UNIVERSITÀ
DEGLI STUDI
FIRENZE

DOTTORATO DI RICERCA IN SCIENZE CHIMICHE

CICLO XXXII

COORDINATORE Prof. Piero Baglioni

ELECTROCHEMICAL STUDY, DESIGN AND REALIZATION OF MODIFIED SUBSTRATE OF ENERGY INTEREST WITH LOW ENVIROMENTAL IMPACT

Settore Scientifico Disciplinare CHIM/01

Dottorando
Dott. Maurizio Passaponti

_____
(firma)

Tutore
Prof. Massimo Innocenti

_____
(firma)

Coordinatore
Prof. Piero Baglioni

_____
(firma)

Anni 2016/2019

Preface

The present thesis work is mainly focused principally on the analysis of new electrocatalysts in the oxygen reduction reaction (ORR) in an alkaline environment, for a future use in fuel cells and in electricity storage systems. We work also in the fields of electrodeposition and surface analysis. Different materials and modified surfaces with a low environmental impact have been studied. Specifically, the catalytic efficiency of carbons obtained from microwave oven-mediated pyrolysis of end-of-life tires and functionalized carbonaceous nanotubes with organic-Pd complexes (Single ion site) was evaluated. The study of the catalysts was carried out with electroanalytical techniques such as cyclic voltammetry (CV), Rotating Disk Electrode (RDE) and Rotating Ring and Disc Electrode (RRDE). Through a punctual and focused characterization with different investigation techniques, such as: SEM / TEM, XRF, XRD, μ-Tomography, XPS besides the use of BET, it was possible to determine which chemical-physical contributions are responsible for the excellent electrocatalytic performance of the samples object of study in half-cell conditions. The samples under study, that showed the best performance in half cells, were tested as cathodes in a fuel cell, obtaining comforting power values. In the last part of the thesis further on-line publications are reported with the research project “Electrochemical study, design and realization of modified substrates of energy interested in environmental impacts”

1 Introduction

This doctoral thesis focuses on studies of potentially cheap materials in electrocatalysis energy applications. What is “energy”? Nowadays energy is life. Indeed, in most developed countries every aspect of human life is strongly connected on energy and its availability. The global economic development and changes in the life’s style and the increase of the world’s population in the last two hundred years has been ascribed to the increasing of fossil energy resources as coal, natural gases and oil and their transformation. In particular, the change of oil into liquid fuel with a high energy density easily be transport and store represented a wonderful energy vector. At the first observation, there are not any problems. But along the time several questions rose up, the energy fossil sources will be there forever? What will happen when petroleum finish? Geo-politic dynamics can be change? Starting from the half of last century, scientist community focused their studies to understand the limited fossil energy resource problems. In 1962 Marion King Hubbert [1] proposed a “bell shaped” graphic for the production of crude oil in the United States. The symmetric curve in Hubbert’s graph (Fig. 1.1) shows clearly a peak. Hubbert's peak or Hubbert's curve is a model that approximates the production rate of a resource over a period of time. In particular, the Hubbert peak refers to the point at which both the production rate and the demand for resources are at maximum, after which it predicts a decline. During this drop, there may be dramatic differences in production and demand as demand continues to increase but production drops overall. Hubbert predicted that crude oil production would peak in the 1970s and then drop drastically over the successive years. On the graph itself, the total area under the curve is the total amount of oil extracted up to a given point in time. Given the

symmetric prediction of the peak, it would mean that around 1970 half of the US oil reserves has been used up. However, there were later unforeseen changes in the production of oil in the US. Mainly, the production of oil from Alaska and advancements in technologies that allowed oil to be extracted from unconventional resources led to what appears to be another peak after the first. Although this growth does exist, the theory of peak oil says that there will be an ultimate peak in oil production when half of the oil reserves remain. The prediction itself was determined by explaining that there is only a finite amount of oil that exists - known as the ultimate recoverable resource and explained that increasing rates of depletion would result in an eventual peak in the amount that could actually be produced as the resources begin to dwindle. Essentially, this ultimate recoverable resource represents the entirety of a McKelvey box, including all undiscovered resources as well as reserves known to exist [2]. Although the shape of the trend is predicted to be a curve, there are a wide number of external factors that may cause the trends to deviate from this model slightly. The idea of peak oil has helped light a the price of petroleum, but now, another peak theory has emerged, this time involving minerals, precious metals gold in particular.

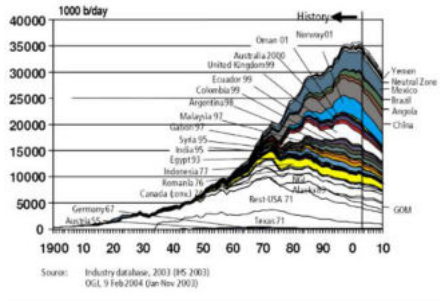

Fig. 1.1 Hubbert's peak of oil: past production and future prevision.

In fact, many analysts of minerals aminers are taking a cue from the assertions from the Bubber's theory, and then begins an inexorable decline accompanied by significantly higher prices. According to them the same concept may been applied equally well to the ingots, as well as to the oil, and can lead to outsized investment returns from the purchase of the minerals, especially precious metals. In this context, for example the golden peak (Fig. b) claim that mining has a discrete number of similarities with oil extraction. Moreover, Hubber's behavior could be extend to some biological resources as for example Caspian caviar in the eighteenth century [3]. Fossil energy or biological resources and minerals and other material systems that the production rate is much faster than regeneration, showing a Hubber's behavior, give us need introduce a new concept of resources: renewable resources. In this case the regenerate the rate of resources is larger than their consumption.

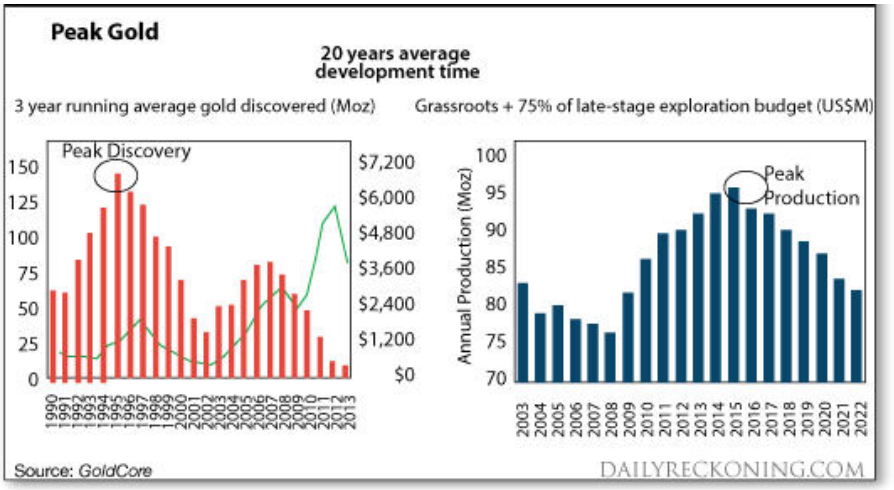

Fig 1.2 Hubbert's peak of gold

1.1 Concept EROEI

As previously mentioned, much of the energy production is currently derived from fossil fuels [4]. The immoderate use of this type of non-renewable resources could cause, in a relatively short time, the depletion of oil, leading to devastating consequences both from the energy point of view and from the political and socio-economic point of view. The dependence on these resources, in particular on the part of the most developed countries, derives mainly from the good energy yield of fossil fuels measured, in the economic sphere, by the EROEI (Energy Returned On Energy Invested) index. This is calculated as the ratio between the energy produced and the energy consumed in the production process [5] for each energy source (Fig 1.3). The EROEI makes it possible to determine whether the latter is capable of satisfying the sometimes unbridled needs of an industrialized society (for which an EROEI of between 5 and 9 is required) [6].

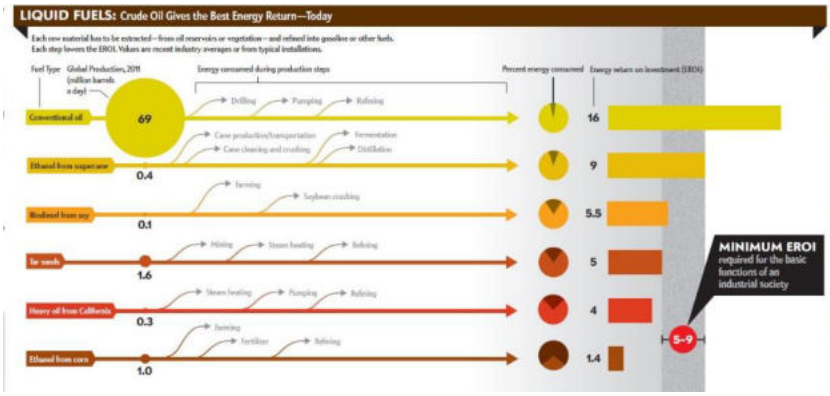

Fig. 1.3 EROEI calculated for the main fossil fuel.

Comparing the values of the EROEI calculated for energy production from fossil fuels and some renewable energy sources (fig. 1.4), we note that in many cases the former show greater efficiency: this is due to the fact that

the constant use of the crude led to more investment in research applied to fossil fuels. As a result, there has been greater technological progress in addition to the development of increasingly effective processing methods, resulting in a high EROEI value. The same cannot be said for alternative systems such as photovoltaic (EROEI = 6) and nuclear (EROEI = 5) [3].

Fig. 1.4 EROEI calculated for the production of energy from renewable sources [3]

The gradual reduction of fossil fuels, together with the considerable environmental impact caused by their use [7], led to find alternative sustainable systems for energy production. In this regard, an example could be the work done by the EERE office (Energy Efficiency and Renewable Energy) of the US Department of Energy. The EERE aims to guide the transition to clean and safe energy sources by promoting the use of electricity from renewable resources by lowering its costs or even encouraging the development of environmentally friendly technologies. An example is the use of fuel cells for powering electric vehicles for city transport [8].

1.2 Purpose of the Research Project

Oxygen is a paramagnetic substance present in nature in the elementary state as a diatomic molecule, O_2. Oxygen has a biological origin, through photosynthesis (both from photosynthetic microorganisms and subsequently from green plants). It is one of the most abundant elements: it forms inorganic compounds (oxides) with most of the elements and in diatomic form it is present both in the atmosphere and in the hydrosphere of our planet.

Oxygen was been obtained in the laboratory in 1774 by chemists Carl Wilhelm Scheele and J. Priestsley for heating some oxides such as manganese dioxide (MnO_2) and HgO mercuric oxide. Subsequently the chemist Antoine-Laurent Lavoiser showed that oxygen was a constituent of the air and called it "prince oxygine". The term oxygen coined by Lavoiser derives from the Greek and means sour, or rather "acid" in fact it was mistakenly believed that this substance was responsible for the acidity. The oxygen reduction reaction (ORR Oxygen Reduction Reaction) is one of the most studied reactions and on which the attention of various research groups is focused, both in the biochemical field as it is involved in the processes of oxidative cellular respiration that in the ambit of energy where there is the interest of exploiting it as a renewable energy source within fuel cells (fuels cells). State of the art low temperature proton exchange membrane fuel cells (PEM-FCs) are compact, yet high power-density systems ideal for automotive applications. Corrosion problems associated with the acidic nature of the proton exchange membrane (PEM) and the high cost of the platinum based anodic and cathodic electrocatalysts and of the Nafion® membrane, are the main limiting factor for these devices. Replacing the PEM with an alkaline anion exchange polymeric electrolyte

(AEM) is one way to overcome these problems. H_2/O_2 fed anion exchange membrane fuel cells (AEM-FCs) are the most attractive alternative to traditional PEMFCs. In fact, the alkaline environment is less corrosive for FC components and allows in principle the use of non-noble metal based catalysts. Platinum-based electrocatalysts are the main limiting factor hindering the large scale development of proton exchange membrane fuel cells, due to the high cost of this metal and to the high Pt loading necessary to speed up the sluggish ORR reaction in H_2/O_2 PEMFCs. Another limiting factor of platinum based catalysts is the CO poisoning effect. Unfortunately, Pt and its alloys are the best catalytic materials for the hydrogen reactions and for the oxygen reduction reaction performed in acidic environments. Platinum is also the only metal that can tolerate the strong acidic environment of proton exchange membranes.

Operating in an alkaline environment is the only way to overcome these issues as in principle non platinum electrocatalysts, even non noble based electrocatalysts, can be used and the reactions kinetics are generally faster with respect to acidic conditions. Alkaline conditions are also much less corrosive for FCs components.

Regarding the cathodic catalyst, in alkaline environment platinum can be replaced by choice of non-noble metals. In this regard the potential cathode electrocatalyst object of this research project, above described and studied in half cell, was tested in complete fuel cell.

At the applied electrochemical laboratories of the University of Florence where I carried out this thesis work, potential catalysts based on pyrolysed carbon were studied starting from waste materials such as tires. A further type of recently synthesized catalyst consists of carbon nanotubes functionalized with organic complexes of some metals including

palladium. To evaluate the catalytic activity of potential catalysts for the ORR we refer to specific parameters of the reaction such as:

• onset potential (Eon)

• mid-wave potential E ½

• number of electrons exchanged in the electrochemical process *n*

The study of the oxygen reduction reaction carried out in an alkaline environment was carried out using electrochemical techniques, in this case cyclic voltammeters (CV) and hydrodynamic techniques RDE (Rotating Disc Electrode) and RRDE (Rotating Ring-Disc Electrode) performing linear voltammeters various rotation speeds of the electrode.

References

1. M.K. Hubbert, *Energy Resources*. (National Academy of Sciences-national Research Council, Washington, 1962), p. 141
2. G.Boyle, B.Everett, S.Peake, J.Ramage. (June 3, 2015). Energy Systems and Sustainability: Power for a Sustainable Future, 2nd Ed. Oxford, UK: Oxford University Press, 2012
3. U. Bardi, Energy prices and resource depletion: lesson from the case of whaling in the nineteenth century. Energy sources Part. B: Econ Plan. Policy 2, 297 (2007)
4. Shafiee, S. & Topal, E. When will fossil fuel reserves be diminished? *Energy Policy* **37**, 181–189 (2009).
5. Murphy, D. J. & Hall, C. A. S. Year in review — EROI or energy return on (energy) invested. *Ann. New York Acad. Sci.* **1185**, 102–118 (2010).
6. Inman, M. The True Cost of Fossil Fuels. *Sci. Am.* **308**, 58–61 (2013).
7. Firor, J. Climate Change Policy: A Survey. *Bull. Am. Meteorol. Soc.*

84, 105 (2003).

8. Office of Energy Efficiency & Renewable Energy. 2016-2020 Strategic Plan and Implementing Framework. 1–36 (2016).

2. Electrochemical technologies

H_2 fuel: a possible solution? In general, an electrochemical cell allows the conversion of chemical energy into electrical energy and vice versa. Electrochemical cells can be classified according to the type of conversion they operate. A galvanic cell (pile or fuel cell) operates by converting chemical energy into electrical energy while electrolyte cells convert energy to electrical energy into chemical energy. In common language the terminology used for devices in which the energy of chemical reactions is converted directly into electricity is mistakenly replaced with that used for devices that serve to store electricity. Accumulators or batteries are devices that can operate both conversions. Reality, the term battery should be more correctly referred to an assembly (in series or, more rarely, in parallel) of more batteries, i.e. a battery of cells. A first classification between batteries and accumulators can be made based on whether they can be rechargeable or non-rechargeable. Respectively, the terminology used distinguishes primary batteries (non-rechargeable) and secondary batteries (rechargeable). Both because of the importance they are increasingly taking on and because of their peculiarity, Fuel cells then form a separate chapter. Fuel cell, from an electrochemical point of view, falls within the classification of primary batteries with the difference that while the latter constitute a "closed" electrochemical system that once exhausted is no longer usable, the fuel cell is an "open" electrochemical system able to exchange material with the environment. Fuel cells are electrochemical devices and represents an attractive technology as energy vector. This system is able of converting the chemical energy of a fuel (usually hydrogen) directly into electrical energy, without intermediate intervention of the Carnot cycle and consequently allow higher conversion yields than

those of the machines conventional thermals. Since fuel cells generate electricity through a chemical process, they are not subjected to the Carnot Limit, so they can extract more energy from fuel (40-70% efficiency) than traditional internal combustion engines (30% efficiency). If fed with H2, no CO2 is emitted by fuel cells. In addition a fuel cell can be recharge quickly with an amount of fresh fuel giving the same performances, while a common battery (lithium battery, e.i.) stops working when it reaches the chemical equilibrium of the redox reaction.

2.1 Fuel Cell

In the search for new energy sources it is important that these respect certain standards of efficiency and eco-compatibility so as to constitute a valid alternative to fossil fuels without constituting a risk for the ecosystem [1]. Among the numerous and valid candidates (such as wind, water, solar, etc.) fuel cells have proved to be a particularly promising option thanks to the large number of possible applications, particularly in the transport field. Fuel cells (or fuel cells) are devices capable of directly converting the chemical energy deriving from the oxidation of a given fuel into electrical energy, avoiding thermal processes. This particular type of pile was developed and described in 1839 by the Welsh chemist Sir William Robert Grove in a letter published in "The London and Edinburgh Philosophical Magazine and Journal of Science" (Fig. 2.1)

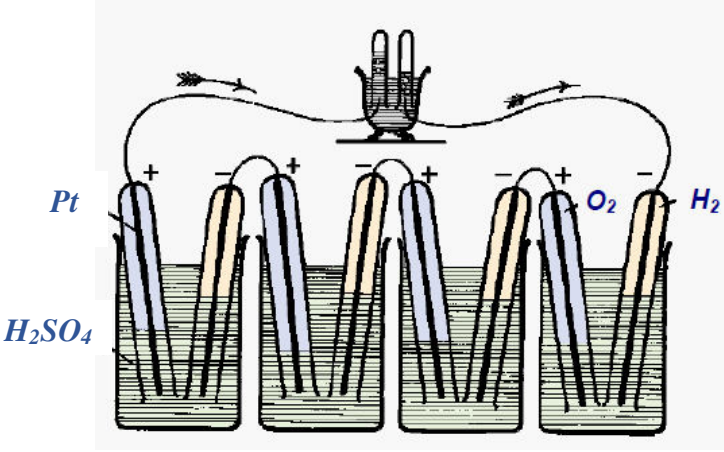

Fig.2.1 Fuel cell scheme proposed by W. R. Grove [2]

The cell described therein consisted of a series of sheets of copper, iron and porcelain plates immersed in a solution of copper sulfate and dilute sulfuric acid [2]. In a second scheme, published in 1842, Grove instead presented a setup in which materials very similar to those currently used for the creation of phosphoric acid fuel cells are used today [3].

Despite being the oldest chemical energy conversion technology known to man, there has not been a serious commitment to the development and use of fuel cells before the twentieth century. Only recently, in fact, the greater interest in alternative methods for energy generation, which do not involve the use of non-renewable resources, has contributed to the increasingly in-depth study of this kind of devices.

One of the major advantages in the use of fuel cells lies in the type of reaction products. In the case of a hydrogen / oxygen fuel cell, for example, the overall reaction leads to the production of water, a by-product that does not constitute a risk factor at the environmental level [4]:

$$H_2 + \frac{1}{2}O_2 \rightarrow H_2O \quad (1)$$

Although there are various types, fuel cells have a common basic scheme: they are composed of two electrodes (anode and cathode) connected by an external circuit and separated by an electrolyte which, in most cases, determines the type of cell [5]. A short overview of the main fuel cells types is reported in table 2.1.

	Polymer Elecrtolyte Membrane Fuel Cells (PEMFCs)	Phosphoric Acid Fuel Cells (PAFCs)	Alkaline Fuel Cells (AFCs)	Molten Carbonate Fuel Cells (MCFCs)	Solid Oxide Fuel Cells (SOFCs)
Electrolyte	proton exchange membrane (Nafion™)	H3PO4 adsorbed on a SiC matrix	concentrated KOH solution	Li2CO3 or Na2CO3 or K2CO3 on ceramic matrix	Zr and Y oxides based ceramics
Ions exchanged	H^+	H^+	OH^-	$CO3^{2-}$	O^{2-}
Working temperature	25-100°C	160-220°C	60-220°C	600-650°C	1000°C
Fuel	hydrogen, alcohols, short chain hydrocarbons	hydrogen, short chain hydrocarbons	hydrogen	hydrogen, short chain hydrocarbons	hydrogen, hydrocarbons
Catalysts	platinum based	platinum based	platinum based, platinum free	platinum based, platinum free	platinum based, platinum free
Applications	household, automotive, portable power supply	stationary high power density supply	automotive, aerospace industry	stationary high power density supply	stationary high power density supply

Table 2.1 Fuel cells classification by working temperature, application and electrolyte..

For example, in a cell with a polymeric membrane, at the anode we see the oxidation of hydrogen with the production of protons. The latter pass through the electrolyte, while the electrons reach the cathode through the external circuit.

$$H_2 \rightarrow 2H^+ + 2e^- \quad (2)$$

Simultaneously with the cathode the electrons react with oxygen. The comburent is reduced to O^{2-} (Eq. 3) which combines with the H^+ products at the anode forming water (Eq. 4).

$$O_2 + 4e^- \rightarrow 2O^{2-} \quad (3)$$

$$O^{2-} + 2H^+ \rightarrow H_2O \quad (4)$$

The electricity generated by the cell depends on the free energy of the reaction. The latter is in turn linked to the potential difference at equilibrium between the two electrodes according to the relation:

$$\Delta G^0 = -nF\Delta E^0 \quad (5)$$

Where *n* represents the number of electrons exchanged, F the Faraday constant and ΔE_0 is the equilibrium potential defined as:

$$\Delta E_0 = E^0_{cathode} - E^0_{anode} \quad (6)$$

The experimentally measured potential actually is far from the thermodynamic equilibrium potential due to overvoltage phenomena (η) due to the passage of current and other effects that cause potential falls, such as the poor mass transport observed in some real systems [4] .

A generic reaction that can occur on the electrode (cathode), $O + n^- \leftrightarrows R$, can be decomposed in a series of elementary steps. In order for the electroactive species to take place, O, it must spread from the massive phase of the solution to the surface of the electrode, be absorbed on it and

here undergoes a reduction; the product obtained, R, must be desorbed and diffused in the mass phase of the solution (Fig. 2.1).

The current produced on the electrode is directly related to the progress of the reaction under examination. If thermodynamically permissible, the forward speed is closely linked to the kinetics of the reaction itself. In this case, the speed depends on the slower elementary process, called the rate determination step, so it affects the amount of current generated.

A certain overvoltage is connected to each current density produced by an elementary process. The total overvoltage can be considered as the sum of the various contributions related to the different phases of the reaction, listed below [6]:

- Overvoltage deriving from mass transfer (ηMT)
- Overvoltage due to electron transfer on the electrode surface (ηCT);
- Overvoltage related to reactions that occur before or after the charge transfer;
- Overvoltage due to phenomena occurring on the electrode surface such as adsorption and desorption.

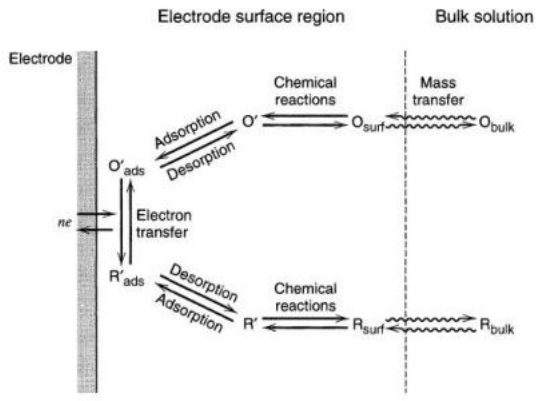

Fig. 2.1 Processes that constitute a generic reaction to the electrode [6]

Being heterogeneous reactions, the actual voltage is expressed as a function of the current density, j, and is defined as:

$$\begin{aligned} \Delta E(j) &= E_c(j) - E_a(j) \\ &= \Delta E_0 - [|\eta_a(j)| + |\eta_c(j)| + R_e j] \end{aligned} \quad (7)$$

Where Re is the resistance of the electrolyte, which contributes to the drop in potential, while ηa (j) and ηc (j) are the overvoltage potentials defined as [4]:

$$\eta_a(j) = E_a(j) - E_{0,a} \quad \text{and} \quad \eta_c(j) = E_c(j) - E_{0,c} \quad (8;9)$$

Overvoltage has an important influence on the efficiency of energy conversion. In general, energy efficiency, ε, is defined as the ratio between usable and produced energy. In a thermal machine the maximum efficiency is limited by the efficiency of Carnot, ε_r^{termic}, defined as:

$$\varepsilon_r^{termic} = \frac{W_r}{(-\Delta H)} = 1 - \frac{T_2}{T_1} \quad (10)$$

In which Wr is the reversible work, -ΔH the variation of enthalpy of the reaction and T1 and T2 the absolute temperatures for the process carried out by the thermal machine.

While Carnot's efficiency often does not exceed 50% [7], fuel cells, in theory, would be able to convert all the energy provided by the reaction. For a cell the efficiency is calculated as:

$$\varepsilon_r^{cell} = \frac{W_e}{(-\Delta H)} = 1 - \frac{T\Delta S}{\Delta H} \qquad (11)$$

In which We is the electric work and ΔS the variation of entropy. In the case of positive ΔS it is also possible to obtain a yield greater than 1 due to the production of electrical energy from the heat coming from the infinite thermal tank [8].

As previously anticipated, in real systems the overpowering phenomena negatively affect the yield. This effect is quantified by electrochemical efficiency, ε_V, which is also a useful value when comparing different fuel cells (with the same reaction):

$$\varepsilon_V = \frac{\Delta E}{\Delta E_0} = 1 - \frac{[|\eta_a(j)| + |\eta_c(j)| + R_e j]}{\Delta E_0} \qquad (12)$$

Another negative contribution to efficiency is given by faradic efficiency, ε_F, defined as:

$$\varepsilon_F = \frac{I_{exp}}{I_{max}} = \frac{n_{exp} \cdot F \cdot v_i}{n_{max} \cdot F \cdot v_i} = \frac{n_{exp}}{n_{max}} \qquad (13)$$

As can be deduced from the equation just described, the faradic efficiency takes into account possible phenomena of heterogeneous catalysis and parallel reactions that decrease the number of electrons exchanged causing a lowering of the produced current.

In summary, the efficiency of a fuel cell, ε_{fc}, can be calculated by combining the contributions just shown:

$$\varepsilon_{fc} = \varepsilon_r^{cella} \cdot \varepsilon_V \cdot \varepsilon_F \cdot \varepsilon_H \cdot U \qquad (14)$$

The last two terms in the equation are respectively the heat yield, ε_H, and the fuel utilization percentage, U [4].

From the constructive point of view fuel cells are generally made up of flat and porous electrodes interspersed with a thin layer of electrolyte. This configuration makes it possible to organize the cells in series, called "stacks", so as to have access to any power (Fig.2.2).

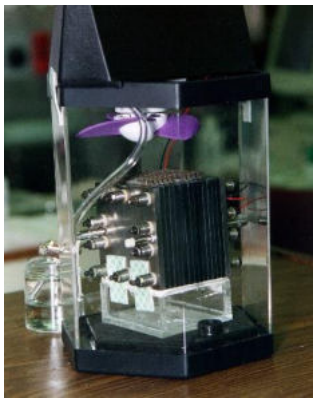

Fig. 2.2 Stack of FCs

2.2 Reactions and Catalysis

2.2.1 Hydrogen oxidation

The reactions that take place in the fuel cell described in the previous paragraph involve the oxidation of the hydrogen to the anode (Eq. 2) and the reduction of the oxygen at the cathode (Eq. 3). Both reactions are thermodynamically favored but, especially in the case of oxygen reduction, there are limits linked to the kinetics that make the intervention of a catalyst necessary. Platinum is generally used for this reaction although more economical solutions are being sought to effectively conduct it.

If a platinum-based catalyst is used, the hydrogen oxidation mechanism consists of a gas adsorption stage on the metal, which causes its

dissociation (Eq. 15), followed by the electrochemical reaction that generates $2H^+$ and two electrons (Eq. 16) [9].

$$2Pt_{(s)} + H_2 \rightarrow (Pt - H_{ads}) + (Pt - H_{ads}) \quad (15)$$

$$(Pt - H_{ads}) \rightarrow H^+ + e^- + Pt_{(s)} \quad (16)$$

Overall we get:

$$H_2 \rightarrow 2H^+ + 2e^- \quad (17)$$

for which $E^0 = 0\ V$.

The problem in this case concerns the storage of pure hydrogen which is particularly complex. Alternative fuels such as natural gas and alcohols are used to contain costs. The latter can be reformed to hydrogen, albeit with the risk of blocking the active sites of the catalyst due to carbon monoxide poisoning, present in the gas as an impurity [4].
Because of this drawback, the development of catalysts in Pt alloys has been proposed, able to increase the catalytic activity with respect to the oxidation of hydrogen [10,11].

2.2.2 Oxygen Reduction Reaction

The oxygen reduction reaction (ORR) takes place at the cathode. In aqueous electrolytes, it can follow two different mechanisms: an indirect mechanism, with two electrons, with the formation of hydrogen peroxide which is subsequently reduced to water:

$$O_2 + 2e^- + 2H^+ \rightarrow H_2O_2 \quad (18)$$

$$H_2O_2 + 2e^- + 2H^+ \rightarrow 2H_2O \quad (19)$$

and mechanism that leads directly to the production of water by exchanging four electrons [12].

$$O_2 + 4e^- + 4H^+ \rightarrow 2H_2O \quad (20)$$

In terms of efficiency, the direct mechanism is preferable as it has a better energy conversion. Furthermore, hydrogen peroxide, formed in the indirect process, can produce free radicals with the risk of probable damage to the system [13]. In any case, both mechanisms depend on a number of adsorption and oxygen dissociation steps, specific for each type of catalyst used [4].

The following are the reaction mechanisms proposed for the catalysts more akin to the work presented in this thesis, namely carbon-based and platinum-based catalysts.

2.2.3 Oxygen Reduction at Carbon Electrodes

The following reaction mechanism has been proposed on glassy carbon electrodes [14]:

$$O_2 \rightarrow O_{2\,(ads)} \quad (21)$$

$$O_{2\,(ads)} + e^- \rightarrow \left[O_{2\,(ads)}\right]^- \quad (22)$$

$$\left[O_{2\,(ads)}\right]^- \rightarrow O^-_{2\,(ads)} \quad (23)$$

$$O^-_{2\,(ads)} + H_2O \leftrightarrows HO_{2\,(ads)} + OH^- \quad (24)$$

$$HO_{2\,(ads)} + e^- \rightarrow OH^-_{2\,(ads)} \quad (25)$$

$$HO^-_{2\,(ads)} \rightarrow HO^-_2 \quad (26)$$

According to this mechanism oxygen, adsorbed on glassy carbon (Eq. 21), is reduced to superoxide ion adsorbed on an inert graphite site (Eq. 22). The migration of the ion to an active site (Eq. 23) allows the formation of the hydroperoxide radical (Eq. 24); the latter is finally reduced to hydroperoxide ion and desorbed (Eq. 25-26). The step that determines the reaction rate is pH dependent and it has been determined that at pH> 10 the decisive step is the migration of the superoxide ion (Eq. 23), while at pH <10 the speed depends on the reduction of oxygen (Eq. 22) [14].

The following mechanism has been proposed on pyrolytic graphite electrodes:

$$O_2 \rightarrow O_{2\,(ads)} \quad (21)$$

$$O_{2\,(ads)} + e^- \rightarrow O^-_{2\,(ads)} \quad (27)$$

$$2O^-_{2\,(ads)} + H_2O \rightarrow O_2 + HO^-_2 + OH^- \quad (28)$$

The step determining the reaction rate is the reduction of oxygen to superoxide ion (Eq. 27) [9].

In both cases the reduction of oxygen takes place through the passage of two electrons with the formation of hydrogen peroxide. This was determined by examining the voltammetric waves recorded in the alkaline environment for the ORR by performing (Fig. 2.3), on a rotating disk and ring electrode (with graphite disk and ring in Pt maintained at 0 V vs. SCE), various scans in the potential range from 0 to -1.1 V (vs. SCE) at the scanning speed of 5 mV / s [15].

The voltammetric profile has two distinct regions, 1 and 2, respectively referable to the formation of H_2O_2 and H_2O.

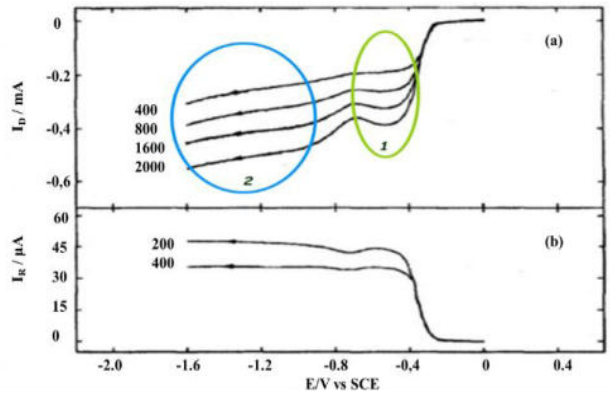

Fig.2.3 Voltammetric waves obtained at a scanning speed of 5mV / s in a 1 M solution of NaOH, saturated with O_2, using a RRDE with a glassy carbon disc (a). Below is the response of the platinum ring maintained at 0 V (vs SCE) (b) [15]

The following scheme (Fig. 2.4) summarizes the different oxygen reduction pathways on platinum electrode [16]:

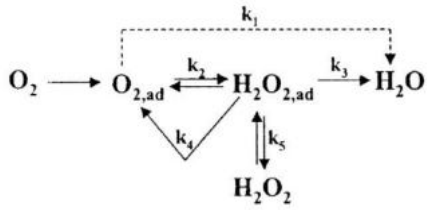

Fig. 2.4 Scheme for the oxygen reduction reaction [16]

It shows (as previously mentioned) that once adsorbed, oxygen can be reduced to water by direct reduction by exchanging four electrons or undergoing a reduction to adsorbed hydrogen peroxide which can then undergo various processes:

• Desorption from the surface of the catalyst;
• Decomposition to oxygen;
• Further reduction to H2O.

Measurements carried out with rotating disk and ring electrodes (RRDE) have shown that the reduction of oxygen on platinum occurs preferably with the transfer of four electrons and the formation of water [9].

2.2.4 Oxygen Reduction on Platinum Electrodes

As regards the reduction on platinum, two reaction mechanisms have been proposed, dissociative and associative, referring respectively to low and high current density ranges.

In the dissociative mechanism the reduction of oxygen occurs without the production of H_2O_2: the adsorption on platinum causes the breakage of the O-O bond leading to the formation of atomic oxygen immobilized on the catalyst (Eq. 29); this undergoes two consecutive reductions that produce H_2O by reforming the catalyst (Eq. 30-31).

$$O_2 + Pt \rightarrow 2\,Pt \cdots O \tag{29}$$

$$2Pt \cdots O + 2H^+ + 2e^- \rightarrow 2Pt \cdots OH \tag{30}$$

$$2Pt \cdots OH + 2H^+ + 2e^- \rightarrow H_2O + Pt \tag{31}$$

The fundamental step that prevents the formation of intermediates, such as hydrogen peroxide, is the rupture, during adsorption, of the oxygen-oxygen bond, so this can be considered a direct mechanism with four electrons [17]. It has been observed that as the overpotential increases, η, the associative mechanism becomes the preferential one [18]:

$$O_2 + Pt \rightarrow Pt \cdots O_2 \quad (32)$$

$$Pt \cdots O_2 + H^+ + e^- \rightarrow Pt \cdots HO_2 \quad (33)$$

$$Pt \cdots HO_2 + H^+ + e^- \rightarrow H_2O + Pt \cdots O \quad (34)$$

$$Pt \cdots O + H^+ + e^- \rightarrow Pt \cdots OH \quad (35)$$

$$Pt \cdots OH + H^+ + e^- \rightarrow H_2O + Pt \quad (36)$$

This mechanism can be considered a re-elaboration of the scheme previously seen since, having the adsorption of O_2 on platinum (Eq. 32), there is the possibility that the breakage of the O-O bond does not occur (Eq. 34). This would cause the formation of hydrogen peroxide, which, as we have seen, can be further reduced to water, or desorbed becoming the final product.

In general, the adsorption of oxygen on platinum is dependent on the overpotential: at high values the adsorbed oxygen is extremely stable and even prevents electronic exchange; the reduction of the overpotential causes the worsening of oxygen stability, allowing the reaction to progress [18].

This phenomenon explains the high overpotentials typical of platinum electrodes that, as explained in paragraph 2.1, influence the efficiency of the cell. Moreover, the use of platinum catalysts implies a considerable increase in the cost of producing the fuel cells and therefore the need to find a less precious metal that is able to catalyze the reaction by reducing production costs.

2.2.5 Oxygen Reduction at Non-Precious Metals

As in most cases, the study and development of catalysts based on non-precious metals was initiated by the observation of a naturally occurring compound capable of catalyzing the reduction of oxygen, or cytochrome. It is an enzyme whose active site consists of an iron ion bound to four nitrogen atoms [19]. In 1964 Jasinski, studying the catalytic activity of cobalt phthalocyanine [20], discovered that catalysis also takes place for simple molecules in which the Me-N4 group is present: this discovery has opened way to numerous researches, still active, on use of macrocycles as catalysts [21–28].

A few years later catalysts were developed that did not include the use of macrocycles [29]: over time the synthesis method was improved by obtaining the electrocatalysts from carbon precursors, nitrogen (NH_3) and metal salts by heat treatment at 500-1000 ° C [30]. In this case the presence of the metal ion has a dual catalytic action: it increases the speed of catalyst formation [31–33] and also improves the activity even for extremely low amounts of iron and cobalt (0.02 wt%) [34].

Another approach adopted to reduce the production costs of fuel cells consists in minimizing the amount of platinum used for the formation of alloys with less noble metals: an example is the catalyst in Pt-Fe alloy supported on carbon (Pt-Fe / C) developed by Li and collaborators [35]. In this study several Pt-Fe / C obtained, for example, at high (900 ° C) or moderate (300 ° C) temperatures were compared: it was observed that Pt-Fe / C prepared at 300 ° C showed the greater surface area electrocatalytic and the best ORR activity, measured using it as a cathode in direct methanol cells.

Given the importance of the metal center influencing the increase in ORR activity, the catalytic properties of different metals were calculated using the density differential theory (DFT) and compared with experimental data. results were presented in two graphs that show the activity of oxygen reduction against the metal-oxygen (Fig. 2.4) and metal-hydroxy binding energy (Fig.2.5).

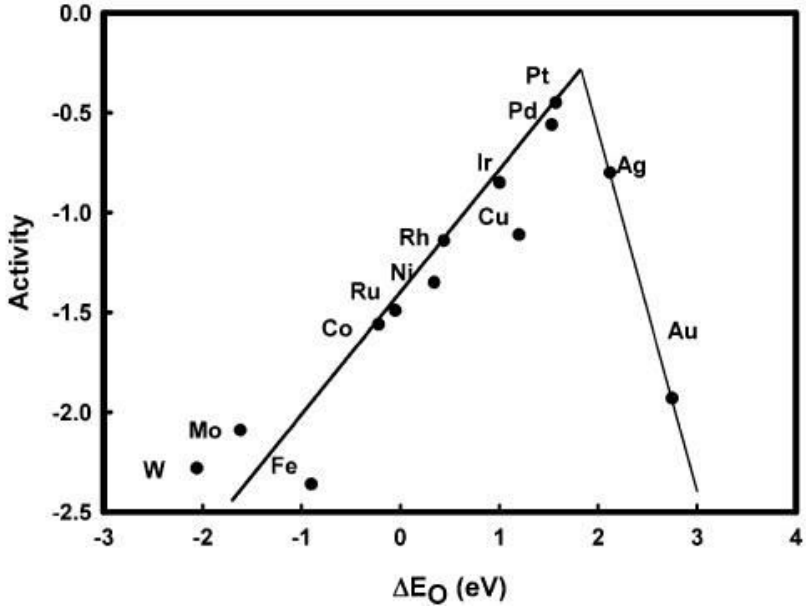

Fig. 2.5 Trend of the catalytic activity of various metals as a function of the strength of the metal-oxygen bond [18]

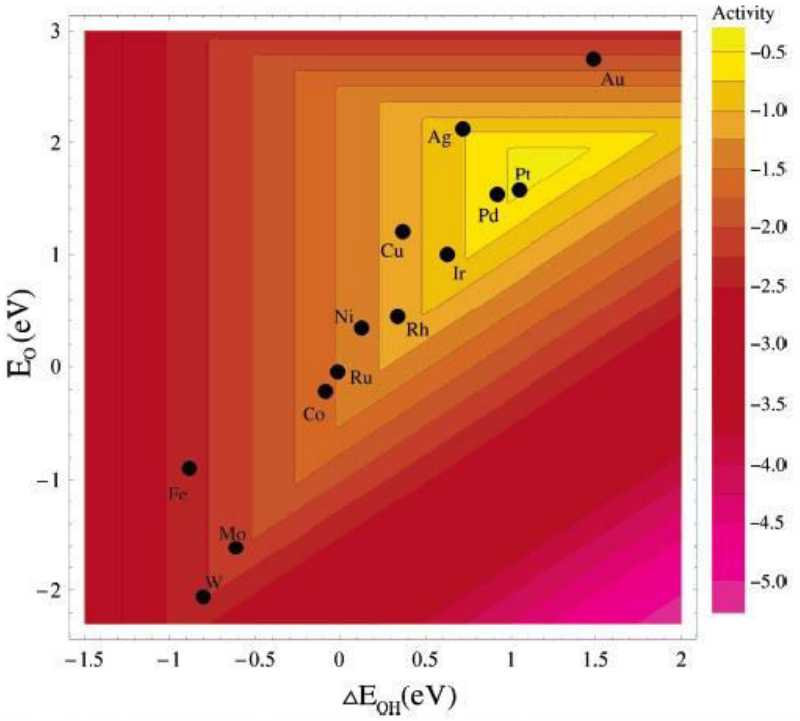

Fig. 2.6 Trend of the catalytic activity of various metals as a function of the strength of the metal-hydroxyl bond [18]

These figures show the increase or decrease in the strength of the bond with oxygen, compared to the value of platinum, causes a worsening of the catalytic activity due to various effects. Nickel for example, to the equilibrium potential, has a bond with O and OH strong enough to prevent proton transfer; on the contrary gold has a very rapid proton transfer but a very bad oxygen absorption [18]. The results obtained here are in agreement with the Sabatier principle which states that the catalytic activity for a given reaction follows a volcano trend in which there is maximum efficiency for a degree of intermediate bond between catalyst and substrate [36]. The catalytic properties of different transition metals have also been investigated on the basis of a new mechanism proposed for the reduction

of oxygen on platinum in an acid environment, obtained by molecular dynamics using the ab-initio method [37]. It consists of three elementary processes that correspond to four values of ΔG:

- Oxygen adsorption on the active site of the metal surface

$$O_2 + M + H^+ + e^- \rightarrow MOOH \qquad (\Delta G_1) \qquad (37)$$

- Dissociation of MOOH

$$MOOH + M \rightarrow MOH + MO \qquad (\Delta G_2) \qquad (38)$$

The following processes may occur after reducing the first electron:

- Reduction by one other electrons

$$O_2 + 2M + H^+ + e^- \rightarrow MOH + MO \qquad (\Delta G_3) \qquad (39)$$

- Reduction by three other electrons

$$MOH + MO + 3H^+ + 3e^- \rightarrow 2H_2O + 2M \qquad (\Delta G_4) \qquad (40)$$

From the analysis of ΔG values for 18 metals, obtained with the DFT method, it was deduced that the metals that favor the formation of the product MOOH (ΔG_1) also facilitate the breaking of the O-O bond, as they make the MOH and MO species more stable . However, this negatively affects the value of ΔG_4 which presents an opposite trend with respect to ΔG_1 [33]. Taking platinum as a reference, since it has the greatest catalytic efficiency, relative ΔGs have been obtained according to the formula:

$$\Delta\Delta G_n = \Delta G_n(M) - \Delta G_n(Pt) \qquad (41)$$

With these data a graph was drawn that shows the abscissa il ΔG relative to the adsorption of oxygen on the metal ($\Delta\Delta G_1$) and on the ordinate one relative to the reduction by the other electrons in the reaction 4 ($\Delta\Delta G_4$ / 3).

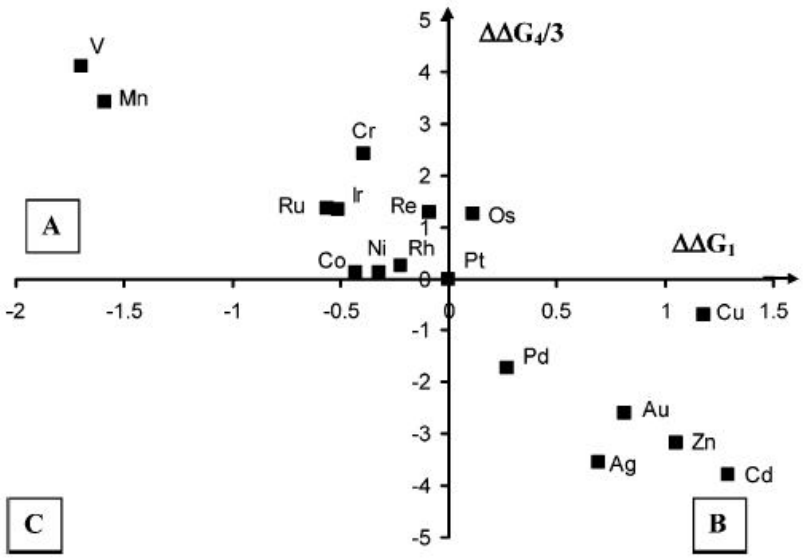

Fig. 2.7 Catalytic activity (relative to Pt) of different metals with respect to different steps of the reaction mechanism [38]

From this diagram, it is possible to deduce how a given metal will affect the oxygen reduction reaction and how effective it will be compared to a platinum-based catalyst. By making the prediction of the relative catalytic activity of metals possible, this graph represents an excellent tool for the design of bimetallic electrocatalysts. An example can be seen in the work realized by Zafferoni et. [39]: it consists in the development of a bimetallic catalyst obtained by electrodeposition of silver and cobalt which, acting on different elementary processes of the oxygen reduction reaction mechanism, cause a synergistic effect on the ORR activity.

References

1. Panwar, N. L., Kaushik, S. C. & Kothari, S. Role of renewable energy sources in environmental protection: A review. *Renew. Sustain. Energy Rev.* **15**, 1513–1524 (2011).
2. Grove, W. R. XXIV. On voltaic series and the combination of gases by platinum. *London, Edinburgh, Dublin Philos. Mag. J. Sci.* **14**, 127–130 (1839).
3. Grove, W. R. LXXII. On a gaseous voltaic battery. *London, Edinburgh, Dublin Philos. Mag. J. Sci.* **21**, 417–420 (1842).
4. Carrette, L., Friedrich, K. A. & Stimming, U. Fuel Cells - Fundamentals and Applications. *Fuel Cells* **1**, 5–39 (2001).
5. Blomen, L. J. M. J. & Mugerwa, M. N. *Fuel cell systems*. (Springer Science & Business Media, 2013).
6. Bard, Allen J; Faulkner, L. R., Swain, E. & Robey, C. *Fundamentals and Applications*. (John Wiley & Sons Inc., 2000).
7. Curzon, F. L. & Ahlborn, B. Efficiency of a Carnot engine at maximum power output. *Am. J. Phys.* **43**, 22–24 (1975).
8. Sharma, B. K. *Electro chemistry*. (Krishna Prakashan Media, 1997).
9. Song, C. & Zhang, J. Electrocatalytic Oxygen Reduction Reaction. *PEM Fuel Cell Electrocatal. Catal. Layers Fundam. Appl.* 89–129 (2008). doi:10.1007/978-1-84800-936-3_2
10. Grgur, B. N., Markovic, N. M. & Ross, P. N. Electrooxidation of H 2 , CO and H 2 / CO mixtures on a well-characterized Pt ± Re bulk alloy electrode and comparison with other Pt binary alloys. *J. Electrochem. Soc.* **43**, 3631–3635 (1998).
11. Grgur, B. N., Markovic, N. M. & Ross, P. N. The Electro-oxidation of H_2 and H_2/CO Mixtures on Carbon-Supported Pt x Mo y Alloy

Catalysts. *J. Electrochem. Soc.* **146**, 1613–1619 (1999).

12. Katsounaros, I. *et al.* Hydrogen peroxide electrochemistry on platinum: Towards understanding the oxygen reduction reaction mechanism. *Phys. Chem. Chem. Phys.* **14**, 7384–7391 (2012).
13. Wang, B. Recent development of non-platinum catalysts for oxygen reduction reaction. *J. Power Sources* **152**, 1–15 (2005).
14. Taylor, R. J. & Humffray, A. A. Electrochemical studies on glassy carbon electrodes: II. Oxygen reduction in solutions of high pH (pH> 10). *J. Electroanal. Chem. Interfacial Electrochem.* **64**, 63–84 (1975).
15. Baez, V. B. & Pletcher, D. Preparation and characterization of carbon/titanium dioxide surfaces—the reduction of oxygen. *J. Electroanal. Chem.* **382**, 59–64 (1995).
16. Jr, P. N. R. & Markovic, N. M. Surface science studies of model fuel cell electrocatalysts. *Surf. Sci. Rep.* **45**, 117–229 (2002).
17. Zhdanov, V. P. & Kasemo, B. Kinetics of electrochemical O 2 reduction on Pt. *Electrochem. commun.* **8**, 1132–1136 (2006).
18. Nørskov, J. K. *et al.* Origin of the overpotential for oxygen reduction at a fuel-cell cathode. *J. Phys. Chem. B* **108**, 17886–17892 (2004).
19. Jaouen, F. *et al.* Recent advances in non-precious metal catalysis for oxygen-reduction reaction in polymer electrolyte fuel cells. *Energy Environ. Sci* **4**, 114–130 (2011).
20. Jasinski, R. A new fuel cell cathode catalyst. *Nature* **201**, 1212 (1964).
21. Li, X., Liu, C., Xing, W. & Lu, T. Development of durable carbon black/titanium dioxide supported macrocycle catalysts for oxygen reduction reaction. *J. Power Sources* **193**, 470–476 (2009).
22. Bagotzky, V. S., Tarasevich, M. R., Radyushkina, K. A., Levina, O. A. & Andrusyova, S. I. Electrocatalysis of the oxygen reduction process

on metal chelates in acid electrolyte. *J. Power Sources* **2**, 233–240 (1978).

23. Koslowski, U. I., Abs-Wurmbach, I., Fiechter, S. & Bogdanoff, P. Nature of the catalytic centers of porphyrin-based electrocatalysts for the ORR: a correlation of kinetic current density with the site density of Fe− N4 centers. *J. Phys. Chem. C* **112**, 15356–15366 (2008).
24. Ziegelbauer, J. M. *et al.* Direct spectroscopic observation of the structural origin of peroxide generation from Co-based pyrolyzed porphyrins for ORR applications. *J. Phys. Chem. C* **112**, 8839–8849 (2008).
25. Maruyama, J., Okamura, J., Miyazaki, K., Uchimoto, Y. & Abe, I. Hemoglobin pyropolymer used as a precursor of a noble-metal-free fuel cell cathode catalyst. *J. Phys. Chem. C* **112**, 2784–2790 (2008).
26. Bogdanoff, P. *et al.* Probing structural effects of pyrolysed CoTMPP-based electrocatalysts for oxygen reduction via new preparation strategies. *J. new Mater. Electrochem. Syst.* **7**, 85–92 (2004).
27. Jahnke, H., Schönborn, M. & Zimmermann, G. Organic dyestuffs as catalysts for fuel cells. in *Physical and chemical applications of dyestuffs* 133–181 (Springer, 1976).
28. Van Veen, J. A. R. & Colijn, H. A. Oxygen Reduction on Transition-Metal Porphyrins in Acid Electrolyte II. Stability. *Berichte der Bunsengesellschaft für Phys. Chemie* **85**, 700–704 (1981).
29. Gupta, S., Tryk, D., Bae, I., Aldred, W. & Yeager, E. Heat-treated polyacrylonitrile-based catalysts for oxygen electroreduction. *J. Appl. Electrochem.* **19**, 19–27 (1989).
30. Wang, H., Cote, R., Faubert, G., Guay, D. & Dodelet, J. P. Effect of the pre-treatment of carbon black supports on the activity of Fe-based

electrocatalysts for the reduction of oxygen. *J. Phys. Chem. B* **103**, 2042–2049 (1999).

31. Matter, P. H., Wang, E., Arias, M., Biddinger, E. J. & Ozkan, U. S. Oxygen reduction reaction catalysts prepared from acetonitrile pyrolysis over alumina-supported metal particles. *J. Phys. Chem. B* **110**, 18374–18384 (2006).
32. Matter, P. H. & Ozkan, U. S. Non-metal catalysts for dioxygen reduction in an acidic electrolyte. *Catal. Letters* **109**, 115–123 (2006).
33. Nallathambi, V., Lee, J.-W., Kumaraguru, S. P., Wu, G. & Popov, B. N. Development of high performance carbon composite catalyst for oxygen reduction reaction in PEM proton exchange membrane fuel cells. *J. Power Sources* **183**, 34–42 (2008).
34. Jaouen, F. & Dodelet, J.-P. Average turn-over frequency of O2 electro-reduction for Fe/N/C and Co/N/C catalysts in PEFCs. *Electrochim. Acta* **52**, 5975–5984 (2007).
35. Li, W. *et al.* Nano-stuctured Pt–Fe/C as cathode catalyst in direct methanol fuel cell. *Electrochim. Acta* **49**, 1045–1055 (2004).
36. Bligaard, T. *et al.* The Brønsted–Evans–Polanyi relation and the volcano curve in heterogeneous catalysis. *J. Catal.* **224**, 206–217 (2004).
37. Wang, Y. & Balbuena, P. B. Ab initio molecular dynamics simulations of the oxygen reduction reaction on a Pt (111) surface in the presence of hydrated hydronium (H_3O)+(H_2O) 2: direct or series pathway? *J. Phys. Chem. B* **109**, 14896–14907 (2005).
38. Wang, Y. & Balbuena, P. B. Design of Oxygen Reduction Bimetallic Catalysts : Ab-Initio-Derived Thermodynamic Guidelines. *J. Phys. Chem. B* **109**, 18902–18906 (2005).

39. Zafferoni, C. *et al.* Synergy of cobalt and silver microparticles electrodeposited on glassy carbon for the electrocatalysis of the oxygen reduction reaction: An electrochemical investigation. *Molecules* **20**, 14386–14401 (2015).

3. Electrochemical techniques

3.1 Introduction to Voltammeters

Voltammetry includes a group of analytical methods in which information is obtained by measuring the current as a function of the potential applied to a polarized working electrode. Polarized electrode means an electrode to which a voltage greater than that required by the Nerst equation has been applied in order for an oxidation or reduction reaction to occur. This electrode is considered ideal if its potential can be modified at will without undergoing permanent changes and can therefore be considered inert. Actually, no polarized electrode is ideal for the whole range of applicable potentials, but some electrodes can be considered as such in wide fields of use as in the case of noble metals such as platinum and gold. Electrodes of this type can be used to study the kinetics of reduction or oxidation processes within the inactivity zone of the material that constitutes the electrode itself.

The electrode at which the process of interest takes place is called the working electrode to which the desired potential is applied by varying the ddp between the latter and a reference electrode. The electrochemical measuring cell will also contain a counter-electrode (or auxiliary electrode) to which the opposite reaction (oxidation or reduction) occurs with respect to that of the working electrode.

The most common work electrodes consist of thin discs of conductive material incorporated at the end of a rod of inert material that contains a metal contact inside it that connects the electrode to the external circuit. The most commonly used conductors are noble metals (gold and platinum),

carbon material (glassy carbon) or other (objet of research) materials deposited on a conductive surface as in the case of the following work.
The range of applicable potentials depends on the electrode material and in the aqueous solution is limited by the oxidation of water to oxygen (positive potentials - upper limit) and by reduction to hydrogen (lower limit - negative); in fact, such reactions would produce currents such as to "cover" other processes. During the scanning and the simultaneous recording of current, the potential is varied as a function of time. Depending on how this variation occurs, voltammetric techniques are classified into:

Classical voltammeters, among which we find hydrodynamic voltammeters: the potential of the working electrode is linearly varied as a function of time, a linear scan is carried out between a starting potential and an arrival potential (Fig. 3.1);

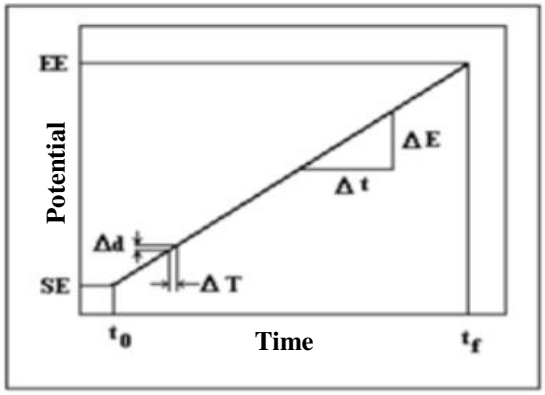

Fig.3.1 Linear voltammeters

Voltammetry with step scanning STC (Staircase Voltammetry): it is a variant in which the potential is increased following steps, that is the potential increases abruptly at regulated time intervals and the current is

recorded in the last moments before the next step, this reduces interference due to capacitive currents (Fig. 3.2);

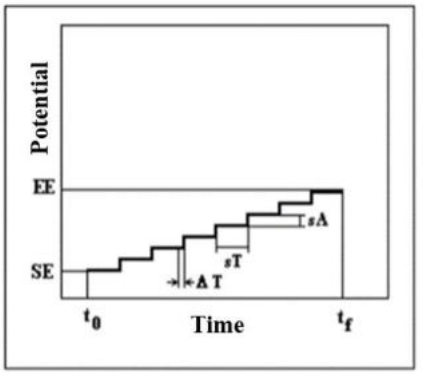

Fig.3.2 Step-type voltammeters

Differential-pulse voltammetry: the potential increases over time following successive excitation pulses and the signal is obtained by superimposing a periodic pulse on a linear scan, the current is recorded alternately at the base and at the maximum height of the pulse, thus obtaining lower detection limits due to the increase in faradic current and the decrease in capacitive current (Fig. 3.3);

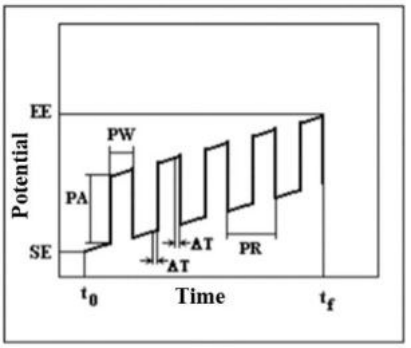

Fig. 3.3 Differential scanning voltammeters.

Square wave Voltammetry: it is a technique similar to the previous one which offers the advantage of being fast and highly sensitive, the signal is obtained by superimposing a periodic pulse on a step signal (Fig. 3.4);

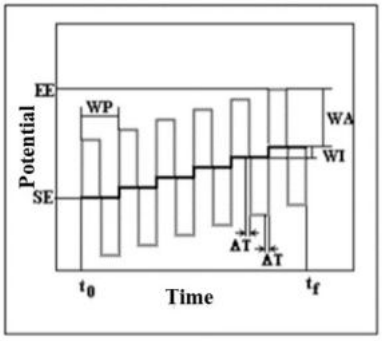

Fig. 3.4 Square-wave differential voltammeters.

Cyclic Voltammetry: a triangular waveform is used so that the potential increases linearly up to a value and decreases with the same slope towards the starting value, or vice versa, in this case we will observe both the reduction reaction and the oxidation reaction that will take place in succession depending on the direction of scanning (Fig. 3.5).

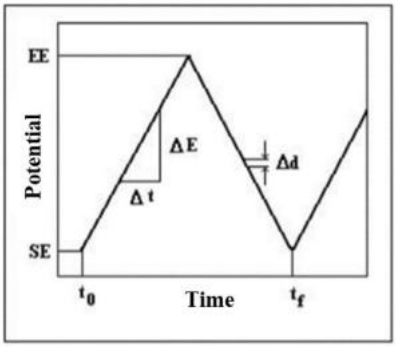

Fig. 3.5 Cyclic Voltammeters.

The graph obtained by recording the current as a function of the potential scan is called a voltammogram and in the case of linear scans it consists of sigmoid-shaped curves in which a limiting current is reached Fig 3.6.

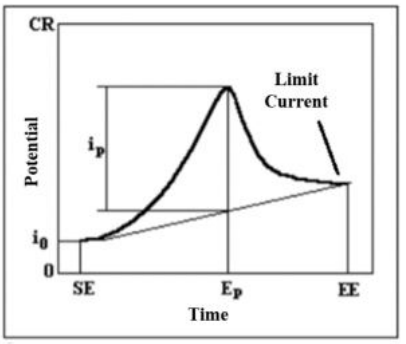

Fig. 3.6 Example of a voltammogram obtained for a linear scan between a SE starting potential and an EE final potential

To understand the trend of the voltammograms it is necessary to introduce the concepts of mass transport, faradic currents, capacitive currents and diffusion layer.

3.1.1 Mass Transport

Mass transport refers to the non-random movement of chemical species within a phase. Mass transport can take place according to three distinct mechanisms: migration, convention and diffusion.

Migration refers to the movement of ions in solution influenced by the force of attraction (or repulsion) of the electric field generated by the electrode. This force decreases exponentially as the distance increases. Fig. 3.7.

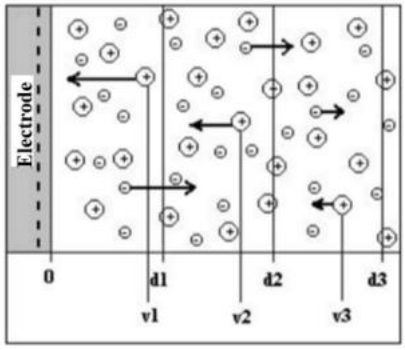

Fig. 3.7 Mass transport for migration

By convention we mean the movements that occur following a temperature gradient (natural convection) or because the solution is subject to agitation (forced convection); in this case we observe a turbulent movement which, when approaching the electrode, becomes laminar and the solution layer in close contact with the surface is stationary Fig.3.8.

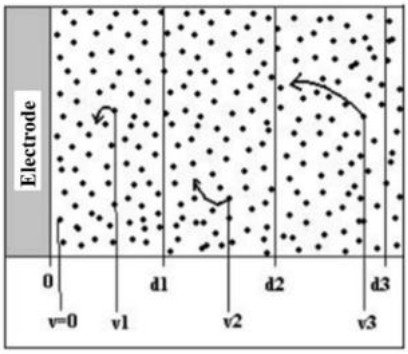

Fig. 3.8 Mass transport by convection

Diffusion means the motion of the species subjected to a concentration gradient and does not depend on the charge of the particles. As the discharge reaction occurs, the solution in the neighborhood of the electrode is depleted of the reacting species as they are consumed and a concentration

gradient is created which recalls the electro-active species from the most distant layers of the solution towards the electrode surface . The diffusion rate is proportional to the concentration gradient and in diffusion of such diffusion processes Fig. 3.9.

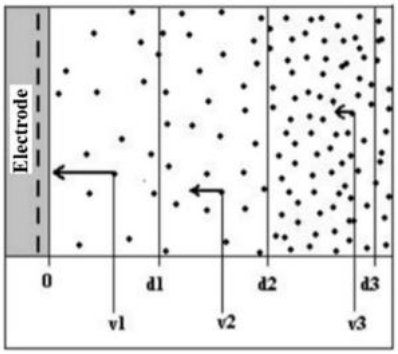

Fig. 3.9 Mass transport by diffusion

3.1.2 Faradic and Capacitive Currents

The electric current that passes through the electrode and is recorded can be of two types: faradic or capacitive.

The faradic current is due to the discharge of the electrochemical species and is proportional to the oxidized or reduced quantity according to Faraday's laws.

The capacitive current is instead due to the discharge of a pseudo-capacitor which is formed at the interphase between the electrode and solution: by imagining a negatively charged electrode it will recall the positive ions present in solution (ions of the support electrolyte) and then a create an electric double layer that behaves like a capacitor Fig. 3.10. Capacitive currents are generally negligible but still constitute background interference.

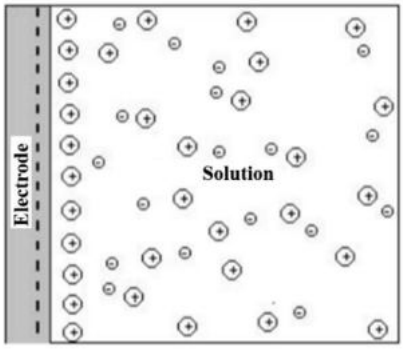

Fig. 3.10 Example of double electric layer at the interface between electrode and solution.

3.1.3 Diffusion layer

Even if the solution is set in motion, a small thickness (layer) of still solution is created around the electrode, said Nernst diffusion layer or stationary state and in which the movement of the particles involved in the reaction occurs by diffusion only (Fig 3.11). The thickness of the layer varies between 10 and 100 μm and depends on the amount of agitation. In these conditions the faradic current reaches a limit value that depends on the speed of diffusion within the Nernstian state which in turn is correlated to the concentration of the massive solution. At a given instant of a steady state process, observing the concentration profiles for solution thicknesses, we will have that the massive solution will have a certain concentration (maintained by agitation) and in the diffusion layer the concentration decreases to a C_0 concentration on the electrode.

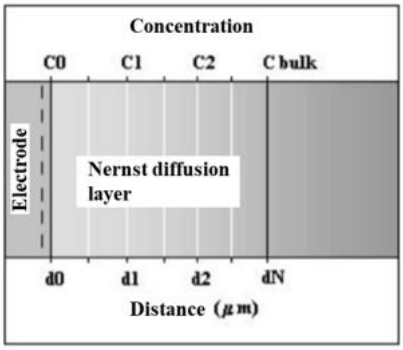

Fig.3.11 Variation of concentration within the diffusion state of Nernst

3.2 Voltammetry in quiet

Consider a process that takes place at rest and we observe the trends of the voltammograms obtained. If we imagine having an electrode immersed in a solution containing an electroactive species and applying a linear scan of the potential. We will find that (Fig. 3.6) initially the current remains stable at a value close to zero (due to the capacitive current); subsequently when the discharge potential is reached the current increases up to a maximum point (the species present around the electrode are consumed) and then it decreases to a limit current that remains constant even increasing the potential. This is because once the molecules have been consumed in the diffusion layer the current will start to decrease and the molecules will begin to be recalled by the massive solution, in these conditions the process is regulated by diffusion. The species reach the electrode at a constant speed and the limit current is reached. The value of the limit current depends on the concentration gradient and therefore on the concentration of the solution, the more the solution is concentrated and the higher the limit current.

The limit current will be proportional to the flow of the species towards the electrode which is expressed by Fick's first law (Eq. 42):

$$\Phi_{x,t} = -D(\delta C/\delta x)_{x,t} \qquad (42)$$

In general, in cyclical voltammeters are performed in order to study the behaviour of a redox pair. This corresponds to performing a reduction reaction and then an oxidation reaction (or vice versa depending on the scanning direction). The extreme potential values at which the inversion occurs are called switching potentials and the scanning in the direction of negative potentials is called direct scanning those in the opposite direction is called reverse scanning. To obtain information on the process the potential scanning must obviously take place within that in which oxidation or reduction of the electroactive species occurs. Figure 3.12 shows an example of cyclic voltammetry where we can observe two peak currents, one referring to the reduction process (the one below) and one referring to the oxidation process (upper peak); for a reversible electrochemical reaction the difference between the two potentials corresponding to the two peak currents is expected to be (43):

$$\Delta E_p = |E_{p,rid} - E_{p,oss}| = 0{,}0592/n \qquad (43)$$

In reality the irreversibility due to the kinetics of the process causes a.ΔEp that exceeds the expected value.

The intensity of the peak current can be expressed with the Randles equation (44), according to which the intensity is proportional to the number of electrons exchanged, to the scanning speed v (V / s), to the area

of the electrode A (cm^2) to the diffusion coefficient D and to the concentration of the massive solution C, and K is a constant of proportionality and is 2,686x105

$$i_p = Kn^{3/2}AD^{1/2}v^{1/2}C \qquad (44)$$

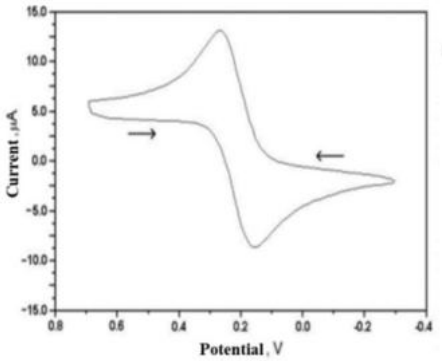

Fig. 3.12 Example of voltammogram obtained in a cyclic voltammetry in quiet

3.3 Hydrodynamic rotating disk voltammetry (RDE)

Hydrodynamic rotating disk voltammetry, differs from that electrochemical technique, previously explained by the fact that the working electrode is subjected to a constant speed rotation (Fig. 3.13). The mass of the solution far from the electrode is subjected to a turbulent flow caused by agitation, approaching towards the electrode a region of laminar flow is met and subsequently the road is stagnant solution called Nerst diffusion layer. Only within the diffusive layer the concentrations vary depending on the distance forming the concentration gradient, since in the areas of laminar and turbulent flow the convention keeps the concentration at its initial value.

The voltammogram that is obtained has the classical form of a wave (Fig.3.14). In the first section the current value is close to zero and is due to the capacitive current. Subsequently the discharge of the electroactive species is observed and the current increases (in absolute value) until reaching a stationary regime where once the species are consumed around the electrode there is a continuous and constant supply of species from the solution to the Nerst layer according to the diffusion process. The thickness of the diffusion layer will be lower the greater the rotation speed, therefore the limit current increases as the solution concentration increases and the electrode rotation speed increases. The potential at which the current is equal to half the limit current is called the half-wave potential $E_{1/2}$ and is closely related to the standard reduction potential of the redox pair even if in reality it is not identical.

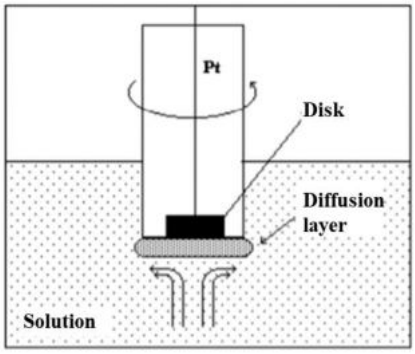

Fig. 3.13 Rotating electrode immersed in a solution

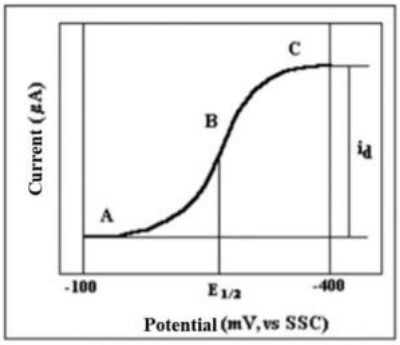

Fig. 3.14 Example of a voltammogram obtained for a linear scan with a rotating electrode.

3.3.1 Levich Equation

Electroanalytical techniques can be used to estimate the number of electrons exchanged in a redox reaction in order to evaluate the efficiency of some electrochemical systems. The calculation of the exchanged electrons can been performed according to two models: the Levich equation and the Koutecky-Levich equation.

The value of the limit current depends on the number of electrons exchanged n, the Faraday constant F, the area of the electrode A, the concentration of the analyte C, the diffusion coefficient D, the kinematic viscosity of the medium v and the angular velocity of rotation of the electrode ω according to equation (45)

$$i_{limite} = 0{,}62nFAC\ D_0^{2/3}\ \omega^{1/2}\ v^{-1/6} \qquad (45)$$

Using the current density defined as the ratio between the current (i) and the electrode area (A), and grouping the constants of the previous equation within a term Kω we get (46):

$$j = \frac{i}{A} = nK_{\omega}\sqrt{\omega} \qquad (46)$$

where:

$$K_{\omega} = 0{,}62FCD^{2/3}v^{-1/6} \quad (cm^{-2}rad^{-1/2}s^{1/2})$$

Still it is convenient to express the rotation speed in revolutions (revolutions per minute) remembering that ω = 2πf / 60, where is the speed in revolutions by minute, the previous equation can be expressed in the form (47):

$$j = nK_{\omega}\sqrt{\frac{2\pi f}{60}} = nK_{\omega}\sqrt{\frac{\pi}{30}}\sqrt{f} \qquad (47)$$

And by grouping in a single constant we obtain the current density as a function of the rotation speed (48):

$$j = nK_f\sqrt{f} \qquad (48)$$

Where:

$$K_f = \sqrt{\frac{\pi}{30}}K_{\omega} \cong 0{,}3236K_{\omega} \quad (cm^{-2}\ rpm^{-1/2}\ min^{1/2})$$

Therefore, bringing in a graph J as a function of √f we obtain a straight line with angular coefficient m = n Kf, from the value of the angular coefficient and knowing the costline Kf it is possible to derive the number of electrons

involved in the electrochemical process. Kf can be calculated by knowing the values of concentration, diffusion coefficient and kinematic viscosity.

3.3.2 Koutecky-Levich Equation

By the Koutecky-Levich equation (49) the number of electrons involved in the redox reaction can also be calculated in the case in which the curve does not present the characteristic sigmoid form.

$$\frac{1}{i} = \frac{1}{i_{cc}} + \frac{1}{k_d\sqrt{\omega}} \qquad (49)$$

Where:

$$k_d = 0{,}62nFACD^{2/3}v^{-1/6}$$

While i_{cc} represents the current value that would be observed if mass transfer was so efficient as to maintain the concentration of the redox species on the electrode surface equal to the mass concentration value.
Using the current density and the number of revolutions per minute (instead of the angular velocity expressed in rad/s) we obtain the relation (50)

$$\frac{1}{j} = \frac{1}{j_{cc}} + \frac{1}{nK_f\sqrt{f}} \qquad (50)$$

With

$$K_f = 0{,}2FCD^{2/3}v^{-1/6}$$

Reporting in a graph 1/j against $1/f^{1/2}$ a series of points can be obtained whose interpolating straight line has as angular coefficient m=1/nKf and as a known term $q=1/J_{cc}$. From the angular coefficient and knowing K_f we can derive the number of electrons exchanged during the process (51):

$$n = \frac{1}{K_f m} \tag{51}$$

3.4 Hydrodynamic Voltammetry with rotating disk-ring electrode (RRDE)

The RRDE technique allows a more direct and complete study of the oxygen reduction reaction as it allows us to estimate both the reaction intermediates and the secondary products.

This rotating electrode hydrodynamic voltammetric technique involves the use of two working electrodes. A central disk and a concentric ring, separated by an insulating layer and mounted on the lower interface of a cylindrical support of inert material in which it has metal contacts and that is screwed to the rotation system. The disc and the ring act as separate working electrodes or a controlled potential is applied to each of them independently of each other (Fig. 3.15).

Fig. 3.15 Electrode that has a Glassy Carbon disc and a platinum ring

The rotation of the electrode causes the solution to drag towards the surface and the laminar motion in the vicinity of the electrode causes a tangential displacement, therefore the concentric geometry ensures that the electroactive species comes into contact with the primary electrode (the central one) and subsequently the products of the reaction are transported to the ring where a second redox reaction takes place, Fig. 3.16.

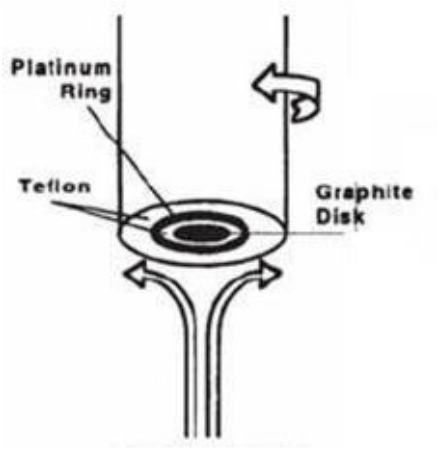

.

Fig. 3.16 Reagent flow on the electrode.

In the RRDE technique the disk current is the sum of all possible faradic currents that occur at that given potential. The electrode rotation causes the removal of the species produced after an electrochemical reaction from the disk to the ring. The latter is held to such a potential as to cause a preferential reaction (the opposite that occurs to the disc) of a single species, in such a way as to estimate the latter.

3.4.1 Study of the ORR by RRDE

The RRDE technique is used in the study of the oxygen reduction reaction where it allows to estimate the number of electrons exchanged and the quantities of water and hydrogen peroxide produced during the reaction.
Potential scanning takes place on the disk while the ring is set to a constant potential so that the oxygen reduction reaction (to give H_2O or H_2O_2) takes place on the disk and the oxidation of the oxygenated water is eventually present at the ring produced on the disc.
In the operating conditions the current measured at the disk I_d is given by the sum of all the charge transfer processes that take place in the working potential range, and therefore is (52):

$$I_D = I_{H2O2} + I_{H2O} \qquad (52)$$

By applying to the ring a potential which is the only oxidation of the hydrogen peroxide produced to the disc, the current recorded to the Ir ring where r stands for ring, is due to the fraction of hydrogen peroxide molecules that reach the disc from the disc ring (Fig. 3.17).

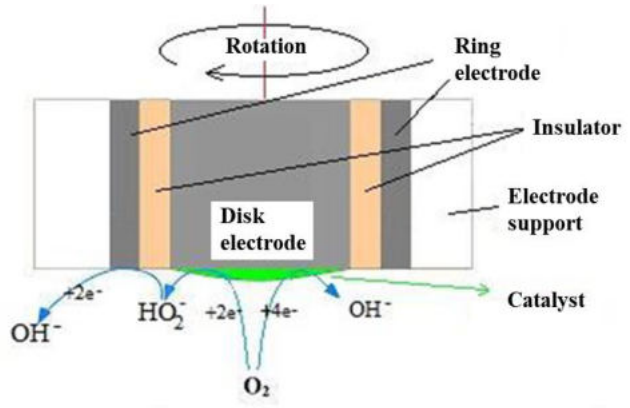

Fig. 3.17 Reactions that occur on the RRDE electrode

It is therefore necessary to introduce a term N (Collection Efficiency) defined as the fraction of matter that passes from the disk to the ring and that the ring manages to "capture". In fact, not all the molecules produced will be able to reach the ring. The theoretical value of this parameter depends on the geometry of the system and can be calculated by knowing the three rays of the electrodes used (disc radius, ring radius and teflon separator radius). The value must be between 0 and 1 and is generally between 0.2-0.3.

A further system for determining the value of N that can be obtained experimentally, by performing a potential scan of a solution containing a known redox pair (generally ferrocyanide / ferricyanide) and performing the ratio between the limit currents of the ring and of the disc (Ir / Id), as reported after.

The fraction of current measured at the disc due to the oxygen molecules reduced to H_2O_2 (I H_2O_2) will be given by the ratio between the current measured in the ring and N (53)

$$I\ H_2O_2 = Ir/N \quad (53)$$

The difference can therefore be obtained from the current due to the reduction of oxygen to water (54):

$$I\ H_2O = Id - I\ H_2O_2 \quad (54)$$

The disc currents that are reduction currents (cathodic) must be made positive.

The ratio between the total current measured on the disc and the number of electrons exchanged (n) must be equal to the sum of the currents caused by the reduction to water and hydrogen peroxide: (55)

$$\frac{I_d}{n} = \frac{I_{H_2O}}{4} + \frac{I_{H_2O_2}}{2} \quad (55)$$

By rearranging the terms one finds the formula for calculating electrons (56).

$$n = \frac{4I_d}{I_d + I_r/N} = \frac{4I_d}{I_d + I_{H_2O_2}} \quad (56)$$

3.4.1.1 Measurements in solution of potassium ferricyanide

Due to the complexity of the systems studied, the collection efficiency, N, was determined experimentally for each sample. For this purpose a cyclic voltammetry was carried out in solution of potassium ferricyanide 5 10^{-3} M in KCl 1 M bubbling an inert gas: N_2.

To prepare the electrolyte solution, appropriately calculated quantities of $K_4[Fe(CN)_6]$ at 99% (Carlo Erba) and KCl (WVR Chemicals) were dissolved in double distilled water and brought to a volume of 250 mL.
After filling the cell and deaerating the solution, a cyclic scan was performed at a speed of 5 mV/s in the potential range from -850 to 100 mV (vs Ag / AgCl in saturated KCl), keeping the working electrode in rotation at 1600 rpm and imposing a constant potential of 600 mV on the ring (vs Ag / AgCl in Saturated KCl).
Once all the operations were completed, the electrode was washed with ethanol to remove the analyzed ink.

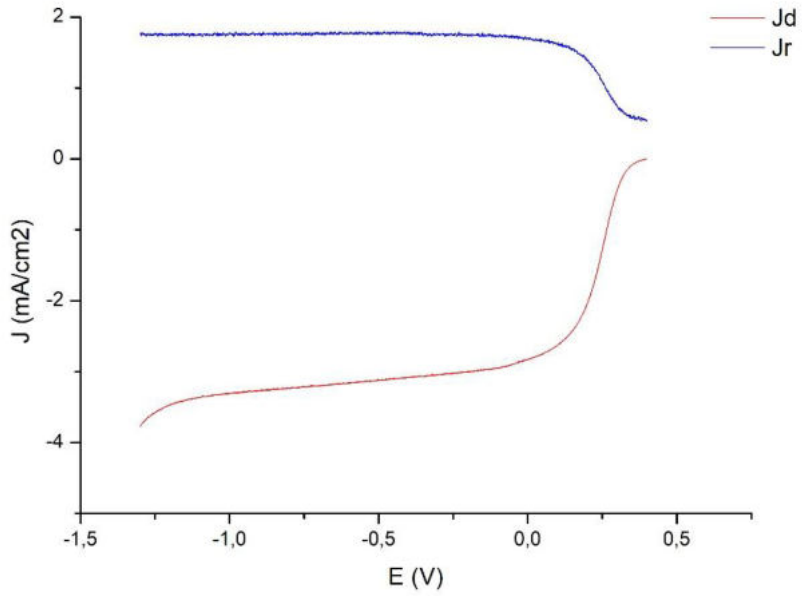

Fig. 3.18 Graph for the determination of N obtained by scanning in the potential range from -850 to 100 mV (vs Ag / AgCl in saturated KCl) at a

speed of 5 mV / s, imposing a potential of 600mV on the ring (vs Ag / AgCl in saturated KCl)

4. Experimental procedure

The experimental procedure allows to evaluate the efficiency of the catalysts. The operational phases carried out for each sample are reported in sequence below:

• Ink preparation

• Preparation of the electrolytic solution and deoxygenation by bubbling nitrogen (N_2)

• Checking the potential of the Ag / AgCl KCl sat reference electrode. + 0.199V vs RHE and preparation of the electrochemical cell

• Electrochemical cleaning of the electrodes

• Drop cast of ink on the surface of the Glassy Carbon disc

• Recording of a quiet cyclic voltammetry in a suitable potential window using the glassy carbon electrode as the main electrode and the platinum ring as a secondary electrode

• Recording of linear voltammeters at five different electrode rotation speeds (400, 800, 1200, 1600, 2000 rpm) using the same potential window

• Ventilation of the solution by bubbling oxygen stored in a cylinder until saturation

• Recording of a cyclic voltammetry

• Recording of the set of linear voltammeters at different rotation speeds

• Preparation of a solution of $K_3Fe(CN)_6$ and registration of linear voltammeters for the determination of Collection Efficiency (N).

4.1 Ink preparation and pre-analytical phases

For a visual observation the samples are presented in the form of dark coloured agglomerates. In order to be deposited on the surface of the

primary working electrode it is necessary to prepare an ink (ink). The preparation of the ink involves the direct weighing of an aliquot of catalyst and the subsequent addition of water, of a polymeric resin which serves to maintain the electrical contact between the catalyst and the surface of the electrode and of ethanol which acts as a solvent for the resin.

The four components are weighed in succession within the same glass vial to obtain the% composition shown in table 4.1. Approximately 2 mg of catalyst is weighed and the quantity in mg of the other necessary reagents is calculated based on the weighing carried out.

	% m/m composition inside the ink
Catalyst	2%
Water	52%
Ion exchange resin, Nafion®	20%
Ethanol	26%

Table 4.1 – Ink composition

The obtained dispersion must be sonicated (to facilitate the breaking of the catalyst lumps) until a homogeneous black ink is obtained in which the catalyst powders are no longer distinguishable. Generally sonification takes 20-30 minutes.

At the end of the sonification using a 10 μL micropipette, a drop of ink is deposited on the surface of the disk, making sure that it remains well confined inside it and does not expand by touching the ring (Fig. 4.1). The drop is allowed to dry for about 20 minutes and after the evaporation of the solvent the surface of the disc appears opaque and the presence of catalyst granules is noted.

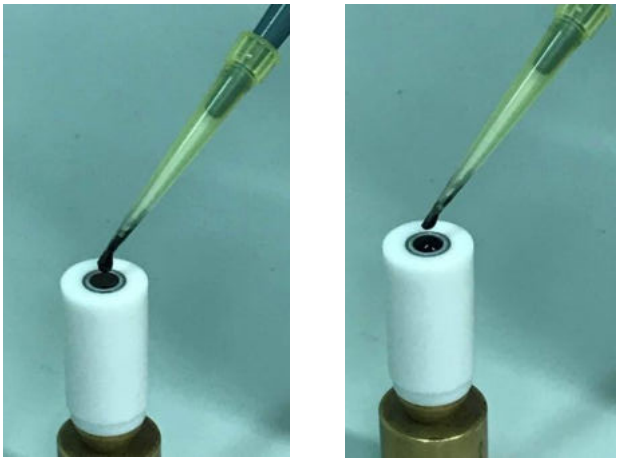

Fig. 4.1 Deposition of ink drop on the glassy carbon disc.

A 0.1M KOH solution is prepared and deoxygenated by bubbling nitrogen for about 20 minutes. The electrochemical cell consists of a glass cell with a central emery neck and side necks that can work with a three-electrode system: the rotating electrode (RRDE), the reference electrode and the counter electrode. There is also an entrance for bubbling the gaseous effluents (O2 and N2). Before starting the measurements, check that there are no air bubbles adhering to the surface of the electrodes.

4.2 Electrochemical Measurement Instrumentation

Table 4.1 summarize the instruments used in the following thesis work, while Figure 4.2 shows the scheme and the picture of complete system of work

Instrument/Component	**Model / Features**
Rotator System	Pine MSR Rotator System It consists of an electric motor that allows to control rotation speed with extreme precision

Roating electrode speed control	Pine Rotatin electrode speed control It allows manual and software adjustment of the electrode rotation speed.
Bi-Potentiostat	Autolab Metrohm potentiostat/galvanostat Instrument which, by means of a suitable internal circuit, is able to apply to the two independent potential electrodes (with respect to the reference electrode) and record the currents due to the electrochemical reaction on the electrodes. On the instrument there are the plugs to be connected respectively with counter electrode, reference electrode, rubbing contact of the disc, rubbing contact of the ring.
Working electrode *Ring / Disk electrodes*	E6 Series Pine Electrodes Flat electrodes characterized by the presence of a Pt ring and an internal glassy carbon disc. The surfaces of the two electrodes supplied by the manufacturer are shown Disk (GC) = 0.1963 cm^2 Ø 5mm Ring (Pt) = 0.11 cm^2
Software	Nova, Autolab Metrohm It allows control of both the potentiostat and the electrode rotation system
Reference electrode	Ag/AgCl/KCl sat. Potential of +197 mV compared to the hydrogen reference electrode (NHE)
Counter elettrode	Pt wire

Table 4.1 Equipment required

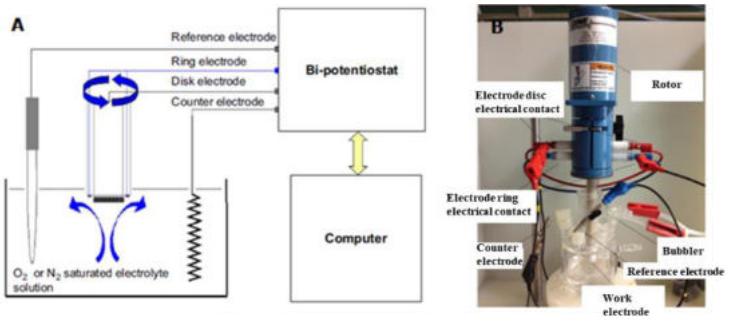

Fig. 4.2 Diagram (A) and picture (B) of the apparatus used for the measurements

Before depositing the catalyst on the surface of the Glassy Carbon disc it is good practice to clean the working electrodes. If the surfaces are particularly inactive it is necessary to carry out a physical treatment that involves a renewal of the surface by lapping: for about a minute the surface of the electrode is abraded on a rotating plate with a special cloth soaked in an aqueous dispersion of alumina particles (Buehler Micropolish II) having an average diameter of 1.0μm. The subsequent removal of alumina residues is carried out by sonication of the electrode in an ethanol solution.

For the electrochemical treatment the two working electrodes are raised to high potentials for small time intervals in order to oxidize the species adhering to the surfaces.

The activity of the platinum ring is evaluated by performing a cyclic voltammetry in an acid environment between 1.2V and -0.2V in which the characteristic trend reported in figure 4.3A must be obtained; in Alkaline solution a different trend is obtained, shown in figure 4.3B. If the traces are different, it is convenient to perform an electrochemical cleaning of the electrode, keeping it at a constant potential of + 2V for about two minutes.

Regarding the cleaning of the Glassy Carbon disc, the disc is connected as the primary working electrode and two / three cycles are performed which involve applying a potential of: + 1.5V then -0 to the electrode for a time of 2min. , 2V and then + 1.5V.

Once the components of the cell are mounted and the solution gurgling nitrogen is de-aired, the set of electrochemical measurements can be started. The platinum ring is used as the primary working electrode and a cyclic voltammetry is performed between + 0.6V towards -0.6V at the scanning speed of 100 mV / s, it is checked that the obtained voltammogram has the usual form 5.3 if this does not happen it is necessary to perform ring cleaning cycles according to the procedure indicated above.

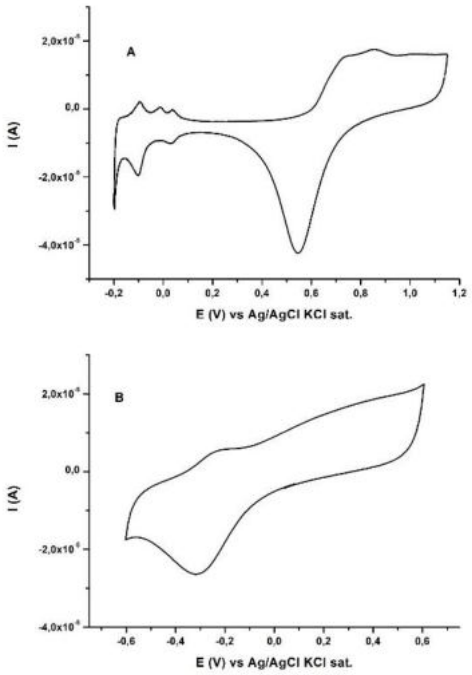

Fig. 4.3 Platinum disk voltammetry in deoxygenated solution A) acid H_2SO_4 1N, B) Basic KOH 1M, scanning speed 100 mV/s

Then the disc is connected as a primary working electrode and the ring as a secondary working electrode, then a cyclic voltammetry is performed at rest with the operating settings shown in table 5.2

Disc	Starting potential	+0,0V
	First vertex	-0,85V (start scanning proceeding to the left)
	Second vertex	+0,3V
	Final Potential	+0,0V vs OCP
	Scan rate	5 mV/s
Ring	Potential (Constant)	+0,6V

Table 4.2 CVs parameters

Five linear voltammeters are recorded at the electrode rotation speeds of 400, 800, 1200, 1600 and 2000 rpm with a scanning speed of 5mV / s according to the potentials shown in table 4.3.

Disc	Starting potential	+0,15V
	Final Potential	-0,85V
	Scan rate	5 mv/s
Anello	Potential (Constant)	+0,6V

Table 4.3 LSVs parameters

After blowing oxygen for about 20 minutes, saturating the solution, cyclic voltammetry is re-performed using the settings shown in table 4.2. The appearance of the oxygen reduction peak should be clear by comparing the disk CVs recorded in nitrogen and oxygen.

The linear scanning voltammeters of the oxygenated solution are performed at the different rotation speeds of the electrode as in table 4.3.

At the end of the measurements carried out on the oxygen reduction reaction, the experimental Efficiency Collection (N) evaluation is

performed using a 0.1M solution of $K_3Fe(CN)_6$. For electrodes used, the parent electrode provides a N value of 0.256. In the present work it is essential to obtain the value of N experimentally since the thin layer of catalyst deposited on the surface of the disk modifies the geometry of the system. Therefore linear voltammeters are performed in the potential range shown in table 4.4 at the different electrode rotation speeds (400, 800, 1200, 1600, 2000 rpm).

Disc	Starting potential	+0,15V
	Final Potential	-0,85V
	Scan rate	5 mv/s
Ring	Potential (Constant)	+0,6V

Table 4.4 LSVs Parameters for the $K_3Fe(CN)_6$ solution

5 Synthetic pathway sample

5.1 Carbon nanotubes

Carbon atoms can give rise to spherical structures called fullerenes which are considered an allotropic form of carbon and have a structure similar to graphite in that they consist of hexagonal rings joined together on a plane, but unlike graphite (which has structure planar) also have pentagonal rings that prevent flatness and favor a spherical folding. Following a rearrangement, the fullerenes can originate tubular structures called carbon nanotubes.

Carbon nanotubes are made up of graphite planes wrapped in a cylindrical shape, the lengths reach a few microns and the diameters at about 100 nm. Depending on the diameter and the arrangement of the hexagons, they can show remarkable electrical and structural properties, aimed at interesting applications in material sciences. Usually they form solid aggregates and are not soluble in water, unless they are functionalized with molecules and polar groups.

There are numerous types of carbon nanotubes but in general they can be classified into two categories (Fig. 5.1):

• Single-Walled Carbon Nano Tube (SWCNTs) or single-walled nanotube, they consist of a single sheet of graphite wrapped around itself to form a cylindrical structure;

• Multi-Walled Carbon Nano Tube (MWCNTs) or multi-walled nanotube, consisting of multiple sheets of graphite wrapped one on top of the other to form a "thick" cylindrical structure.

The central body of the nanotube is formed only by hexagons (such as graphite) while the curved ends representing the closing points of the nanotube (the caps) are formed by hexagons and pentagons (as in the fullerene). Carbon nanotubes show interesting chemical-physical properties, they can behave both as conductors and semiconductors (depending on the diameter and geometry) and are characterized by a strong mechanical resistance due to all the forces of cohesion of the structure. The electrical conductivity is graphitic and can occur both on the plane of the orbitals π and within the nano tube itself and in this case there is no heating effect following a current passage. Thanks to these properties the nanotubes are designed for the realization of microcircuits and in electrochemistry they can therefore function as electrodes or in any case they can be used to coat the surface of a conductor.

The versatility in the field of application of these nanomaterials is due to the possibility of functionalization, that is, it is possible to "cover" the surface of the nanotube with covalently linked molecules or functional groups or adsorbed through Van der Waals interactions. This functionalization modifies its characteristics and gives it peculiar properties. Therefore functionalised nanotubes can find applications in multiple scientific-technological fields.

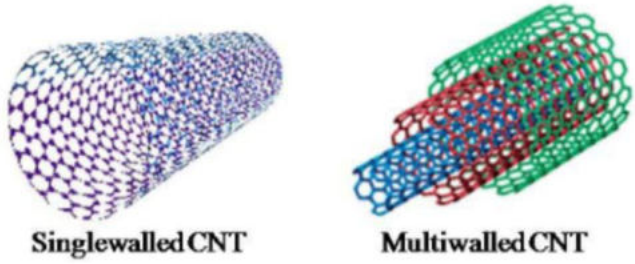

Fig. 5.1 Single-walled and multi-walled carbon nanotubes

5.2 Carbon nanotubes under study

In the present work of thesis, multi-walled carbon nanotubes (MWCNTs) functionalized with azamacrocyclic that complex inorganic cations were used. The adsorption of azamacrocyclic complexing agents on the graphitic surface allows to obtain active sites consisting of single metal ions and therefore a considerable saving in terms of the mass of precious metal used inside the catalyst (Fig.5.2).

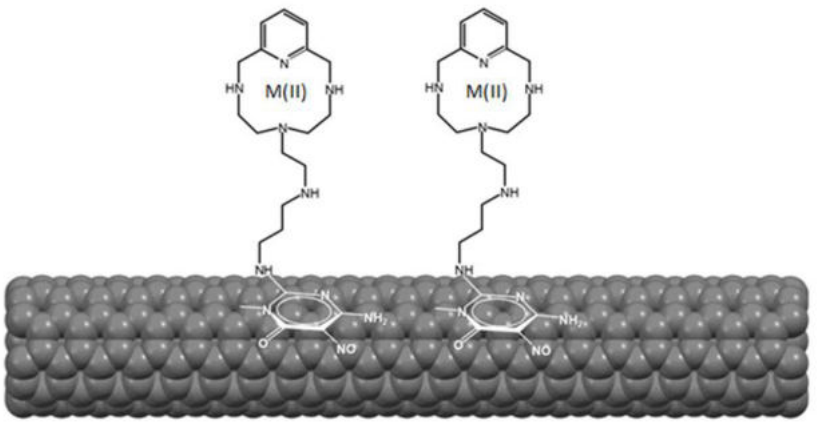

Fig.5.2 Azamacrocycle adsorbed on the surface of the carbon nanotube, a metal cation is complexed inside the terminal macrocycle.

5.3 Publication on Inorganic Chemistry acs

In this paragraph the work published in the scientific journal **Inorganic Chemistry is reported** entitled "Towards Supported Single-Ion Heterogeneous Catalysts: Pd (II) Complexes with High Efficiency in Oxygen Reduction Reaction in Alkaline Media". This work explains and summarizes (both in the main manuscript and in the information support) the entire study and research path, considering also the various steps, related to the functionalized MWCNTs samples **object of study**. As can be seen, the results obtained, in particular for the MWCNTs / HL2- (PdII) sample, are very interesting**. F**or this reason MWCNTs / HL2- (PdII) sample was chosen to use it as a cathodic catalyst in the assembly of a complete fuel cell test.

Inorganic Chemistry
Cite This: Inorg. Chem. 2018, 57, 14484−14488
Communication
pubs.acs.org/IC

MWCNTs-Supported Pd(II) Complexes with High Catalytic Efficiency in Oxygen Reduction Reaction in Alkaline Media

Maurizio Passaponti,[†,§] Matteo Savastano,[†,‡,§] M. Paz Clares,[⊥] Mario Inclán,[⊥] Alessandro Lavacchi,[∥] Antonio Bianchi,[*,†] Enrique García-España,[*,⊥] and Massimo Innocenti[*,†]

[†]Department of Chemistry "Ugo Schiff", University of Florence, via della Lastruccia 3, 50019 Sesto Fiorentino, Italy
[‡]CSGI, University of Florence, via della Lastruccia 3, 50019 Sesto Fiorentino, Italy
[⊥]Supramolecular Chemistry Group, Institute of Molecular Sciences, University of Valencia, 46980 Paterna, Spain
[∥]ICCOM-CNR, via Madonna del Piano 10, 50019 Sesto Fiorentino, Italy

Supporting Information

ABSTRACT: We report here the remarkable catalytic efficiency observed for two Pd(II) azamacrocyclic complexes supported on multiwalled carbon nanotubes (MWCNTs) toward oxygen reduction reactions. Beyond a main (>90%) 4e⁻ process and an onset potential close to or better than those of commercial Pt electrodes, the MWCNTs functionalization strategy, aimed at chemically defined Pd(II)-based catalytic centers, allowed the half-cell to exceed the proton-exchange-membrane fuel-cell reference/target mass activity efficiency set by the U.S. Department of Energy for 2020 (440 mA/mg_{PGM} at 0.9 V vs reversible hydrogen electrode).

Fuel cells are promising candidates for sustainable future energetic technology. Oxygen reduction reaction (ORR) allows the release of chemical energy stored in the vector molecule H_2 in the form of electrical work without producing any waste but innocuous H_2O molecules. For this reason, ORR is regarded as a highly strategic reaction, upon whose efficiency the near-future energy storage and powering technology depend.

The use of a cathode catalyst is mandatory to achieving a satisfying ORR conversion rate. Although many efforts have been made and several C-based nanomaterials have been assessed, Pt-based catalysts remain unchallenged as of today in terms of the produced current density (J), low onset potential (E_{on}), and avoidance of production of the reactive H_2O_2, rather favoring direct conversion to H_2O.[1] Because Pt and the so-called Pt group metals (PGMs) are rare and expensive—one of the key unsolved issues for the widespread use of fuel cells—much research effort has been oriented to reduce the required amount of metal to reach the desired performances.[2−6] As the useful timespan for the replacement of fossil fuels narrows, international protocols and agreements with specific objectives and deadlines are stipulated. The upcoming 2020 efficiency goal for fuel cells was expressed in this same spirit, i.e., in terms of mass activity, by the U.S. Department of Energy, requiring that a threshold current is produced per quantity of PGM under certain conditions [440 mA/mg_{PGM} at 0.9 V vs reversible hydrogen electrode (RHE)] in acidic media.[7]

Herein we report a hydrodynamic study on the half-cell, as is the best practice for benchmarking ORR catalyst performances,[8,9] conducted on two novel Pd(II)-based catalysts in alkaline solutions because Pt-free alkaline fuel cells were recently proven[10−12] to be efficient in delivering stable performances and a power density above 1 W/cm^2. One of our new catalysts exceeds the target mass activity value by over 10%, featuring an E_{on} value identical or better than that of a Pt electrode (0.91 V vs RHE) and an almost exclusive (96.5% at 0.9 V vs RHE) 4e⁻ process, i.e., selectively promoting the direct conversion of O_2 to H_2O (see Table 1). Such features were made possible by the supramolecular architecture of our supported catalysts, enabling homogeneous distribution on multiwalled carbon nanotubes (MWCNTs) of the Pd(II) complexes, without disrupting either the nanostructured nature of the substrate or its π-delocalized system.

Table 1. Catalytic Performances of Our Catalysts Immobilized in a Polymeric Film on a Glassy Carbon Electrode[a]

catalyst	E_{on}[b] (V)	n_e at +0.164 V[c] RRDE	n_e at +0.164 V[c] RDE (K-L[d])	mass activity[d] (mA/mg_{PGM})
MWCNT/HL1-Pd(II)	0.91	3.64	3.51 (R^2 =0.999)	173
MWCNT/HL2-Pd(II)	0.95	3.78	3.70 (R^2 =0.999)	493
Pt electrode	0.91		4.10 (R^2 =0.999)	

[a]The activity of a Pt electrode is reported as a reference. [b]Details on the E_{on} determination are given in Figure S1. [c]vs RHE. [d]Calculations provided in Table S1. [e]at 0.9 V vs RHE. [f]Koutechy−Levich plots provided in Figure S2.

The catalysts MWCNT/HL1-Pd(II) and MWCNT/HL2-Pd(II) evaluated in this work (Figure 1) were obtained through a supramolecular approach. High-purity (99.9% C) graphitized MWCNTs were chosen as substrates, both in view of the usefulness of nanostructured C in catalysis and for their unspoiled electrical properties.[13] Their noncovalent functional-

Received: September 21, 2018
Published: October 24, 2018

DOI: 10.1021/acs.inorgchem.8b02695
Inorg. Chem. 2018, 57, 14484−14488

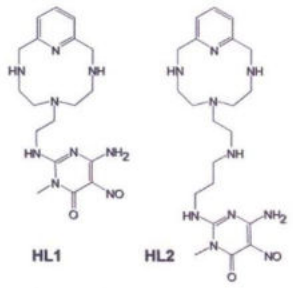

Figure 1. Ligands HL1 and HL2.

ization with either HL1 or HL2 (Figure 1) by spontaneous chemisorption in H_2O according to previously described procedures[14,15] afforded the MWCNT/HL1 and MWCNT/HL2 hybrid materials, without disrupting the delocalized π-electron systems of the CNTs. Adsorption of HL1, HL2, and analogous pyrimidine derivatives on graphitic surfaces from aqueous solutions was previously reported to happen mainly through the electron-deficient pyrimidine residue, rather than involving the protonated amine chain, as H_2O actively competes for the ammonium groups.[14−17] The adsorbed ligand amount is compatible with single-layer coverage [cf. the Supporting Information (SI), p S4], and multilayer adsorption is discarded according to previously reported ligand adsorption isotherms on MWCNTs, showing simple Langmuir-type adsorption behavior.[14]

Complexation of Pd(II) to the surface azamacrocyclic functionalities of these materials at pH 5.0 afforded the final catalysts MWCNT/HL1-Pd(II) and MWCNT/HL2-Pd(II), possessing a homogeneous distribution of discrete Pd(II) ions at the surface. Such complexes possess an activated position in the cation's first coordination sphere, consisting of an ancillary chloride ligand, as previously reported for analogous systems[14] and reverified in the present case through X-ray photoelectron spectroscopy (XPS; Figure S3) and scanning electron microscopy (SEM)−energy-dispersive spectroscopy (EDS) analysis (Figure S4). Characterization and stability of the complexes under ORR conditions (pH and potential range) are reported in the SI. Previous reports substantiated the tendency of HL1 to flatten on the CNT surface upon Pd(II) complexation [moving from MWCNT/HL1 to MWCNT/HL1-Pd(II) reduces the Brunauer−Emmett−Teller (BET) surface area], while this is not observed for HL2 (moving from MWCNT/HL2 to MWCNT/HL2-Pd(II) has almost no effect on the BET surface area). This was ascribed to both the higher loss of degrees of freedom required for folding of the longer spacer arm back onto the surface and its increased hydrophilicity due to protonation of the extra amino group (pK_a = 7.51(6); working pH 5.0).[14]

Samples were prepared according to the described methodologies.[14] Details of the catalyst preparation are given in the SI. The final Pd contents in the catalysts were assessed as 0.242 mmol of Pd/g of MWCNT/HL1 and 0.258 mmol of Pd/g of MWCNT/HL2.

The electrocatalytic performances of these catalysts toward ORR were evaluated in an alkaline aqueous solution (0.1 M KOH) by cyclic voltammetry (CV). Electrochemical measurements were performed using a three-electrode cell consisting of an Ag/AgCl/saturated KCl reference electrode, a Pt counter electrode, and either a rotating-disk electrode (RDE) or a rotating-ring-disk electrode (RRDE). Immobilization of the catalysts on the working electrode was achieved by preparing an ink for each functionalized sample, consisting of the Pd(II)-functionalized MWCNTs dispersed in a polymeric membrane (Nafion), which was then cast onto a rotating glassy carbon (GC) electrode. Samples were prepared according to reported procedures:[18] a detailed description is available in the SI. A commercial Metrohm Pt polycrystalline electrode (⌀ 3 mm) was employed to benchmark the performances of our catalysts.

Figure 2 shows the ORR polarization curves recorded at 1600 rpm for each sample at a potential scan rate of 5 mV/s. The

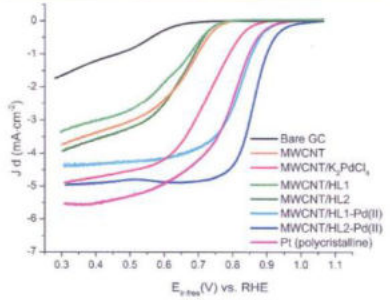

Figure 2. RRDE disk currents showing the ORR activities of the investigated catalysts. Rotation rate: 1600 rpm. Scan rate: 5 mV/s.

polarization curves for the bare GC electrode, as well as for the GC electrode functionalized with the same strategy with pristine MWCNTs, MWCNT/HL1, MWCNT/HL2, and MWCNT/K_2PdCl_4, are also reported. Relevant data on each electrode performance are given in Table S2. The preparation and characterization of MWCNT/K_2PdCl_4, where Pd species are directly adsorbed on MWCNTs because of Cπ−dπ interactions,[19] are provided in the SI. During the RRDE CV measurements, the Pt ring electrode was held at a potential of +0.50 V vs Ag/AgCl/saturated KCl to ensure the complete oxidation of H_2O_2 eventually produced at the sample−GC disk electrode. All electrochemical profiles and background currents (under N_2-saturated conditions) are subtracted from the respective curves to remove capacitive contributions (Figure S5). The catalytic activities, in terms of both E_{on} and current values, increase depending on the catalyst nature in the order: bare GC < pristine MWCNTs ≈ MWCNT/HL1 ≈ MWCNT/HL2 < MWCNT/K_2PdCl_4 < MWCNT/HL1-Pd(II) < MWCNT/HL2-Pd(II). This rules out significant catalytic properties of the substrate and CNT-supported ligands in our case, while it highlights the prominent role of Pd(II) and the ligands in enhancing their catalytic activities. Table S2 collects the electrochemical parameters for all systems.

As displayed in Figure 2, the E_{on} values observed for the MWCNT/HL1-Pd(II) and MWCNT/HL2-Pd(II) catalysts are very close to the benchmark values determined in the same conditions with a commercial Pt working electrode. Data in

DOI: 10.1021/acs.inorgchem.8b02695
Inorg. Chem. 2018, 57, 14484−14488

Table 1 reveal that, in the case of MWCNT/HL2-Pd(II), the E_{on} value is even better (i.e., more positive) than that observed for the Pt electrode.

The number of exchanged electrons per O_2 molecule is invariably very close to 4, signifying an almost exclusive conversion of O_2 into H_2O. Interestingly, very close values are found by either direct evaluation with RRDE or extrapolation of RDE polarization curves through the Koutechy−Levich (K.L.) equation[20−22] (Table 1). For this purpose, ORR polarization curves were recorded from 400 to 2000 rpm (step of 400 rpm) with a potential scan rate of 20 mV/s (Figure S6). Sample linear-sweep voltammograms at different scan rates (200 mV/s) are reported in Figure S7. Close convergence of the RRDE and K.L. extrapolated data for exchanged electron number suggests high homogeneity of the electrode surface. SEM images of the electrode surface are displayed in Figure S8. Measured ring and disk currents for MWCNT/HL2 at the suggested potential of 0.9 V vs RHE demonstrate that, under the said conditions, the direct conversion to H_2O efficiency increases, reaching 96.5%; the full dependence of ne^- versus voltage for Pd-containing catalysts is presented in Figure S9.

With regard to the mass activity, both catalysts show satisfactory results, with MWCNT/HL1-Pd(II) reaching 173 mA/mgPd and MWCNT/HL2-Pd(II) scoring 493 mA/mgPd (Table 1).

Although other strategies based on Pd species are reported, involving either metallic thin-film electrodes[23] or Pd(0) nanoparticles (NPs) immobilized onto heteroatom-doped C surfaces,[24−27] this feat of the mass activity was only made possible by the careful design of catalysts to achieve supported discrete ions. As pointed out elsewhere,[28] single-atom catalysts would be the ultimate way of maximizing the mass/atom activity of PGM metals. Moving from randomly doped systems to supported discrete macrocyclic complexes with a well-defined chemical identity is a mandatory step in that direction.

XPS spectra of the as-prepared catalysts, reported in Figure 3a, show that all Pd ions are present as a Pd(II) complex. Ink preparation and subsequent ORR assays do not tamper much with the nanostructure of the catalyst, as proven by the complete preservation of features in the C 1s region. Pd does not change its oxidation number upon use of the catalysts; i.e., all Pd ions remain as Pd(II). After use, new small peaks appear (Figure 3b), which do not change during at least 1000 cycles (Figure S11) and are consistent with the formation of either PdO[29] or clusters of Pd with surface oxy/hydroxyl groups[20] (Figure 3), while most of the metal is still bound to the ligand, demonstrating that we really are in the presence of Pd(II)-complex active sites. Indeed, among the many TEM images aquired, only few (Figure S10) show the presence of tiny localized traces of NPs, which cannot justify the observed activity. Also, the slight shift in the binding energy of the Pd 3d signal and the lack of a chlorine peak in the used catalysts suggest that the original ancillary chloride ligand was shed in favor of a hydroxide anion. Binding and activation (i.e., for proton exchange) of such H_2O-related species under the reversible conditions granted by the strong binding to a tridentate azamacrocycle are probably the key mechanisms subtending to the observed catalytic activity of these Pd(II) complexes.

According to characterization of the as-prepared and after-use catalysts, we cannot detect any major differences between MWCNTs/HL1-Pd(II) and MWCNTs/HL2-Pd(II) in either the overall composition, metal oxidation state, or Pd(II) coordination environment. For these reasons, we are led to

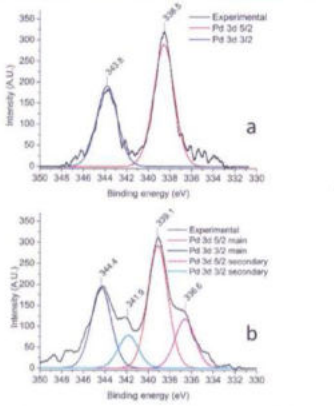

Figure 3. High-resolution XPS spectra in the Pd 3d region of (a) the as-prepared MWCNT/HL2-Pd(II) catalyst and (b) the MWCNT/HL2-Pd(II) GC electrode after use (1 CV from +0.1 to −0.85 V vs Ag/AgCl/saturated KCl).

think that the longer spacer of HL2, protruding from the MWCNTs surface, either produces a brushlike arrangement of the catalytic sites, better suited for capturing gaseous reagents from the solution, or promotes a cooperative mechanism involving two neighboring Pd(II) centers.

The stability of the catalysts has also been addressed. Concerning Pd leakage, SEM−EDS analysis of the fresh and after-use (1000 cycles) MWCNT/HL2 catalysts show the same percent abundance of Pd in both samples (Figure S4). The presence of Pd in the electrolyte solution was also checked by inductively coupled plasma mass spectrometry after 1000 CV scans, revealing no traces of the metal. Preliminary data indicate that our most promising catalyst, MWCNT/HL2-Pd(II), is able to maintain its performances over time, with no bias observed for the produced current density or exchanged electron numbers per O_2 molecule over a 1.5 h test in galvanostatic operating conditions (i.e., simulating a working fuel cell) at −0.80 V vs Ag/AgCl/saturated KCl (Figure S12). Moreover, catalytic performances are also maintained over 1000 CV scans at 200 mV/s (Figure S13). Nevertheless, further investigation is needed to evaluate the long-term stability of the catalyst for fuel-cell applications.

In conclusion, herein we reported novel Pd(II) catalysts for ORR, one of which exhibits a half-cell PGM mass activity exceeding state-of-the-art reference goals. Both systems feature E_{on} values comparable or better than those of a commercial Pt electrode and a predominating (90% or above; cf. Figure S9) $4e^-$ process, leading to the direct production of H_2O. Furthermore, we demonstrated that beyond Pd(0) species, also Pd(II) complexes are feasible as active sites for ORR catalysts. Taking for granted that the working mechanism will be the object of upcoming studies, its understanding, together with the good stability displayed by the developed catalysts, foreshadows their rapid placement in practice and evaluation in a complete fuel cell. For the reasons above, we strongly believe that these

DOI: 10.1021/acs.inorgchem.8b02695
Inorg. Chem. 2018, 57, 14484−14488

findings will prompt further studies and developments toward affordable cost-effective solutions for the renewable energetic technology of the immediate future.

■ ASSOCIATED CONTENT

Supporting Information

The Supporting Information is available free of charge on the ACS Publications website at DOI: 10.1021/acs.inorgchem.8b02695.

Synthetic procedures, preparation of modified electrodes, details of the mass activity calculation, details and definition of the electrochemical measurements and stability tests, SEM−EDS and XPS analyses of MWCNT/HL2-Pd(II) as-prepared and after use, still CVs in KOH 0.1 M solutions saturated with N_2/O_2 for both catalysts, linear-sweep voltammograms at different spin rates at a 20 mV/s scan rate for both catalysts, K.L. plots at −0.80 V versus Ag/AgCl/saturated KCl, and TEM images of after-use MWCNT/HL2-Pd(II) (PDF)

■ AUTHOR INFORMATION

Corresponding Authors

*E-mail: antonio.bianchi@unifi.it.
*E-mail: enrique.garcia-es@uv.es.
*E-mail: m.innocenti@unifi.it.

ORCID

Antonio Bianchi: 0000-0002-1082-3911
Enrique García-España: 0000-0002-4601-6505

Author Contributions

§M.P. and M.S. contributed equally.

Notes

The authors declare no competing financial interest.

■ ACKNOWLEDGMENTS

Financial support from the Italian MIUR (Project 2015MP34H3), Spanish Ministerio de Economia y Competitividad (Projects CTQ2016-78499-C6-1-R and Unidad de Excelencia MDM 2015-0038), and Generalitat Valenciana (Project PROMETEOII2015-002) is gratefully acknowledged.

■ REFERENCES

(1) Morozan, A.; Jousselme, B.; Palacin, S. Low-platinum and platinum-free catalysts for the oxygen reduction reaction at fuel cell cathodes. *Energy Environ. Sci.* **2011**, *4*, 1238−1254.

(2) Zheng, Y.; Jiao, Y.; Jaroniec, M.; Jin, Y. G.; Qiao, S. Z. Nanostructured metal-free electrochemical catalysts for highly efficient oxygen reduction. *Small* **2012**, *8*, 3550−3566.

(3) Zhu, C. Z.; Dong, S. J. Recent progress in graphene-based nanomaterials as advanced electrocatalysts towards oxygen reduction reaction. *Nanoscale* **2013**, *5*, 1753−1767.

(4) Wang, D.-W.; Su, D. Heterogeneous nanocarbon materials for oxygen reduction reaction. *Energy Environ. Sci.* **2014**, *7*, 576−591.

(5) Yu, D.; Nagelli, E.; Du, F.; Dai, L. Metal-Free Carbon Nanomaterials Become More Active than Metal Catalysts and Last Longer. *J. Phys. Chem. Lett.* **2010**, *1*, 2165−2173.

(6) Song, C.; Zhang, J. Electrocatalytic Oxygen Reduction Reaction. In *PEM Fuel Cell Electrocatalysts and Catalyst Layers: Fundamentals and Applications*; Zhang, J., Ed.; Springer: New York, 2008; pp 89−134.

(7) U.S. Department of Energy. *Office of Energy Efficiency and Renewable Energy*, https://www.energy.gov/eere/fuelcells/doe-technical-targets-polymer-electrolyte-membrane-fuel-cell-components.

(8) Kocha, S. S.; Shinozaki, K.; Zack, J. W.; Myers, D. J.; Kariuki, N. N.; Nowicki, T.; Stamenkovic, V.; Kang, Y.; Li, D.; Papageorgopoulos, D. Best Practices and Testing Protocols for Benchmarking ORR Activities of Fuel Cell Electrocatalysts Using Rotating Disk Electrode. *Electrocatalysis* **2017**, *8* (4), 366−374.

(9) Shao, M.; Chang, Q.; Dodelet, J.-P.; Chenitz, R. Recent Advances in Electrocatalysts for Oxygen Reduction Reaction. *Chem. Rev.* **2016**, *116* (6), 3594−3657.

(10) Wang, L.; Bellini, M.; Miller, H. A.; Varcoe, J. R. A high conductivity ultrathin anion-exchange membrane with 500+ h alkali stability for use in alkaline membrane fuel cells that can achieve 2 W cm^{-2} at 80 °C. *J. Mater. Chem. A* **2018**, *6*, 15404−15412.

(11) Omasta, T. J.; Peng, X.; Miller, H. A.; Vizza, F.; Wang, L.; Varcoe, J. R.; Dekel, D. R.; Mustain, W. E. Beyond 1.0 W cm^{-2} Performance without Platinum: The Beginning of a New Era in Anion Exchange Membrane Fuel Cells. *J. Electrochem. Soc.* **2018**, *165*, J3039−J3044.

(12) Miller, H. A.; Lavacchi, A.; Vizza, F.; Marelli, M.; Di Benedetto, F.; D'Acapito, F.; Paska, Y.; Page, P.; Dekel, D. R. A Pd/C-CeO_2 Anode Catalyst for High-Performance Platinum-Free Anion Exchange Membrane Fuel Cells. *Angew. Chem., Int. Ed.* **2016**, *55*, 6004−6007.

(13) Serp, P.; Machado, B.; *Nanostructured Carbon Materials for Catalysis*; RSC Catalysis Series 23; The Royal Society of Chemistry: Cambridge, U.K., 2015; Chapter 7, pp 370−375.

(14) Savastano, M.; Arranz-Mascarós, P.; Bazzicalupi, C.; Clares, M. P.; Godino-Salido, M. L.; Gutiérrez-Valero, M. D.; Inclán, M.; Bianchi, A.; García-España, E.; López-Garzón, R. Construction of green nanostructured heterogeneous catalysts via non-covalent surface decoration of multi-walled carbon nanotubes with Pd(II) complexes of azamacrocycles. *J. Catal.* **2017**, *353*, 239−249.

(15) Savastano, M.; Arranz-Mascarós, P.; Bazzicalupi, C.; Clares, M. P.; Godino-Salido, M. L.; Guijarro, L.; Gutiérrez-Valero, M. D.; Bianchi, A.; García-Espana, E.; López-Garzón, R. Polyfunctional Tetraaza-Macrocyclic Ligands: Zn(II), Cu(II) Binding and Formation of Hybrid Materials with Multiwalled Carbon Nanotubes. *ACS Omega* **2017**, *2* (7), 3868−3877.

(16) López-Garzón, R.; Godino-Salido, M. L.; Gutiérrez-Valero, M. D.; Arranz-Mascarós, P.; Melguizo, M.; García, C.; Domingo-García, M.; López-Garzón, F. J. Supramolecular assembling of molecular ion-ligands on graphite-based solid materials directed to specific binding of metal ions. *Inorg. Chim. Acta* **2014**, *417*, 208−221.

(17) Godino-Salido, M. L.; López-Garzón, R.; Gutiérrez-Valero, M. D.; Arranz-Mascarós, P.; Melguizo-Guijarro, M.; López de la Torre, M. D.; Gómez-Serrano, V.; Alexandre-Franco, M.; Lozano-Castelló, D.; Cazorla-Amorós, D.; Domingo-García, M. Effect of the surface chemical groups of activated carbons on their surface adsorptivity to aromatic adsorbates based on π-π interactions. *Mater. Chem. Phys.* **2014**, *143* (3), 1489−1499.

(18) Miller, H. A.; Bellini, M.; Oberhauser, W.; Deng, X.; Chen, H.; He, Q.; Passaponti, M.; Innocenti, M.; Yang, R.; Sun, F.; Jiang, Z.; Vizza, F. Heat treated carbon supported iron(ii)phthalocyanine oxygen reduction catalysts: elucidation of the structure-activity relationship using X-ray absorption spectroscopy. *Phys. Chem. Chem. Phys.* **2016**, *18*, 33142−33151.

(19) Savastano, M.; Arranz-Mascarós, P.; Bazzicalupi, C.; Bianchi, A.; Giorgi, C.; Godino-Salido, M. L.; Gutiérrez-Valero, M. D.; López-Garzón, R. Binding and removal of octahedral, tetrahedral, square planar and linear anions in water by means of activated carbon functionalized with a pyrimidine-based anion receptor. *RSC Adv.* **2014**, *4*, 58505−58513.

(20) Arrigo, R.; Schuster, M. E.; Xie, Z.; Yi, Y.; Wowsnick, G.; Sun, L. L.; Hermann, K. E.; Friedrich, M.; Kast, P.; Havecker, M.; Knop-Gericke, A.; Schlogl, R. Nature of the N−Pd Interaction in Nitrogen-Doped Carbon Nanotube Catalysts. *ACS Catal.* **2015**, *5*, 2740−2753.

(21) Wang, Y.; Zhang, D.; Liu, H. A study of the catalysis of cobalt hydroxide towards the oxygen reduction in alkaline media. *J. Power Sources* **2010**, *195*, 3135−3139.

(22) Teschner, D.; Vass, E.; Havecker, M.; Zafeiratos, S.; Schnorch, P.; Sauer, H.; Knop-Gericke, A.; Schlogl, R.; Chamam, M.; Wootsch, A.

DOI: 10.1021/acs.inorgchem.8b02695
Inorg. Chem. 2018, 57, 14484−14488

Alkyne hydrogenation over Pd catalysts: A new paradigm. *J. Catal.* **2006**, *242*, 26−37.
(23) Tsui, L.; Zafferoni, C.; Lavacchi, A.; Innocenti, M.; Vizza, F.; Zangari, G. Electrocatalytic activity and operational stability of electrodeposited Pd−Co films towards ethanol oxidation in alkaline electrolytes. *J. Power Sources* **2015**, *293*, 815−822.
(24) Arrigo, R.; Wrabetz, S.; Schuster, M. E.; Wang, D.; Villa, A.; Rosenthal, D.; Girsgdies, F.; Weinberg, G.; Prati, L.; Schlogl, R.; Su, D. S. Tailoring the morphology of Pd nanoparticles on CNTs by nitrogen and oxygen functionalization. *Phys. Chem. Chem. Phys.* **2012**, *14*, 10523−10532.
(25) Arrigo, R.; Schuster, M. E.; Abate, S.; Wrabetz, W.; Amakawa, K.; Teschner, D.; Freni, M.; Centi, G.; Perathoner, S.; Havecker, M.; Schlogl, R. Dynamics of palladium on nanocarbon in the direct synthesis of H_2O_2. *ChemSusChem* **2014**, *7*, 179−194.
(26) Bard, A. J.; Faulkner, L. R. *Electrochemical Methods: Fundamentals and Applications*, 2nd ed.; John Wiley & Sons, Inc.: New York, 2001; p 856.
(27) Wang, L.; Lavacchi, A.; Bevilacqua, M.; Bellini, M.; Fornasiero, P.; Filippi, J.; Innocenti, M.; Marchionni, A.; Miller, H. A.; Vizza, F. Energy Efficiency of Alkaline Direct Ethanol Fuel Cells Employing Nanostructured Palladium Electrocatalysts. *ChemCatChem* **2015**, *7*, 2214−2221.
(28) Liu, J. Catalysis by Supported Single Metal Atoms. *ACS Catal.* **2017**, *7* (1), 34−59.
(29) Wu, Q.; Rao, Z.; Yuan, L.; Jiang, L.; Sun, G.; Ruan, J.; Zhou, Z.; Sang, S. Carbon supported PdO with improved activity and stability for oxygen reduction reaction in alkaline solution *Electrochim. Electrochim. Acta* **2014**, *150*, 157−166.

DOI: 10.1021/acs.inorgchem.8b02695
Inorg. Chem. 2018, 57, 14484−14488

Supplementary Material for

MWCNTs-Supported Pd(II) Complexes with High Catalytic Efficiency in Oxygen Reduction Reaction in Alkaline Media.

Maurizio Passaponti,[a‡] Matteo Savastano,[a,b‡] M.Paz Clares,[c] Mario Inclán,[c] Alessandro Lavacchi,[d] Antonio Bianchi,[a*] Enrique García-España[c*] and Massimo Innocenti.[a*]

[a] Department of Chemistry "Ugo Schiff", University of Florence, via della Lastruccia 3, 50019 Sesto Fiorentino, Italy.

[b] CSGI, University of Florence, via della Lastruccia 3, 50019 Sesto Fiorentino, Italy.

[c] Supramolecular Chemistry Group, Institute of Molecular Sciences, University of Valencia, 46980 Paterna, Spain.

[d] ICCOM-CNR, via Madonna del Piano 10, 50019 Sesto Fiorentino, Italy.

Contents

Synthetic procedures

Synthesis of HL1 and HL2

The synthesis of HL1 (HL1·0.5MeOH·H_2O) and HL2 (HL2·MeOH·H_2O) was previously performed.[1]

Synthesis of (PdHL1)Cl_2

K_2PdCl_4 (37.5 mg, 0.115 mmol) dissolved in 0.5 cm^3 of water was added to a boiling solution of HL1·0.5MeOH·H_2O (50 mg, 0.115 mmol) in 20 cm^3 of an acetone/ethanol 1:1 (v:v) mixture. The purple ligand solution turned orange. This solution was evaporated almost to dryness and successively diluted with 10 cm^3 of hot ethanol. The procedure (evaporation/ethanol addition) was repeated three times, until the solution became opalescent. Precipitation of the complex as fine powder occurred while maintaining the solution at room temperature overnight. The solid complex was filtered, washed with ethanol and dried in vacuum at 35 °C (42 mg, 0.073 mmol, 63%). Elem. anal. Calcd for $C_{18}H_{27}N_9O_2PdCl_2$: C, 37.35; H, 4.70; N, 21.78. Found: C, 37.05; H, 4.81; N, 21.64. ^1H NMR (400 MHz, D_2O, pH 7, 298 K): δ 8.00 (t, 1H), 7.50 (d, 2H), 4.79 (s, 4H), 3.50-2.60 (m, 15H). UV-vis spectra of the complex (5×10^{-4} M) at different pH values are reported in the following figure. Stability of the complex was verified by periodical recording of these spectra: no changes were observed during 20 days.

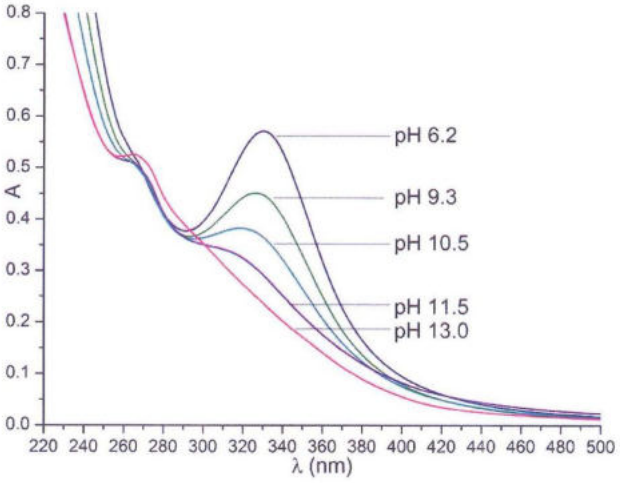

S2

Synthesis of (PdHL2)Cl_2

The synthesis of this complex was performed, by adopting the procedure above described for (PdHL1)Cl_2, from K_2PdCl_4 (32 mg, 0.098 mmol) and HL2·MeOH·H_2O (50 mg, 0.098 mmol). Yield: 45 mg, 0.071 mmol, 72%. Elem. anal. Calcd for $C_{21}H_{34}N_{10}O_2PdCl_2$: C, 39.67; H, 5.39; N, 22.03. Found: C, 39.46; H, 5.48; N, 21.88. ^{1}H NMR (400 MHz, D_2O, pH 5, 298 K): δ 8.03 (t, 1H), 7.52 (d, 2H),4.70 (s, 4H), 3.85 (t, 2H), 3.35-2.99 (m, 17H), 2.16 (q, 2H). UV-vis spectra of the complex (5×10^{-4} M) at different pH values are reported in the following figure. Stability of the complex was verified by periodical recording of these spectra: no changes were observed during 20 days.

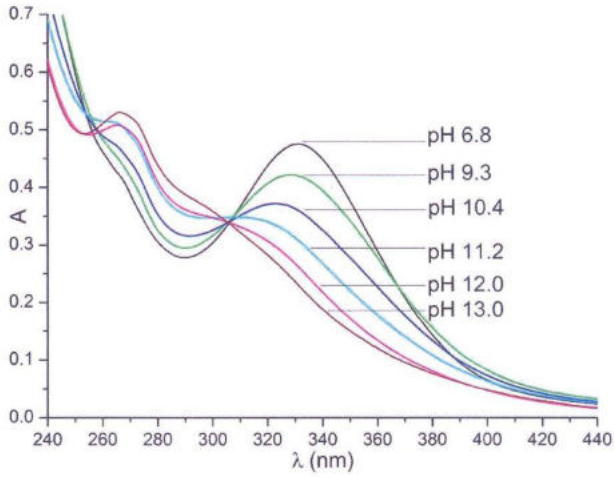

S3

Preparation of MWCNT/HL1-Pd(II) and MWCNT/HL2-Pd(II)

Functionalization of MWCNTs with HL1-Pd(II) and HL2-Pd(II) complexes was performed according to previously described procedures.[1] The main difference between literature data and the current study is the choice of the graphitic support: instead of the already reported Thin MWCNTs (Nanocyl, Ref 3100, Spain, with metal ox-ides content $\leq 5\%$)[1-2] we opted for an even less functionalized substrate, hoping that an unsoiled sp^2 network would help electron transfer processes; for this reason, we employed graphitized MWCNT (outer diameter 8-15 nm, inner diameter 3-5 nm) with a minimum C content of 99.9%, which were purchased from Nanostructured & Amorphous Materials, Inc. (Houston, TX 77084, USA) and used as received. Chemisorption of HL1 and HL2 ligands was performed as already described, suspending a weighted amount of MWCNTs in mM aqueous solutions of the ligands at pH 7.5 maintaining a 1 mg(MWCNTs)/1 ml(solution) ratio. The dispersions were equilibrated for 3 days in a thermostated shaker at 298.1 K. The amount of adsorbed ligands was then evaluated by UV-Vis absorption. The resulting MWCNT/HL1 and MWCNT/HL2 hybrid materials were recovered by filtration, carefully washed with distilled water and dried in vacuum at constant weight. Ligands desorption has been performed in the same way by re-suspending the materials in pure water at pH 5.0 (the value at which Pd(II) adsorption is performed, see below) to eliminate HL1 and HL2 molecules retained in a non-specific way or non-properly adsorbed on the surface. The amount of desorbed ligands was again quantified by UV-Vis measurements. The resulting MWCNT/HL1 and MWCNT/HL2 materials were then recovered once more by filtration and dried to constant weight. The final amount of adsorbed ligands was found to be 0.211 mmol/g(MWCNT) and 0.330 mmol/g(MWCNT) for HL1 and HL2 respectively.

Pd(II) adsorption on the resulting MWCNT/HL1 and MWCNT/HL2 materials was performed by suspending the hybrid materials in 5 10^{-4} M solution of K_2PdCl_4, working at pH 5.0 and in the presence of 1 M KCl to avoid the hydrolysis of the metal. Visible adsorption of the solution was monitored until the completion of the adsorption (4 days). The resulting MWCNT/HL1-Pd(II) and MWCNT/HL2-Pd(II) hybrid materials were once more recovered by filtration and dried in vacuum to constant weight. The final amount of adsorbed Pd(II) were found as follows: 0.242 mmol(Pd)/ g(MWCNT/HL1) and 0.258 mmol(Pd)/ g(MWCNT-HL2). Surface coverage is 1.1 complexes per nm^2 for MWCNT/HL1-Pd(II) and 1.7 complexes per nm^2 for MWCNT/HL2-Pd(II). Calculated size of molecular boxes large enough to accommodate the ligands in optimized conformation were previously reported.[1]

Elem. anal. Calcd for MWCNT/HL1-Pd(II) (as defined above): C, 92.43; H, 0.51; N, 2.35. Found: C, 92.17; H 0.58; N, 2.43.

Elem. anal. Calcd for MWCNT/HL2-Pd(II) (as defined above): C, 90.25; H, 0.91; N, 3.83. Found: C, 90.41; H 1.02; N, 3.91.

Preparation of MWCNTs/K_2PdCl_4

Functionalization of MWCNTs with K_2PdCl_4 was performed repeating the Pd(II) functionalization step as described above. Rather than a metal coordination on defective sites, which should be rather insignificant on graphitized 99.9% C MWCNTs, most of the adsorption is thought to happen mainly due to Cπ-dπ interactions.[3] According to the weaker nature of such forces compared to coordinative bonds, the amount of adsorbed Pd species is found considerably lower, namely 0.044 mmol of Pd(II)/ g(MWCNTs), i.e. almost 6 times less than in the presence of ligands.

Table S1. Details of Mass Activity Calculation.†

Sample	% w/w Pd (MWCNTs)	mg Pd (Ink)	mg Pd (Drop)	J (0.9 vs RHE) (mA cm^{-2})	Mass Activity (0.9 vs RHE) (mA $cm^{-2}mg_{Pd}^{-1}$)
MWCNT/HL1-Pd(II)	2.47	0.049	$1.48\ 10^{-3}$	0.257	**173**
MWCNT/HL2-Pd(II)	2.63	0.052	$1.57\ 10^{-3}$	0.774	**493**

†w/w % of Pd in the MWCNT/HL1-Pd(II) and MWCNT/HL2-Pd(II) catalysts is calculated as follows. The determined mmol(Pd)/g (MWCNT/ligand) are converted into a weight increase assuming that all Pd(II) is adsorbed as $PdCl_2$, since no other possible counteranions are expected to be present in a 1 M Cl^- aqueous solution at pH 5.0 (hydroxide being ruled out due to pH; also said conditions, ionic strength and pH, were selected according to literature thermodynamic data to avoid the hydrolysis of $PdCl_4^-$ entirely), and drying procedure to constant weight is performed thoroughly.

If one assumes to be working on 1.0 g of MWCNT/ligand hybrid material, the total mass of MWCNT/ligand/Pd (i.e. after metal adsorption) can be easily calculated by adding the mass of the determined mmol(Pd)*F.W.($PdCl_2$). The w/w % of metal is then calculated by dividing the mass of Pd (as mmol(Pd)*A.W.(Pd)) and dividing for the total weight of the system (1.0 g of MWCNT/ligand plus the mass of adsorbed $PdCl_2$). Please note that in the presence of additional adsorbates (like residual water molecules), this would overestimate the real w/w % of Pd: this would ultimately reflect itself in an underestimation of the mass activity, so systematic errors, if any, would produce an improvement of the reported mass activity results.

mg of Pd in the ink and on the drop-casted electrode are calculated according to the dilution and methodologies described in the Preparation of modified electrode section (e.g. accounting for the fact that the ink is 2% w/w in the MWCNT-supported catalyst, et. cetera).

Finally, mass activity has been calculated by dividing the current density for the total amount (in mg) of Pd.

S7

Table S2. Synoptic view of determined $E_{1/2}$ and E_{on} values of all investigated catalysts.

Catalyst	$E_{1/2}$ (V vs RHE)	E_{on} (V vs RHE)
Bare GC	0.55	0.69
MWCNTs	0.69	0.79
MWCNT/HL1	0.66	0.77
MWCNT/HL2	0.67	0.77
MWCNT/K_2PdCl_4	0.74	0.88
MWCNT/HL1-Pd(II)	0.83	0.91
MWCNT/HL2-Pd(II)	0.86	0.95
Pt	0.82	0.91

S8

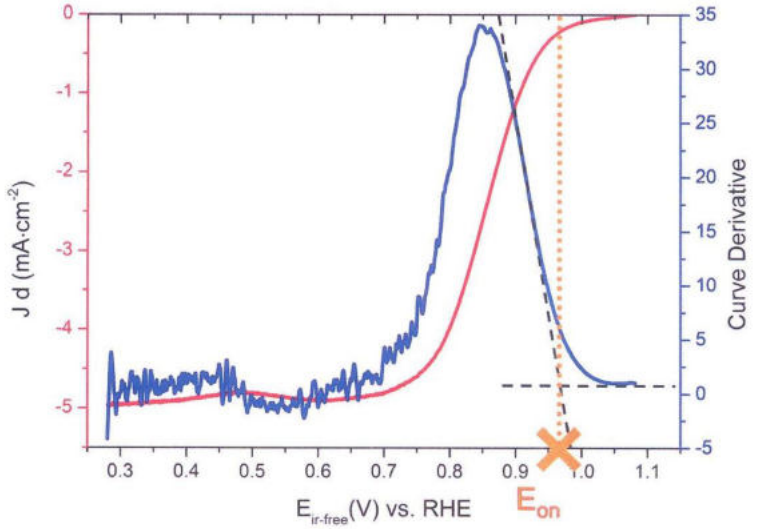

Figure S1. Graphical definition of E_{on} as employed in this paper. E_{on} value is determined from the polarization curve using its first derivative as the intersection between the derivative inflection point and its baseline. Displayed polarization curve is the one for the MWCNT/HL2-Pd(II) catalyst.

S9

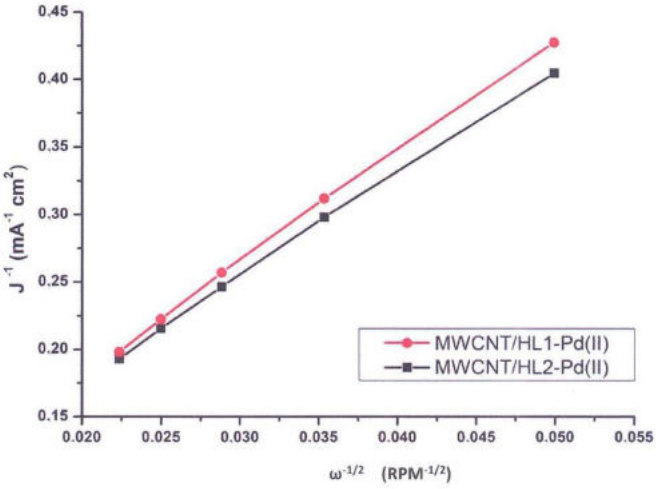

Figure S2. Koutecky-Levich plots at -0.80 V vs Ag/AgCl/sat. KCl.

S10

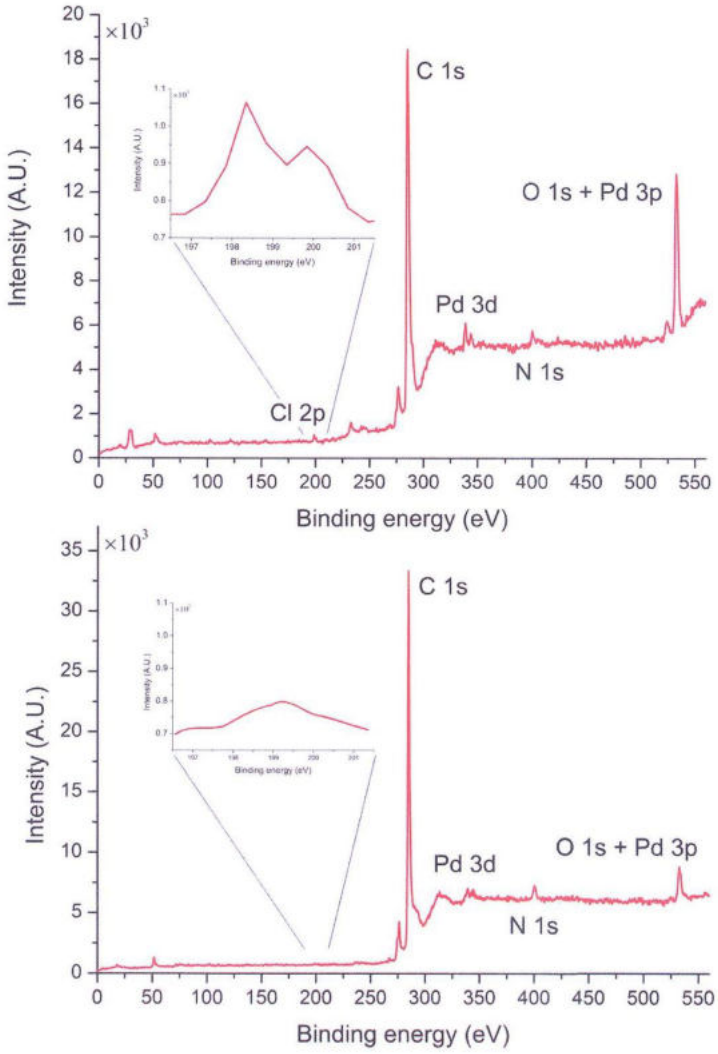

Figure S3. XPS survey spectra of the MWCNT/HL2-Pd(II) catalyst as prepared (top) and after use (bottom), showing the exchange of the ancillary chloride ligand.

S11

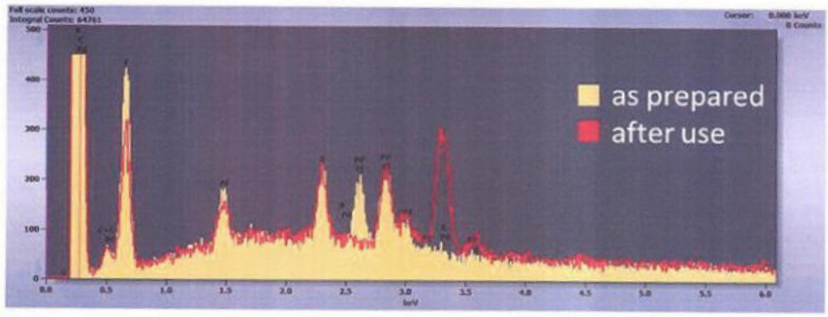

	as prepared		after use	
Element[a]	Weight %	Atom %	Weight %	Atom %
C *K*	84.4	90.5	87.7	93
F *K*	12.9	8.8	9.4	6.3
Al *K*	0.3	0.1	0.2	0.1
S *K*	0.5	0.2	0.4	0.2
Cl *K*	0.5	0.2	0	0
K *K*	0	0	1	0.3
Pd *L*	1.4	0.2	1.3	0.2
Total	100	100	100	100

[a] *K* and *L* indicate the spectral line used for quantification.

Figure S4. SEM-EDS analysis of MWCNT/HL2-Pd(II) as prepared and after use (1000 CV cycles, ≈ 2.8 h) showing invariance of Pd content and exchange of the ancillary chloride ligand. Analysis has been performed using a Hitachi S-2300 SEM equipped with a Thermo Scientific NSS7 EDS analyser. Accelerating voltage: 20kV. Analysis software: Pathfinder 2.2

S12

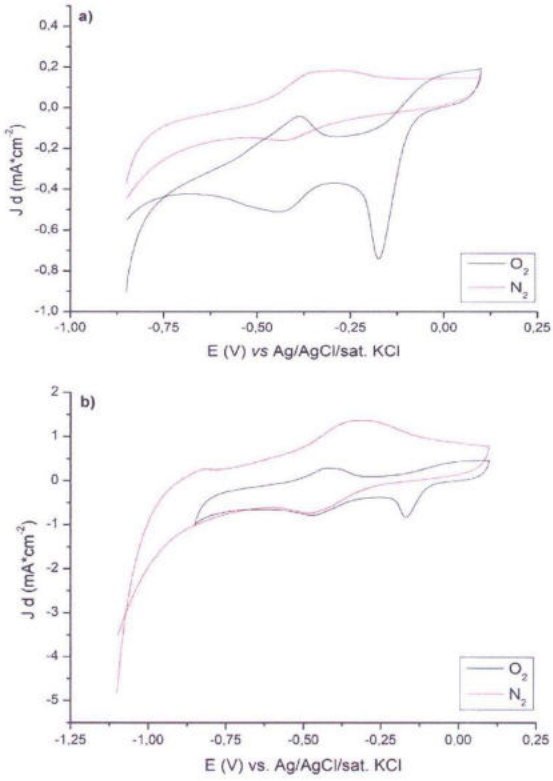

Figure S5. Still CVs in KOH 0.1 M solution saturated with N_2 (red line)/O_2 (black line) for MWCNT/HL1-Pd(II) sample (a) and MWCNT/HL2-Pd(II) sample (b).

S13

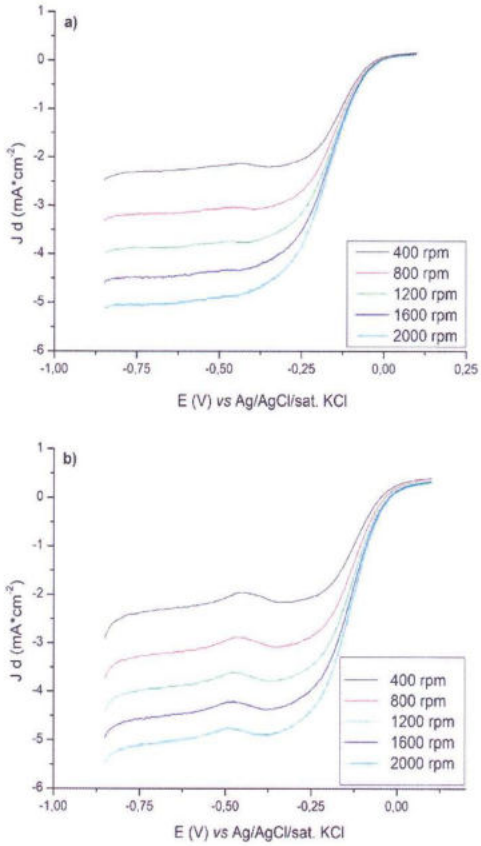

Figure S6. Linear sweep voltammograms recorded at different spin rates (400; 800; 1200; 1600; 2000 rpm) at 20 mV/s scan rate. (a) MWCNT/HL1-Pd(II) sample; (b) MWCNT/HL2-Pd(II) sample.

S14

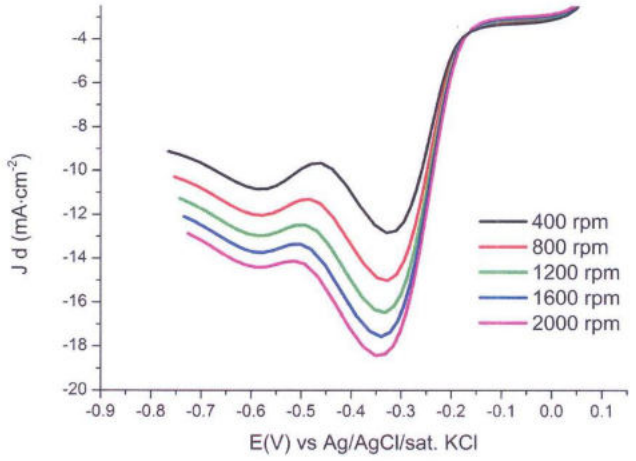

Figure S7. Linear sweep voltammograms of MWCNT/HL2-Pd(II) recorded at different spin rates (400; 800; 1200; 1600; 2000 rpm) at 200 mV/s scan rate.

S15

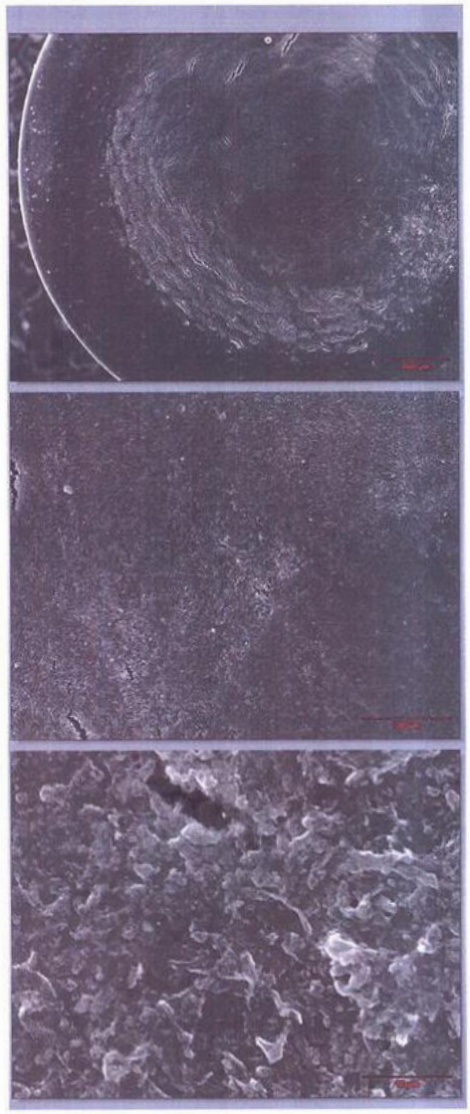

Figure S8. SEM micrographs showing the as-prepared MWCNT/HL2-Pd(II) electrode surface. Recorded on a Hitachi S-2300 instrument.

S16

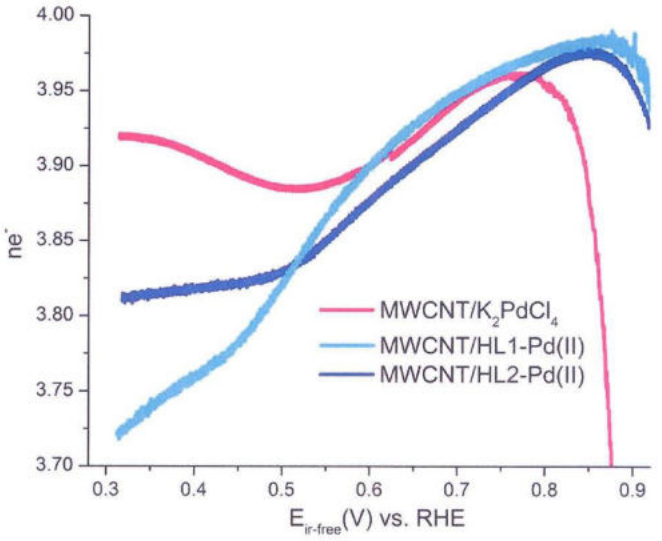

Figure S9. Dependency of number of exchanged electrons per O_2 molecule vs voltage for Pd-containing catalysts.

S17

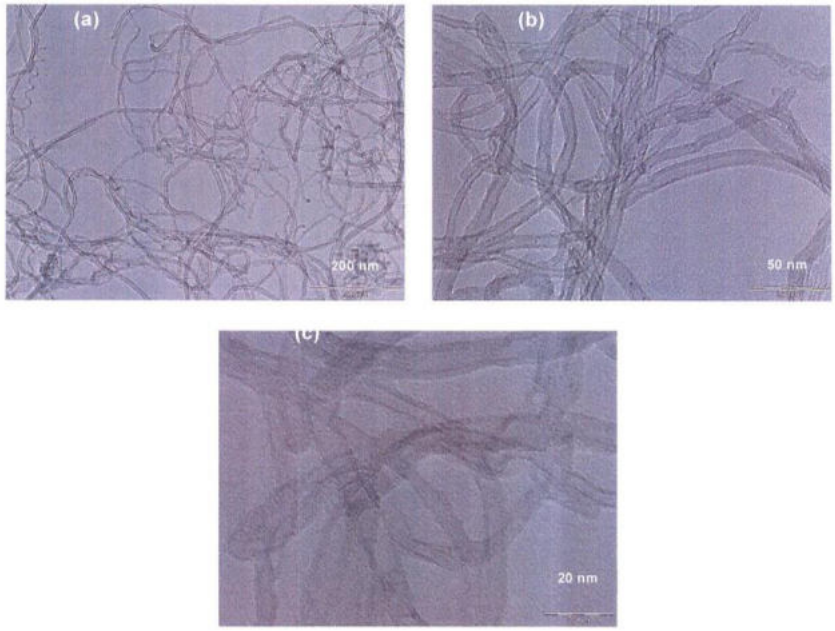

Figure S10. TEM Images of the after-use MWCNT/HL2-Pd(II) catalyst. Image (b) was selected among the many images acquired to show that rare and tiny traces of Pd(0) nanoparticles can be locally observed.

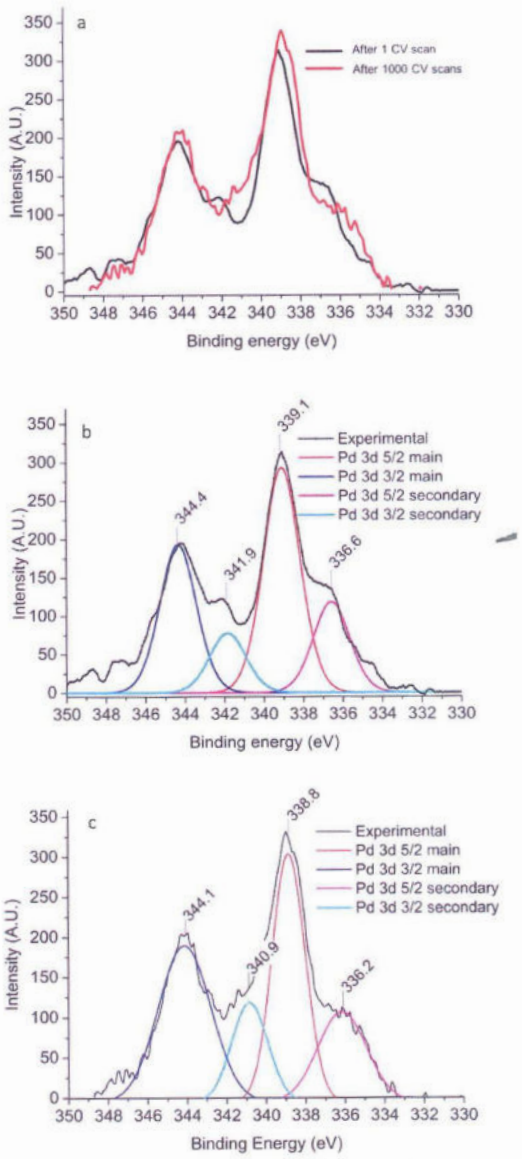

Figure S11. High resolution XPS spectra in the Pd 3d region of the MWCNT/HL2-Pd(II) GC electrode after 1 CV and 1000 CV cycles (CV scans from anodic to cathodic potential, stop at -0.85 V vs Ag/AgCl/sat. KCl). (a) Experimental spectra. (b) Fitted spectrum of the catalyst after 1 CV scan. (c) Fitted spectrum of the catalyst after 1000 CV scans.

S19

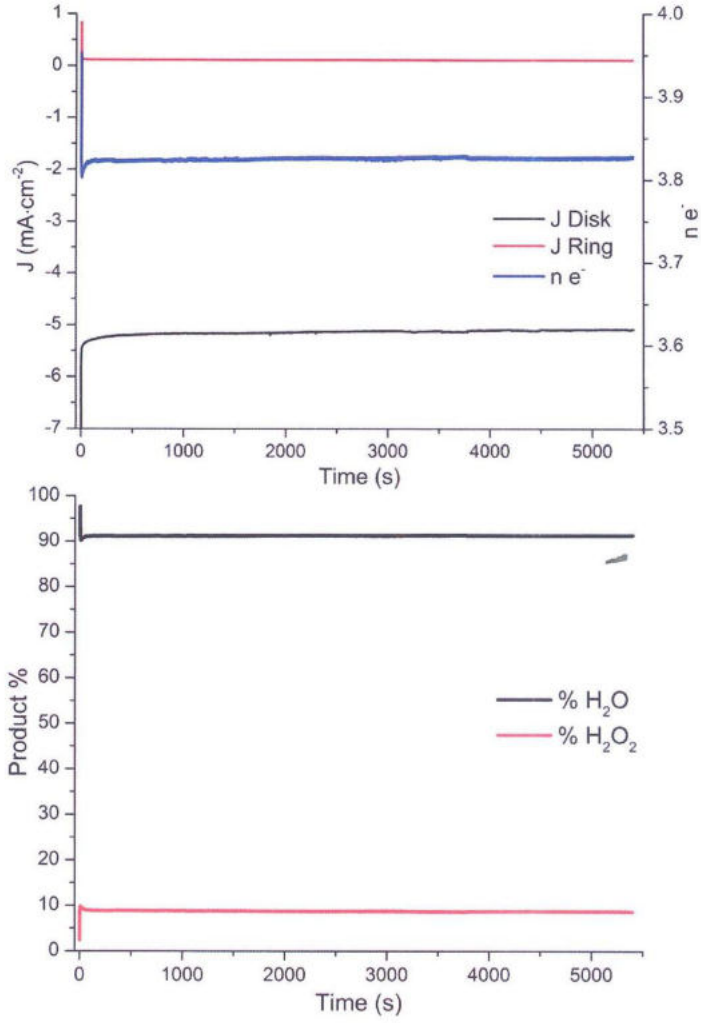

Figure S12. MWCNT/HL2-Pd(II) 1.5 hours stability test results; top: time evolution of ring and disk current densities and number of exchanged electrons per O_2 molecule; bottom: time evolution of water and hydrogen peroxide yields (as percentage).

S20

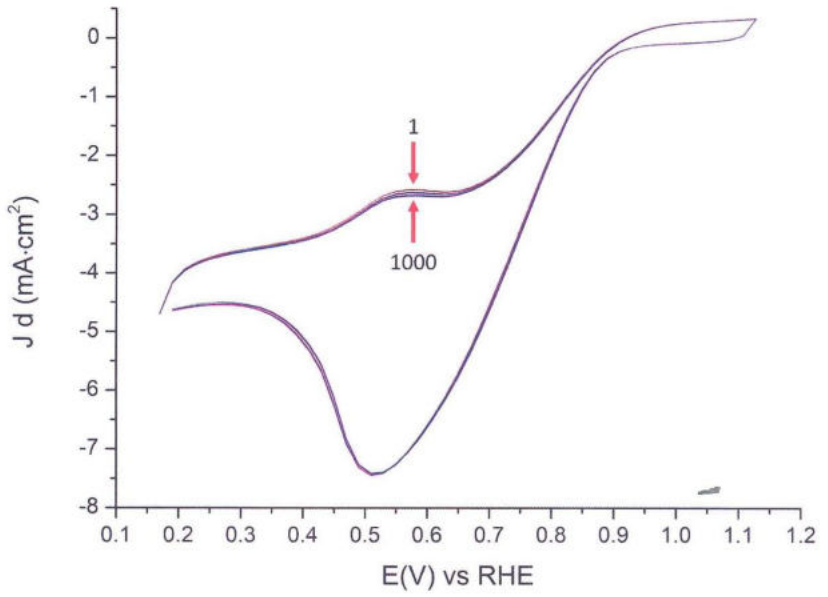

Figure S13. Stability of the MWCNT/HL2-Pd(II) catalysts over 1000 CV scans (1600 rpm, 200 mV/s). 1 voltammogram is plotted every 200 scans.

S21

References

1. Savastano, M.; Arranz-Mascarós, P.; Bazzicalupi, C.; Clares, M. P.; Godino-Salido, M. L.; Gutiérrez-Valero, M. D.; Inclán, M.; Bianchi, A.; García-España, E.; López-Garzón, R. *J. Catal.* **2017**, *353*, 239-249.

2. Savastano, M.; Arranz-Mascarós, P.; Bazzicalupi, C.; Clares, M. P.; Godino-Salido, M. L.; Guijarro, L.; Gutiérrez-Valero, M. D.; Bianchi, A.; García-España, E.; López-Garzón, R. *ACS Omega* **2017**, *2* (7), 3868-3877.

3. Savastano, M.; Arranz-Mascarós, P.; Bazzicalupi, C.; Bianchi, A.; Giorgi C.; Godino-Salido, M. L.; Gutiérrez-Valero, M. D; López-Garzón R. *RSC Adv.* **2014**, *4*, 58505.

4. Newman, J. *J. Electrochem. Soc.* **1966,** *113*(5), 501-502

S22

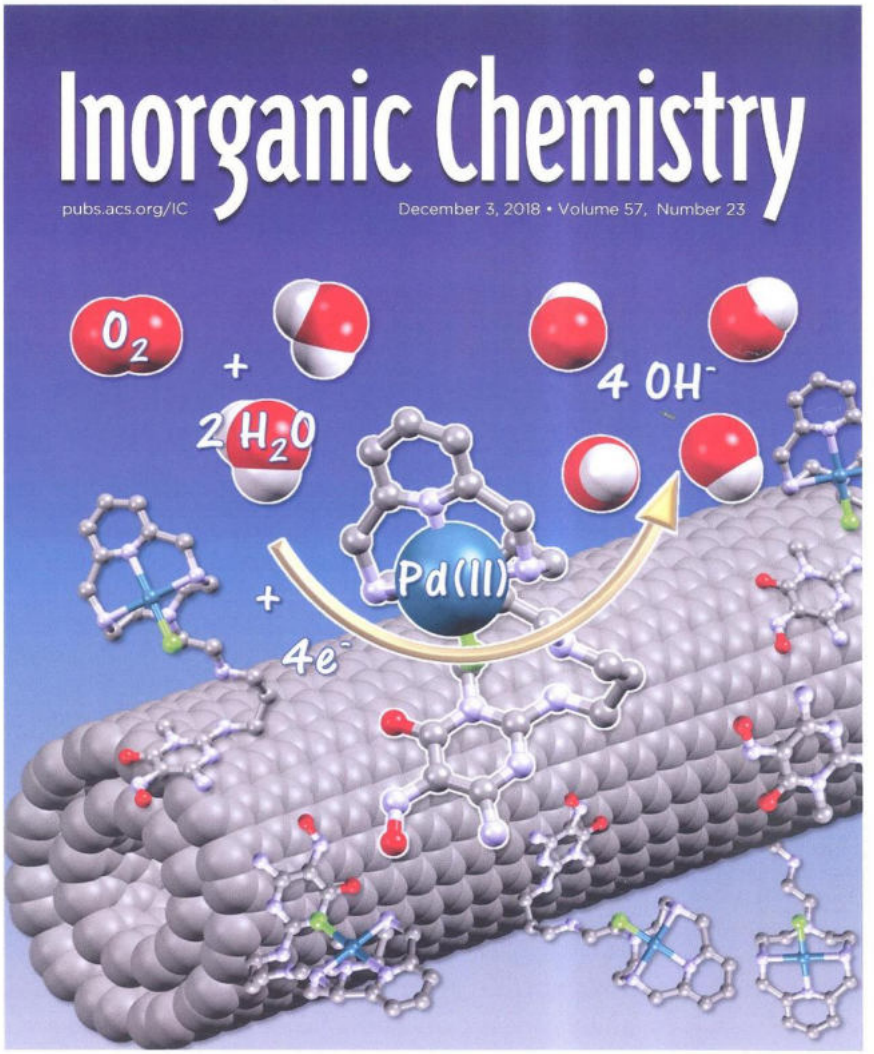
Inorganic Chemistry
pubs.acs.org/IC
December 3, 2018 • Volume 57, Number 23
O2
+
2 H2O
4 OH-
Pd(II)
+
4e-
ACS Publications
Most Trusted. Most Cited. Most Read.
www.acs.org

6 Recycle pathway sample

6.1 Microwave Assisted Pyrolysis (MAP)

Pyrolysis is a thermochemical decomposition process in which the heat supplied promotes a series of radical chain reactions capable of breaking down polymers into simpler compounds. The process is conducted in an oxygen-free environment, created by insufflating inert gases such as He, N_2 and CO_2, in order to avoid combustion phenomena due to high temperatures. During pyrolysis the material to be pyrolized is heated up to a maximum temperature, called pyrolysis temperature, to which it is kept for a specific time useful for completing the reaction. Some important parameters in pyrolysis are: the type of reactor used, the temperature, and the presence of any catalysts. The value chosen for these parameters strongly influences the composition of the pyrolysis products, so by adequately setting the experimental conditions it is possible to production of a product compared to the others. Generally high temperatures and long residence times promote the production of gas, while lower temperatures promote the formation of solid products. It is possible, for example, to obtain a better liquid yield at moderate values of residence time and pyrolysis temperature. Classical pyrolysis uses a conventional heating method which involves increasing the temperature of the walls of the container which then transfers the thermal energy to the sample, heating it. This type of pyrolysis has several disadvantages due to conventional heating such as: low heating efficiency and long reaction times, caused by the slow transfer of thermal energy between the container and the sample. An alternative and convenient method to classical pyrolysis involves the use of microwaves for heating the sample. In this case we talk about

microwave-assisted pyrolysis or microwave assisted pyrolysis. The microwaves are electromagnetic waves or waves composed of two fields, magnetic and electric, oscillating at a certain frequency on two planes perpendicular to each other. In this case, microwaves occupy in the electromagnetic spectrum the frequency range between 0.3 and 300GHz, corresponding to wavelengths between 1 mm and 1 m (fig. 6.1).

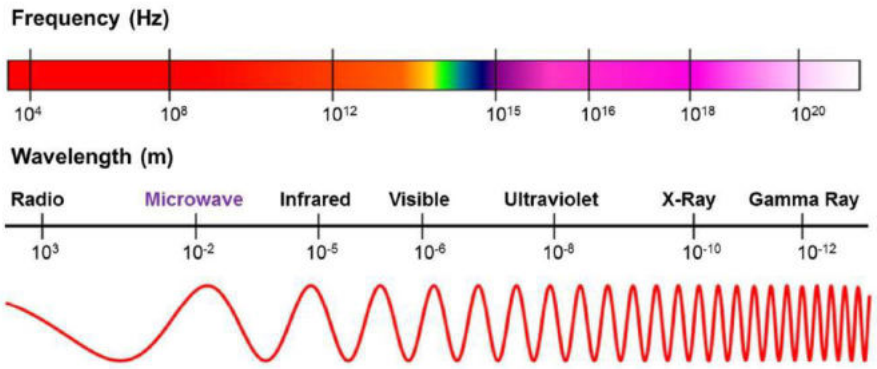

Fig.6.1 Electromagnetic spectrum.

The use of microwaves in pyrolysis experiments is possible if a substance capable of absorbing microwaves is present in the sample, allowing the transformation of electromagnetic energy into thermal energy. Energy conversion is mainly due to two phenomena: ionic migration and dipolar polarization. Ionic migration makes the greatest contribution to heating; it generates heat due to the collisions between the charged particles that, moving along the electric field, collide with each other. Dipolar polarization is instead an effect that takes place in polar liquids and is related to the realignment of the dipoles, due to the fluctuating electric field, the continuous realignment of the dipoles causes friction and molecular shocks which in turn generate heat. The different behaviour of the various

materials with respect to microwave radiation has made it possible to distinguish them in three categories:

• Insulators - materials that are transparent to microwaves and therefore not subject to this type of heating (teflon, quartz);
• Conductors - materials capable of reflecting radiation (metals);
• Absorbents - also called dielectrics - are materials capable of interacting with microwaves absorbing radiation.

Since only the last class is able to undergo the processes that lead to microwaved heating it has been called dielectric heating. The use of microwaves provides a more effective method of heating than conventional heating: the substantial difference, as well as the main advantage of dielectric heating, lies in the mechanism of heat transfer to the sample.
Figure 6.2 shows the heating patterns for the two methods.

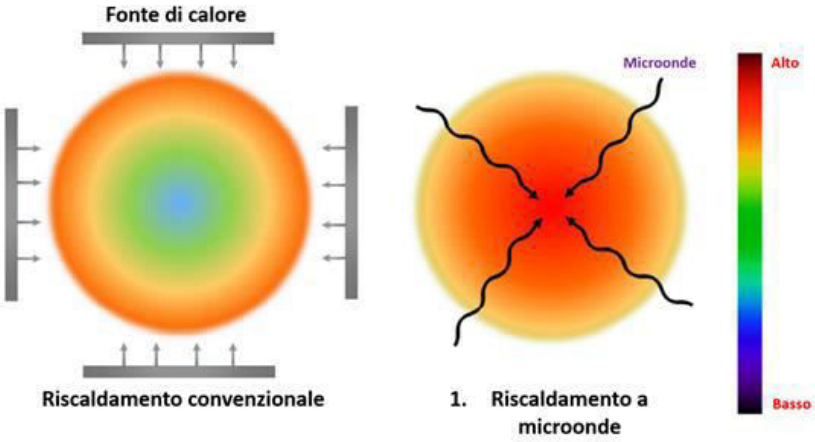

Fig. 6.2 Temperature diagram for two heated objects for conventional heating (left) and microwave heating (right)

In conventional heating the heat is transferred to the external walls of the container which then transfers the thermal energy to the sample. In this way there is a considerable use of energy, necessary to heat the sample and the walls of the container as well as increasing the temperature exclusively on the surface of the sample itself, thus obtaining a heating that is not very effective and uniform. In the dielectric heating the waves pass through the insulating materials, often used for the construction of the containers, being absorbed directly by the sample. This effect allows to heat the sample avoiding the formation of temperature gradients, typical of conventional heating. Furthermore, not involving contact heat transfer, this method avoids all the problems and limits related to thermal conductivity, density or specific heat of materials. In figure 6.2 it is possible to notice that the centre of the sample is much warmer than the external zones. The cause is attributable to the inhomogeneity of the magnetic field that generates hot spots, called hot spots or micro cells. These small electric arcs, lasting a few fractions of a second, confined to a very small space, are able to reach temperatures high enough to influence the yield of the products by increasing the gasification of the sample. Although it requires the presence of an absorbent, microwave-assisted pyrolysis enjoys all the advantages deriving from dielectric heating such as the high reaction speed which influences the yield of the products, the high heating efficiency and the rapid transfer of heat for which temperature variations between 10 and 200 ° C / s have been recorded. The yield of the products obtained through MAP is linked to various experimental aspects, for example: the reactor used, the reaction time, the applied power, the particle size, and the temperature. As explained at the beginning of the paragraph, the latter has the greatest contribution: at high temperatures the intermediate products present in the

pyrolysis gases can undergo thermal cracking by increasing the formation of gaseous species or, for fairly long residence times, it is It is possible to observe an increase in coal, formed by secondary reactions.

Another important contribution is given by the power applied as it influences the heating time which in turn has an effect on the solid yield and on the calorific value of the coal produced.

6.2 Chars obtained from MAP of Waste tyres (PFU)

Given their complexity, the disposal and recycling of PFU (Fig. 6.1) is a very complicated process.

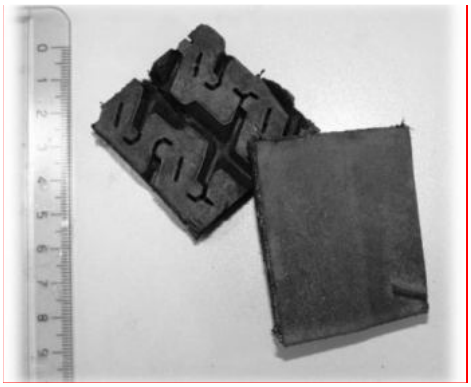

Fig. 6.1 Exhausted Michelin Agilis 81 195/65 R16C tire used for coal production [68]

The main methods of recovery of these waste are divided into three classes:

- Physical methods
- Chemical methods
- Thermal methods.

In the first case it is possible to obtain rubber powders or granules which are used for paving roads; the granulate can also undergo a chemical treatment useful for the recovery of the rubber and the subsequent application in various fields. Thermal processes instead aim at energy recovery: one of the most sustainable methods for PFU disposal is pyrolysis. The presence in tires of an excellent absorbent such as carbon black (used as a filler) allows in particular the use of microwave-mediated pyrolysis, with all the advantages previously exposed. The gaseous products of pyrolysis are composed of a mixture of gases with a high calorific value which can therefore be used as a fuel. The chars obtained represent the second type of samples tested for the oxygen reduction reaction during this doctorate.

6.3 Publication on Journal of Power Sources

In this paragraph the work published in the scientific Journal “Journal of Power Sources” entitled "*Recycling of waste automobile tires: Transforming char in oxygen reduction reaction catalysts for alkaline fuel cells* ". This work explains and summarizes (both in the main manuscript and in the information support) the entire study and research path, considering also the various steps:

• the importance of the power / mass^2 ratio (P / M^2) during pyrolysis, consequently electrochemical performance;

• the influence of a second heat treatment in the presence of oxygen;

• characterization of the materials studied.

Journal of Power Sources 427 (2019) 85–90

Contents lists available at ScienceDirect

Journal of Power Sources

journal homepage: www.elsevier.com/locate/jpowsour

Recycling of waste automobile tires: Transforming char in oxygen reduction reaction catalysts for alkaline fuel cells

Maurizio Passaponti [a], Luca Rosi [a,b], Matteo Savastano [a], Walter Giurlani [a], Hamish A. Miller [c], Alessandro Lavacchi [c], Jonathan Filippi [c], Giovanni Zangari [d], Francesco Vizza [c,*], Massimo Innocenti [a,c,**]

[a] Department of Chemistry "Ugo Schiff" University of Florence, via della Lastruccia 3, 50019, Sesto Fiorentino (FI), Italy
[b] Consorzio Interuniversitario Reattività Chimica e Catalisi (CIRCC), Via Celso Ulpiani 27, Bari, Italy
[c] CNR-ICCOM, via Madonna del Piano 10, 50019, Sesto Fiorentino (FI), Italy
[d] University of Virginia, 395 McCormick Rd, Charlottesville, VA, 22904, USA

ARTICLE INFO

Keywords:
Waste automotive tires
Recycling
Microwave pyrolysis
Alkaline ORR catalysts

ABSTRACT

The recycling of scrap automotive tires is made difficult by a number of factors. They are composed of a complex matrix that includes hazardous materials, not to mention a gigantic annual production rate. Herein we report a novel approach tackling the recovery and valorization of chars, the least valuable by-product of waste-tire pyrolysis, through the transformation into highly efficient Oxygen Reduction Reaction (ORR) catalysts for use in alkaline fuel cells and metal air batteries. The study has been performed on chars obtained from Microwave Assisted Pyrolysis (MAP). Each sample has been characterized by metal content (ICP-MS), specific surface area (BET), porosity, crystallinity and nature of inorganic components embedded in the carbonaceous matrix (XRPD). The most promising samples exhibit an ORR onset potential of −90 mV (RHE) and a 4e⁻ mechanism. Two main factors are found to contribute to the enhanced ORR activity. Firstly, a large specific surface area and porosity and secondly the presence of a high concentration of ZnO particles embedded within the carbon matrix.

1. Introduction

Global climate change and the detrimental effects on human health of air pollution (smog) [1] have contributed to raise awareness of the problems associated with modern society's dependence on fossil fuels for both energy and raw chemicals. The dramatic growth in the number of combustion engine powered vehicles is responsible in large part for our environmental problems, both due to the emission of greenhouse gases and in terms of solid waste disposal [2,3]. With regard to the latter, scrap tires are a major long-standing and unresolved issue [4]. Currently, about 1.5 billion waste tires are produced yearly, including 2.6 million tons for just Europe alone [5]. More than 80% of the worldwide production of scrap tires is concentrated in a few macro-areas (USA, EU, China, India and Japan), where strict protocols and regulations have been applied (e.g. EU Directive 31/1991) [6]. It should also be mentioned that tires are particularly problematic considering that in their worn-out state their mass is essentially the same as when they were produced. In particular, the chemical composition of scrap tires poses serious problems. Landfill storage is prohibited in most countries, due to flammability and leakage of toxic chemicals. For this reason, whole tires are recycled to produce mats for playgrounds, athletic surfaces, and also to make cement; since 1994 the fraction of waste tires going to landfills has decreased from 60% to 5% in 2015 [7].

Thermal treatments, such as pyrolysis, have been developed as an efficient strategy to reclaim useful chemicals, often in the form of fuels, or from scrap tires [8]. Pyrolysis is a thermal decomposition process performed at high temperature in an inert atmosphere, which allows the transformation of complex substances into simple molecules. Starting materials are invariably converted into three phases: gas, liquid and solid. The liquid and gas phases are at present considered the most valuable (i.e. possessing the highest economic value). The gas phase consists generally of small molecules (H_2, C_1—C_4 hydrocarbons, CO_2, CO and H_2S) [8]. The oil (i.e. the liquid phase) obtained is generally a complex mixture of aliphatic, aromatic, heteroaromatic and polar

* Corresponding author.
** Corresponding author. Department of Chemistry "Ugo Schiff" University of Florence, via della Lastruccia 3, 50019, Sesto Fiorentino (FI), Italy.
E-mail addresses: francesco.vizza@iccom.cnr.it (F. Vizza), m.innocenti@unifi.it (M. Innocenti).

https://doi.org/10.1016/j.jpowsour.2019.04.067
Received 18 February 2019; Received in revised form 28 March 2019; Accepted 16 April 2019
0378-7753/

compounds, which has been investigated both as potential fuels and/or source of purified chemicals [8–11]. The solid residuals, often referred to as chars, have been tentatively used to produce carbon black and/or activated carbon with some success in the production of activated carbon electrodes for supercapacitors [12–14]. Chars contain significant amounts (from a few to several thousand ppm) of different metals embedded in a heterogeneous matrix in the form of isolated chemical entities or particulate matter (e.g. oxides, sulfides, etc.). Such compounds are introduced during vulcanization and other stages of rubber manufacture. The heterogeneous nature of the mixture makes an affordable separation and recovery of metals from scrap tires very difficult.

In this paper, we propose an effective way to exploit the presence of nano-sized metallic or metal oxides/sulfide particles dispersed in the carbonaceous matrix obtained after char formation [15,16]. We demonstrate that a simple post pyrolysis heat treatment can be used to produce materials with high activity for the electrocatalytic oxygen reduction reaction (ORR) [17–19].

The morphology and porosity of the materials can be optimized by these treatment conditions. The optimized preparation method leads to a high surface area carbon based matrix containing ZnO/ZnS particles. Both the high surface area and the dispersion of ZnO particles are responsible for the enhanced ORR activity. The recycling of tires as ORR catalysts is an interesting process that has the potential to become much more relevant should a massive switch from fossil fuels to fuel cell vehicles may occur: in this case, this process may lay the foundations for the closed-loop recycling of end of life tires. Herein we report a hydrodynamic study (rotating ring-disk elec trode, RRDE) on the half-cell, as is the best practice for benchmarking ORR catalyst performances.

2. Experimental section

2.1. Fabrication of materials

A commercial tire (Michelin model Agilis 81–195/65 R16C) was chopped into chip (8 cm^3) samples. The tire chips were first dried for 24 h at 338 K in a ventilated oven. The pyrolysis were carried out in a microwave oven working at 2.45 GHz, with two external microwave generators each having an absorption of 1.2 kW electric power for a total of 2.4 KW, capable of delivering up to 2 KW of microwave power inside the oven. The oven was designed and produced by Microglass srl (Pordenone, Italy). The oven was also equipped with a wide angle measuring infrared thermometer. As just reported in previous papers the infrared thermometer provides an average temperature within the tyres mass and the surrounding gas.

Samples were placed in a 500 mL borosilicate Erlenmeyer flask inside the oven; the liquid and gas formed during pyrolysis were separated from the solid char residue that remained in the flask inside the oven. A sample of commercial tire was treated using the following Microwave Assisted Pyrolysis (MAP) conditions (2.4 kW, 10 min) under inert atmosphere (N_2) [8,11,12]. This sample was then subjected to further heat treatments as follows. Samples were placed in quartz vials and treated for 1 h at 4 different temperatures (150 °C, 300 °C, 450 °C or 600 °C) within a conventional oven under static air.

2.2. Physical characterization

Elemental analysis was performed using a PerkinElmer CHNS/O Analyzer model 2400 series II (CHNed by nitrog). Information on the BET surface area and pore structure was obtained by adsorption isotherm using a Coulter SA 3100 instrument and X ray μ-Computed Tomography (μ-CT) data set using a Bruker Skyscan 1172. Metal content was evaluated through ion coupled plasma-mass spectroscopy (ICP-MS) analysis, carried out using a MW mineralizer, CEM Mars Xpress and ICP-MS thermo Xseries2.

Crystal lattice parameters and structures were determined by X-Ray Powder Diffraction (XRPD). XRPD data were collected at room temperature by using a Bruker New D8 DaVinci diffractometer equipped with a Bruker LYNXEYE-XE detector (Cu−Kα radiation, 40 kV × 40 mA, scanning range $2\theta = 8–70°$).

TEM-EDX analysis was carried out on a TEM CM 12 PHILIPS instrument with CRYO-GATAN UHRST 3500e microanalysis EDAX.

2.3. Electrochemical measurements

Rotating ring disk electrode (RRDE) cyclic voltammetrry (CV) and Linear Sweep Voltammograms (LSV) experiments were performed in a Pyrextm (Princeton Applied Research) glass cell filled with a 0.1 M KOH solution. The reference electrode was a commercial Ag/AgCl/sat. KCl (Princeton Applied Research) with a potential of +197 mV respect to the NHE. A platinum wire was used as counter electrode. A PGSTAT 100 N bi-potentiostat was used to perform the experiments.

The ring current was recorded simultaneously with the disk current. Measurements were performed using a ring-disk electrode (E6 Series) from Pine Instrument Co. Consisting of a glassy carbon (GC) disk insert (ø 5 mm; A = 0.196 cm2) and a Pt ring (A = 0.11 cm^2). The RRDE measurements were carried out using a modulated speed rotator (MSR) model 636 A from Pine Instrument Co. The working electrode for RRDE measurements was prepared as follows: catalyst (10 mg) was dispersed in 0.220 g of water, 0.112 g of ethanol and 0.084 g of a Nafion solution (5 wt% in lower aliphatic alcohols and water). The resulting ink was sonicated for 30–45 min and was drop cast onto the glassy carbon electrode (3 mg). The as-prepared electrode was then dried at room temperature. All RRDE experiments were carried out at a scan rate of 5 mV/s and at 1600 revolutions per minute (rpm) in the potential range from −0.85 to +0.1 V vs Ag/AgCl/sat. KCl in alkaline medium, while the Pt ring electrode was held at a potential of +0.50 V. Galvanostatic analysis at selected potential values were performed within a 300 s framework. N_2 or O_2 were used to purge the solution and achieve an O_2-free or an O_2-saturated electrolyte solution. To assess the number of transferred electrons per O_2 molecule occurring during the ORR process, the fractional yields of HO_2^- were calculated from the RRDE experiments as;

$$X\ HO_2^- = (2I_{ring}/N)/(I_{disk} + I_{ring}/N)$$

the electron transfer number was calculated by;

$$n = 2 \times HO_2^- + 4 \times I_2O = 4\ I_{disk}\ /(I_{disk} + I_{ring}/N)$$

The HO_2^- collection efficiency of the ring electrode N ($N = I_{ring}/I_{disk}$) [27] was determined experimentally for each sample. Calibration was performed using the $K_3Fe(CN)_6$ redox couple. LSVs for 10 ppm $K_3Fe(CN)_6$ solutions were recorded in N_2-saturated KOH 0.1 M solution at 1600 rpm using a 5 mV/s potential scan rate to empirically determine the collection number. The number of exchanged electron per O_2 molecule (n e^-) are reported. A commercial Metrohm $Pt_{polycrystalline}$ electrode (ø 3 mm) was employed to benchmark the performance of the materials presented in this report. Acid treatment.

2.4. Acid treatment

The sample obtained by heat treatment at 450 °C was treated with a 1:1 (v:v) mixture of 98% H_2SO_4 and 70% HNO_3 for 24 h at room temperature, followed by washing with deionized water and drying.

3. Results and discussion

3.1. Preparation and characterization

Chars possessing different physical, chemical and catalytic properties were obtained by varying the MAP conditions as described in our previous reports [10,11,16–24]. The most promising sample in terms of

porosity, specific surface area and electrocatalytic activity, was used to study the ORR activity after further heat treatment under controlled conditions (Table 1). Refer to the SI for analysis of the various CHAR materials. The chosen starting material was obtained from a sample of commercial tire by pyrolysis MAP conditions (2.4 kW, 10 min) under inert atmosphere (N_2). This material was then heat treated for 1 h at four temperatures (150, 300, 450, 600 °C) under static air conditions. All samples were characterized with respect to their chemical composition (CHN elemental analyses), metal content (ICP-MS), specific surface area (nitrogen adsorption isotherms) and porosity/morphology (X ray μ-CT): these data are reported in Tables 1 and 2 and Tables S1 and S2.

Table 1 lists important data regarding the elemental composition and BET surface area. Heating the starting CHAR material leads to a decrease in the %C due to partial oxidative decomposition of the carbon in the sample in the presence of oxygen from the air. In the sample prepared at 600 °C this process is almost complete. The most important change observed is the large increase in BET surface area and pore volume for the sample prepared at 450 °C (72–296 $m^2 g^{-1}$ and 0.46–1.03 $cm^3 g^{-1}$). The increase in surface area is also apparent from X ray μ-CT analysis. The three dimensional reconstruction shown in Fig. 1 depicts the microstructure shifting from a solid coal-like materials towards a sponge-like architecture, demonstrating a major increment in porosity/exposed surface. The effect of heat treatment depends strongly upon the temperature used. Samples were heat-treated in static air: at 150 and 300 °C a limited and similar mass loss (about 30%) was observed, while the sample treated at 600 °C underwent an almost complete combustion, losing about 97% of its weight. TG analysis confirms the nature of the sample decomposition during heating. Fig. 2(a) shows TG analysis data of the CHAR under air, at a temperature ramp of 20° min^{-1}. The sample is stable up to around 400 °C, when weight loss accelerated and by 600 °C more than 90% of the sample sublimated. A sample of CHAR held at 450 °C in air for 1 h (Fig. 2(b)) exhibits a constant loss of weight through combustion (20–25 μg min^{-1}). After 1 h about 50% of the sample weight had been lost. For this reason the preparation time was held at 1 h as further exposure to air at this temperature would lead to complete combustion of the sample. As anticipated, various metals are found in significant amounts within the starting material: in order of abundance Zn (up to 85000 ppm), due to its widespread use as accelerator for the vulcanization process, followed by Fe (up to 5000 ppm) [21], Cu, Co, Ni, Cd and Cr (Table 1) [22]. In addition, analysis of the metals present after acid treatment of the sample at 450 °C shows a large quantity of Zn has been removed. The high BET surface area and pore volume is also maintained after acid treatment (Table S5).

XRPD traces of each sample are shown in Fig. 3. The patterns show the presence of several crystalline inorganic components demonstrating the simultaneous presence of different transition metals in the form of mixed sulfides and oxides, with a marked prevalence of β ZnS. The treatment at high temperatures has a major impact on the chemical properties, affecting the concentration and nature of the particulate metal containing species embedded in the char starting material. Moreover, there is a marked shift from metal sulfide to metal oxide components, that results from the oxidation of sulfur to volatile SO_2, causing a net decrease in sulfur content. Overall, this results in an enrichment in metal oxides, with ZnO replacing β ZnS as the main inorganic component in a temperature dependent fashion.

Table 1
Physical properties.

Sample	%wt loss	BET $m^2 g^{-1}$	Pore volume $cm^3 g^{-1}$	Pore surface area $m^2 g^{-1}$
CHAR	–	72	0.46	67
150	26	50	0.55	56
300	28	55	0.55	61
450	57	296	1.03	196
600	97	83	0.62	76

Table 2
Metal content from ICP-MS analysis. Values in ppm (mg/kg).

Sample	Cd	Co	Cr	Cu	Fe	Ni	Zn
CHAR	3.1	162	2.0	72	984	13	3760
450	4.9	473	14	408	4720	32	85607
450 after acid wash	1.4	–	11	61	2586	3	1200

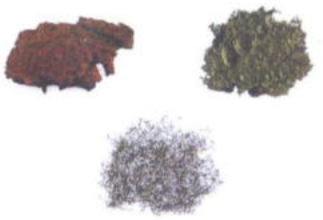

Fig. 1. Morphological features of the CHAR sample before (upper left) and after (upper right) annealing at 450 °C in N_2 according to their XRD μ-CT three-dimensional reconstructions and metal particle distribution (gold colored) of sample 450. (For interpretation of the references to color in this figure legend, the reader is referred to the Web version of this article.)

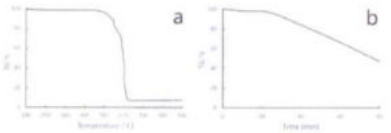

Fig. 2. TG analysis of CHAR starting material in air, a) ramp from 40 to 900 °C at 20° min^{-1} and b) ramp 40–450 °C (20° min^{-1}) followed by stable temperature 450 °C.

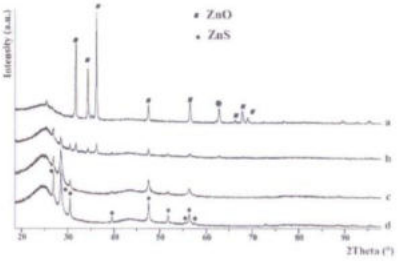

Fig. 3. Powder XRD analysis of treated samples; a) 600 °C, b) 450 °C, c) 300 °C and d) 150 °C.

The nanoscale surface morphology of the samples prepared at 150, 300 and 450 °C was investigated using TEM. Representative images are shown in Fig. 4 and also in the SI. Generally, the samples are

characterized by agglomerated carbon particles (30–50 nm). Large metal crystallites of ZnO can also be observed in clusters in the sample prepared at 450 °C, in agreement with the XRD analysis. EDX analysis confirms the elemental composition as ZnS in the materials treated at 150 and 300 °C (Figs. S3-S5). The sample prepared at 450 °C shows a similar morphology; the EDX analysis however shows the loss of S from the Zn particles, confirming the transformation of ZnS to ZnO as observed in the XRD analysis (see SI for complete EDX analysis) (see Fig. 4).

3.2. Electrochemical characterization

At first, we have studied the electrochemical behavior of each sample by cyclic voltammetry in 0.1 M KOH (pH = 13) purged with either N_2 or O_2. Cyclic voltammograms (CVs) for the four representative samples are shown in Fig. 5. In all cases, a clear and irreversible oxygen reduction peak that is not present under N_2-saturated conditions is observed under O_2 (black vs. red curve). A summary of the electrochemical data is also presented in Table 3.

The electrochemical data in Table 3 and the RRDE analysis presented in Fig. 6 reveal that the samples annealed at 150 °C and 300 °C exhibit catalytic properties closely related to that of the parent CHAR material (see SI for CHAR CV), with at best a very slight anodic shift of the E^{onset} [25]. Such a shift is increased significantly for the 450° sample, which demonstrates a major enhancement with respect to the starting material, maintaining a high number of transferred electrons per O_2 molecule while possessing an E^{onset} value (−0.09 V vs. Ag/AgCl/sat. KCl), shifted much closer to the Pt electrode benchmark compared to the precursor material (Fig. 6). The material prepared at 600 °C is, instead, the worst catalyst reported in this paper. The material prepared at 450 °C shows the best performance as it represents a compromise between the enhancement of porosity and specific surface area, promoting catalytic activity, and the retention of the carbon structure to support electron transfer processes (i.e. enabling significant conductivity).

This demonstrates that physical properties, i.e. the microstructure of the samples and their ability to support electron transfer, mainly determined by the heat treatment conditions, correlate with the observed catalytic performances. The chemical composition, which is also modified by the heat treatment process as discussed previously, also plays a major role in the enhancement of catalytic activity. Relevant changes in the material can be rationalized in three main categories: i) relative increase of metal content, ii) overall reduction of S content, iii) conversion of Zn sulfide into Zn oxide. At relatively low temperature (e.g. 150–300 °C), the CHAR loses about 30% of its weight upon heating: according to XRD (Fig. 3) the ZnS is not converted into ZnO; furthermore the metal quantity are expected to increase due to the mass loss, as it is reasonable that those metals are not lost during heat treatment.

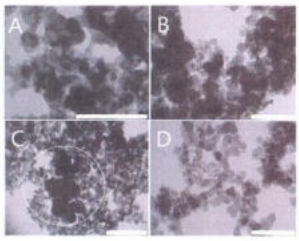

Fig. 4. TEM images of treated samples; A) 150 °C, B) 300 °C, C) and D) 450 °C. Scale bars 200 nm. The region indicated by a circle contains large ZnO crystallites in the 450 sample (scale bars = 200 nm).

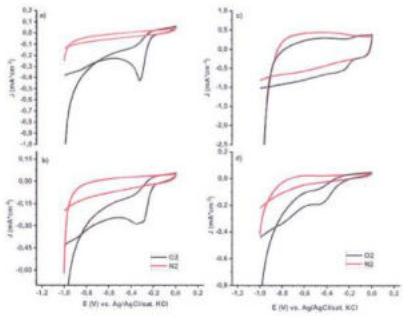

Fig. 5. CVs in quiescent 0.1 M KOH aqueous solution with either saturated O_2 (black) or N_2 (red). Heat treated samples a) 150, b) 300, c) 450 and d) 600 (°C) in N_2. (For interpretation of the references to color in this figure legend, the reader is referred to the Web version of this article.)

Table 3
Synopsis of electrochemical data.

Sample	E_{onset} [a] (V)	RRDE[b]		
		n e⁻ Calcd.[c] N Emp.	n e⁻ Calcd.[d] N Th[e]	n e⁻ calcd.[c] Averaged
CHAR	−0.21	3.65 (0.248)		
150	−0.21	3.69 (0.27)	3.50	
300	−0.19	3.67 (0.253)	3.71	
450	−0.09	3.62 (0.254)	3.63	3.69
600	−0.26	–	2.59	
Pt	−0.06	4.10[f]		
450_1[g]	−0.11			3.88

[g] sample 450 after acid treatment.
[a] vs. Ag/AgCl/sat.KCl.
[b] disk potential −0.55 V vs Ag/AgCl/sat.KCl; ring potential +0.50 V vs Ag/AgCl/sat. KCl.
[c] Number of exchanged electrons per O2 molecule (n e−) according to empirical collection numbers N Emp. (in brackets).
[d] Number of exchanged electrons per O2 molecule (n e−) according to theoretical collection number N Th. = 0.256; taken from ref 15.
[e] Time average of n e−over 300 s working time.
[f] Calculated from Rotating Rind Disk Electrode (RRDE) experiments.

The β ZnS, which is the prime inorganic component of the CHAR, is gradually replaced by ZnO at higher heat treatment temperature. This is probably the most important point, as ZnO possesses different electrical properties, namely a lower bandgap than ZnS, and significantly lower band edges, facilitating electron hopping [26]. This may indeed promote electron transfer processes as also reported in the framework of photocatalytic water splitting. Moreover, it has been recently demonstrated that nanosized ZnO obtained by calcination of ZnS exhibits enhanced catalytic properties compared to commercial or directly prepared ZnO nanoparticles. However, it is noteworthy that the transformation of ZnS to ZnO is known to produce a superior amount of oxygen vacancies compared to directly prepared ZnO nanoparticles due to the atomic size difference between O and S, which causes a lattice mismatch during the conversion of the sulfide into oxide. Such intrinsic features can boost catalytic activity. These factors can also explain the noticeable enhancement in catalytic activity observed for heat treated samples, the main reason being the shifting in the nature of active sites from.

ZnS to ZnO. Most likely, the overall increase of ZnO content together

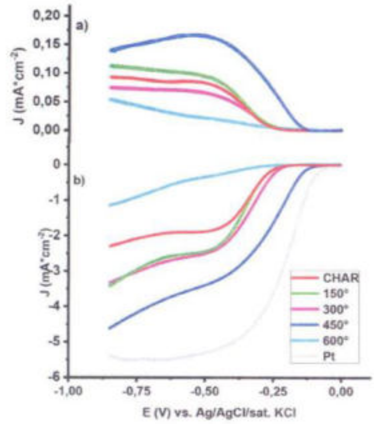

Fig. 6. ORR RRDE electrocatalytic performance of samples obtained from the heat treatment of the CHAR. a) Ring and b) Disk currents are shown respectively. The activity of the CHAR a"d commercial Pt (no ring data)"wor"ing electrode are reported "s"en"hmarks.

with a large increase in surface area provide synergistic contributions to the overall catalytic performances.

The sample prepared at 450 °C was found to be the best compromise for the maximization of the catalytic activity. Due to its remarkable performance we decided to further characterize the material concerning its short-time stability (300 s). RRDE was used in galvanostatic mode to simulate a working fuel cell at a fixed potential. The disk electrode potential was held at −0.55 V and the ring electrode was held at +0.50 V vs. Ag/AgCl/sat. KCl, respectively, for 300 s. Fig. 7 shows plots of the galvanostatic analysis results. After a few seconds the current density reaches constant values for ring and disk current densities, which remain constant during the analysis, indicating the robustness of the catalyst. The time-averaged number of exchanged electrons per O_2 molecule (3.69) shows that direct conversion to water is the main process. Also, the results are in perfect agreement with those observed from RRDE LSVs analysis (Table 3). The ORR activity was studied after the acid treatment and it was found that it is essentially unchanged (Fig. 6). A slightly worse onset potential is observed but the material performs better in terms of electrons transferred and a lower production of HO_2^- (Fig. 8 and Table 3). Despite a large quantity of zinc was removed with the acid treatment, there is still sufficient ZnO present for the catalysis of the ORR.

4. Conclusion

In this paper we demonstrate a novel approach for the reuse of a problematic waste such as waste tires. The chars obtained from pyrolysis, considered to have little to no economic value, may instead be transformed through a simple heat treatment into highly efficient catalysts for the ORR at virtually no cost and free from precious metals. The electrocatalytic behavior of the samples has been fully characterized and correlated to the physico-chemical and electrochemical properties. The catalyst physical properties, particularly the microstructure, porosity and specific surface area have been investigated. During heat treatment the β ZnS present is converted into ZnO, together with a significant

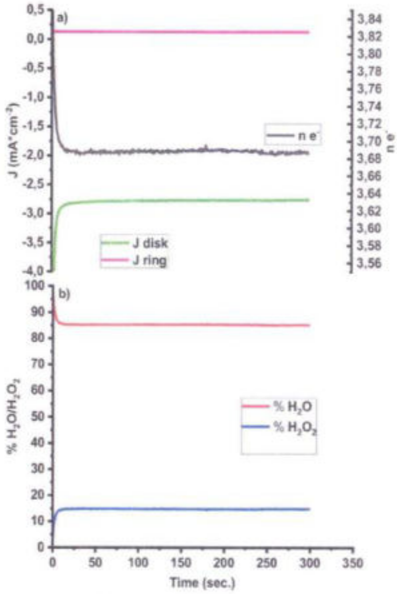

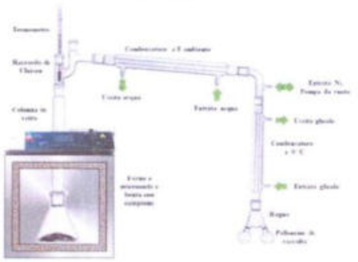

Fig. 7. Short-time stability test (galvanostatic RRDE experiment) for the sample annealed at 450 °C; (a) ring and disk currents, together with the number of exchanged electrons per O_2 molecule over time; (b) relative percentage production of H_2O and H_2O_2.

increase in total metal content. The sample prepared at 450 °C exhibits an onset potential for the ORR of −110 mV compared to a Pt electrode and a conversion efficiency of O_2 into H_2O, above 85%. Moreover, this catalyst proved stable at constant potential. This study has shown that waste CHAR derived from end of life tires can be easily transformed into a high performance electrocatalyst for the ORR. In further studies we are going to assess the performance of a complete alkaline fuel cell and acidic half-cell studies. We strongly believe that those findings will

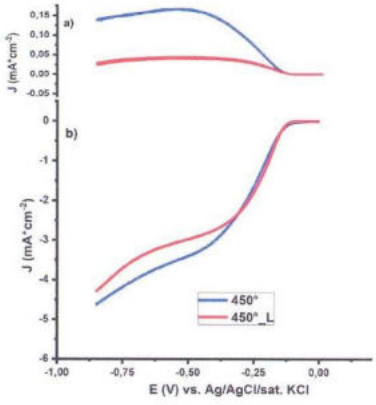

Fig. 8. ORR RRDE electrocatalytic performance of sample 450 before and after (450-L) acid treatment.

stimulate further studies towards the think-out-of-box electrocatalyst production from waste for the renewable energetic technology.

Acknowledgements

The authors thank Ente Cassa di Risparmio di Firenze for funding (project EnergyLab). PRIN 2018 Project funded by Italian Ministry MUIR Italy (N° 2017YH9MRK). L.R is grateful to the Ente Cassa di Risparmio di Firenze Foundation for funding the project "Value from Waste" (n. 201 4.0703).

Appendix A. Supplementary data

Supplementary data to this article can be found online at https://doi.org/10.1016/j.jpowsour.2019.04.067.

References

[1] Climate Change and Health – WHO (World Health Organization) Fact Sheets, 2018. http://www.who.int/news-room/fact-sheets/detail/climate-change-and-health.
[2] Worldwide Motorization Rate 2015 – OICA (International Organization of Motor Vehicles Manufacturers), 2018. http://www.oica.net/world-vehicles-in-use-all-vehicles-2/.
[3] Ambient (Outdoor) Air Quality and Health - – WHO (World Health Organization) Fact Sheets, 2018. http://www.who.int/en/news-room/fact-sheets/detail/ambient-(outdoor)-air-quality-and-health.
[4] R.C. Dower, S.D. Rand, P.F. Scodari, The Scrap Tire Problem: A Preliminary Economic Analysis, EPA (United States Environmental Protection Agency) Environmental and Economics Research Inventory. Resource available online at:, 1985 https://www.epa.gov/environmental-economics/scrap-tire-problem-preliminary-economic-analysis-1985.
[5] Worldwide Perspective – ETRMA (European Tyre and Rubber Manufacturer Association), 2018. http://www.etrma.org/tyres/ELTs/worldwide-perspective.
[6] European Council Directive, Waste Landfill Directive (1999/31/EC, 1999) Official Journal of the European Communities, Brussels, Belgium.
[7] S. Ramasada, M. Khalida, C.T. Ratnam, A. Luqman Chuah, W. Rashmi, Prog. Mater. Sci. 72 (2015) 100.
[8] P.T. Williams, Waste Manag. 33 (2013) 1714.
[9] J. Scheirs, W. Kaminsky (Eds.), Feedstock Recycling and Pyrolysis of Waste Plastics, John Wiley & Sons Ltd., Chichester, West Sussex, England, 2006.
[10] A. Undri, S. Meini, L. Rosi, M. Frediani, P. Frediani, J. Anal. Appl. Pyrolysis 103 (2013) 149.
[11] A. Undri, L. Rosi, M. Frediani, P. Frediani, Fuel 115 (2015) 600.
[12] M. Boota, M. Paranthaman, A.K. Naskar, Y. Li, K. Akato, Y. Gogotsi, ChemSusChem 8 (2015) 3576.
[13] M. Zhi, F. Yang, F. Meng, M. Li, A. Manivannan, N. Wu, ACS Sustain. Chem. Eng. 2 (2017) 1592.
[14] Y. Wang, P.B. Balbuena, J. Phys. Chem. B 109 (2005) 18902.
[15] C. Zefferoni, G. Cioncoloni, M.L. Foresti, L. Dei, E. Carretti, F. Vizza, A. Lavacchi, M. Innocenti, Molecules 20 (2015) 14386.
[16] M. Passaponti, L. Rosi, M. Frediani, E. Salvietti, A. DeLuca, A. Giaccherini, M. Innocenti, ECS Trans 78 (2017) 1935.
[17] Z.F. Pan, R. Chen, L. An, Y.S. Li, J. Power Sources 365 (2017) 420.
[18] Z.F. Pan, L. An, T.S. Zhao, Z.K. Tang, Prog. Energ. Combust. 66 (2018) 141.
[19] L. Wang, A. Lavacchi, M. Bevilacqua, M. Bellini, P. Fornasiero, J. Filippi, M. Innocenti, A. Marchionni, H.A. Miller, F. Vizza, ChemCatChem 7 (2015) 2214.
[20] F. Loglio, M. Innocenti, F. D'Acapito, R. Felici, G. Pezzatini, E. Salvietti, M. L. Foresti, J. Electroanal. Chem. 575 (2005) 161.
[21] F. Motazemi, M.T. Afzal, Renew. Sustain. Energy Rev. 28 (2013) 317.
[22] A. Undri, L. Rosi, M. Frediani, P. Frediani, in: U. Chandra (Ed.), Microwave Heating, InTech, Janeza Trdine 9, 51000 Rijeka, Croatia, 2011, p. 219 (Chapter 10).
[23] H.A. Miller, M. Bellini, W. Oberhauser, X. Deng, H. Chen, Q. He, M. Passaponti, M. Innocenti, R. Yang, F. Sun, Z. Jiang, F. Vizza, Phys. Chem. Chem. Phys. 18 (2016) 33142.
[24] C. Hagelüken, Recycling of (critical) metals, in: G. Gunn (Ed.), Critical Metals Handbook, John Wiley & Sons, Ltd., Chichester, West Sussex, England, 2014.
[25] M. Passaponti, M. Savastano, M. Paz Clare, Mario Inclán, Alessandro Lavacchi, A. Bianchi, E. García-España, M. Innocenti, Inorg. Chem. 57 (2018) 14484.
[26] A. Brayek, S. Chaguetmi, M. Ghoul, I. Ben Assaker, R. Chtourou, P. Decorse, P. Beaunier, S. Nowak, F. Mammeri, S. Ammar, RSC Adv. 8 (2018) 11785.
[27] U.A. Paulus, T.J. Schmidt, H.A. Gasteiger, R.J. Behm, J. Electroanal. Chem. 495 (2001) 134.

Supporting Information

Recycling of Waste Automobile Tires: Transforming Char in Oxygen Reduction Reaction Catalysts for Fuel cells

Maurizio Passaponti,[a] Luca Rosi,[a] Matteo Savastano,[a,b] Walter Giurlani,[a] Hamish A. Miller,[c] Alessandro Lavacchi,[c] Jonathan Filippi,[c] Giovanni Zangari,[d] Francesco Vizza,[c*] Massimo Innocenti[a,c*]

m.innocenti@unifi.it, francesco.vizza@iccom.cnr.it

[a] Department of Chemistry "Ugo Schiff" University of Florence, via della Lastruccia 3, 50019 Sesto Fiorentino (FI), Italy; [b] Consorzio Interuniversitario Reattività Chimica e Catalisi (CIRCC). Via Celso Ulpiani 27. Bari. Italy; [c] CNR-ICCOM, via Madonna del Piano 10, 50019 Sesto Fiorentino (FI), Italy; [d] University of Virginia, 395 McCormick Rd, Charlottesville, Virginia 22904, USA

Synthesis of CHAR materials by MAP

The analyzed samples were obtained from a commercial tire waste (Michelin model Agilis 81- 195/65 R16C). The starting material was chopped into 2 cm x 2 cm chips and dried for 24 h at 65 °C in a ventilated oven before each experiment. The pyrolysis tests were carried out in an oven capable of up to 6 kW microwave (MW) power (Figure S1). A wide-angle measuring infrared thermometer completed the heating system. Equal amounts of chopped tire masses (m) were pyrolyzed at different MW power (P) under inert atmosphere (N_2). Experimental conditions are given in Table S1. Effects of different specific powers (MW power to sample mass ratio, P/m) in the 24-48 kW/kg range have been explored to obtain the CHAR_1 to CHAR_4 sample pool (Table S1), resulting in different chemico-physical properties. Prior to heating, each of the samples was inserted inside the oven in a borosilicate flask connected to a glass condensing system, so that liquids and gases could be collected in a flask and in a gasometer, respectively. Pyrolysis experiments were stopped and considered complete when no further gas evolution was detected, assuming that all susceptible organic material has been detached from the residue; hence, pyrolytic time was also specific power dependent (Table S1). The CHAR samples were recovered from the reactor as brittle pieces, milled to a homogeneous powder, separated from the leftover metal wires originally present in the tire with a magnet, and finally stored in a desiccator.

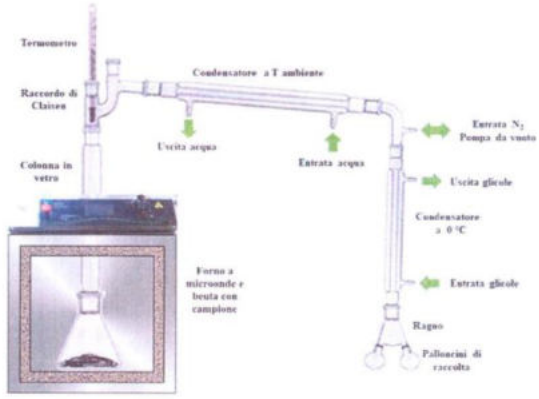

Figure S1: MAP apparatus.

Table S1. a) Experimental conditions for MAP treatment of tire samples: parameters and data; b) Experimental condition for CHAR heat treatment parameters and data.

a) MAP	*MW Power (W)*	*Tyre sample (g)*	*Char Weight (g)*	*Solid Yield (wt%)*	*MAP Time (min)[a]*	*Specific Power (kW/kg)[b]*
CHAR_1	1200	50	26.50	53	37	24
CHAR_2	1600	50	24.50	49	25	32
CHAR_3	1800	50	24.50	49	20	36
CHAR_4	**2400**	**50**	**24.00**	**48**	**11**	**48**
b) Heating	*Temperature °C*	*Char Weight before (mg)*	*Char Weight after (mg)*	*Solid Yield (wt%)*	*Heating Time (min)*	
150	150	20.4	15.1	74	60	
300	300	19.5	14.0	72	60	
450	450	18.9	10.8	43	60	
600	600	27.1	1.2	4.5	60	

[a] Completion time evaluated as the time after which no further gas evolution could be detected;

[b] MW Power (P) to mass (m) ratio (P/m).

Table S2. CHN Elemental analysis, BET specific surface area and X ray μ-CT data for all MAP samples.

Sample	*Elemental Analysis*			*BET area (m^2/g)*	*X ray μ-CT Surface/Volume*
	%C	%H	%N		
CHAR_1	86.97	1.00	0.33	29.60	7.4
CHAR_2	89.14	0.82	0.58	34.38	65.0
CHAR_3	85.68	0.67	0.35	41.30	15.7
CHAR_4	89.77	0.61	0.26	72.40	191.5

Table S3. Metal content from ICP-MS analysis. Values in ppm (mg/kg).

Sample	*Cd*	*Co*	*Cr*	*Cu*	*Fe*	*Ni*	*Zn*
CHAR_1	3.0	30	2.0	71.0	973	22	2980
CHAR_2	2.4	34.8	5.0	129	674	26	3180
CHAR_3	1.8	30.1	2.0	132	3543	18	2820
CHAR_4	3.1	162	2.0	72	984	13	3760

Table S4. Synopsis of electrocatalytic activity of all CHAR samples.

Sample	E_{on} [a] *(V)*	*RRDE*[b] *n e^- Calcd.*[c]
CHAR_1	-0.26	3.08 (0.249)
CHAR_2	-0.21	3.18 (0.252)
CHAR_3	-0.21	3.24 (0.225)
CHAR_4	-0.21	3.65 (0.248)

[a] vs. Ag/AgCl/sat.KCl;

[b] disk potential -0.55 V vs Ag/AgCl/sat.KCl; ring potential +0.50 V vs Ag/AgCl/sat. KCl;

[c] Number of exchanged electrons per O_2 molecule (n e^-) according to empirical collection numbers N Emp. (in brackets);

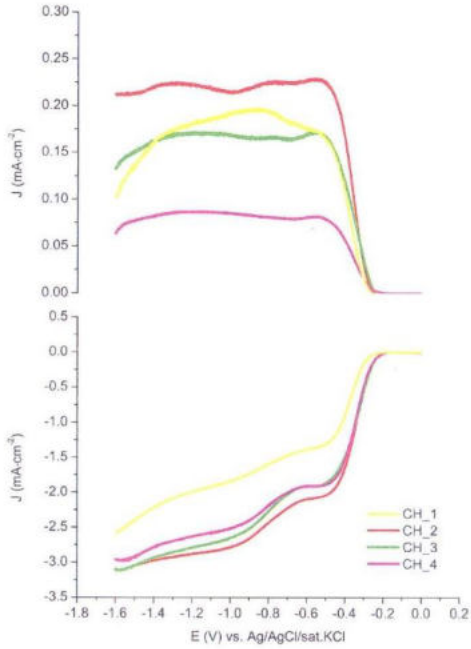

Figure S2. RRDE electrocatalytic performance for the ORR of CHAR materials from MAP. (Lower) Disk and (upper) Ring currents.

TEM-EDX analysis

TEM analysis has been carried out on samples (150, 300, 450) combined with EDX analysis.

Figure S3 SAMPLE150

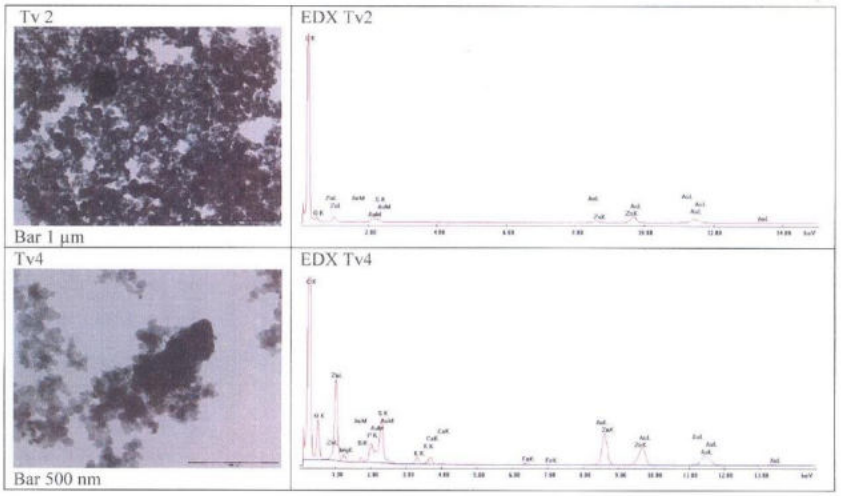

EDX Tv2

Element	Weight %
C K	82.4
O K	1.2
S K	0.6
Zn K	1.1
Au L	14.6
Total	100.0

EDX Tv4

Element	Weight %
C K	59.8
O K	5.4
Mg K	0.5
Si K	0.3
P K	1.8
S K	3.8
K K	0.7
Ca K	0.8
Fe K	0.3
Zn K	8.9
Au K	17.7
Total	100.0

Figure S4 SAMPLE 300

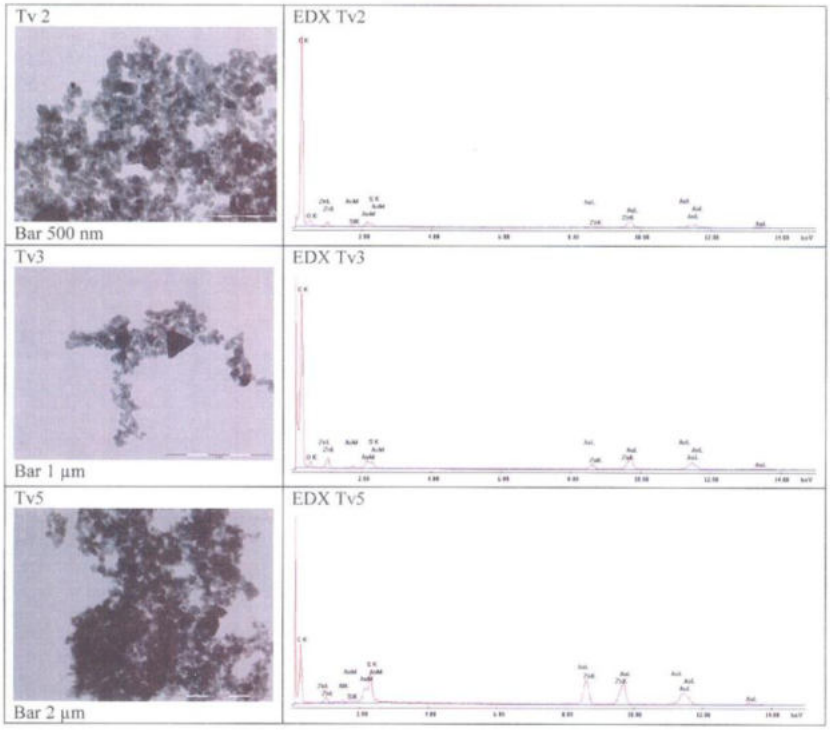

EDX Tv2

Element	Weight %
C K	78.7
O K	1.9
Si K	0.2
S K	0.5
Zn K	0.9
Au K	17.7
Total	100.0

EDX Tv3

Element	Weight %
C K	68.2
O K	1.4
S K	1.1
Zn K	2.6
Au L	26.8
Total	100.0

EDX Tv5

Element	Weight %
C K	27.6
Al K	0.3
Si K	0.4
S K	5.9
Zn K	16.2
Au L	49.7
Total	100.0

Figure S5 SAMPLE 450

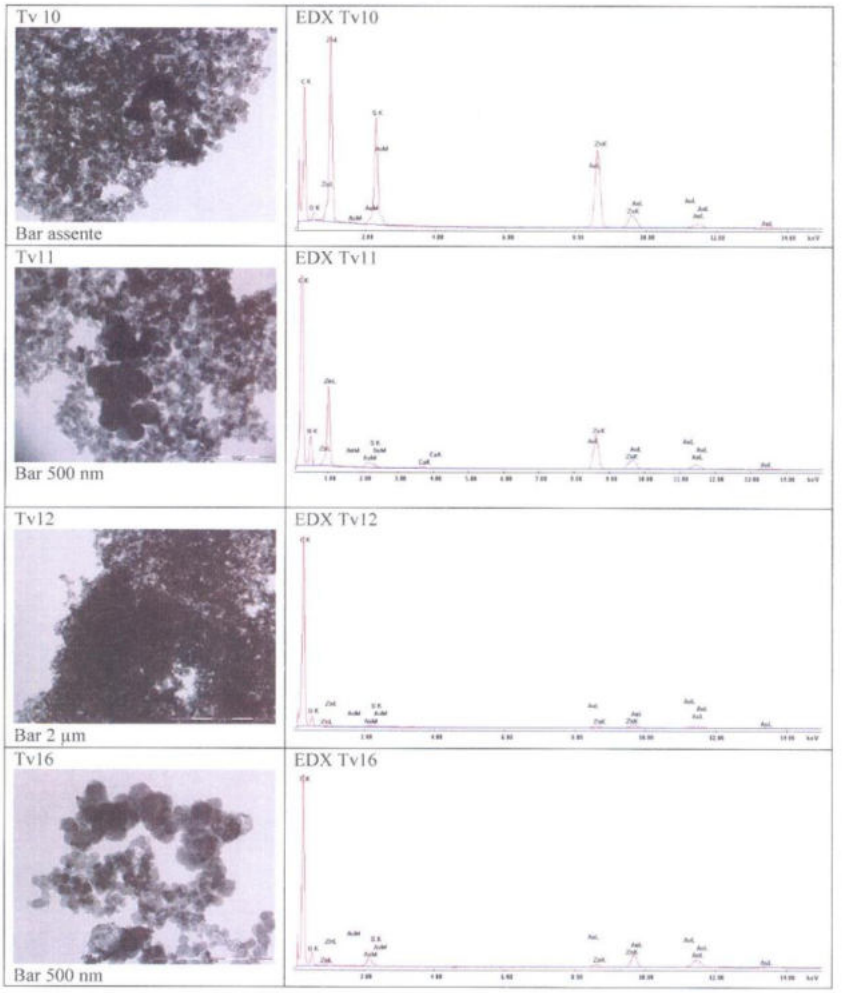

EDX Tv10

Element	Weight %
C K	40.1
O K	1.6
S K	14.1
Zn K	34.1
Au L	10.1
Total	100.0

EDX Tv11

Element	Weight %
C K	70.6
O K	5.3
S K	0.4
Ca K	0.2
Zn K	12.6
Au L	11.0
Total	100.0

EDX Tv12

Element	Weight %
C K	87.0
O K	3.3
S K	0.3
Zn K	1.3
Au L	8.1
Total	100.0

EDX Tv16

Element	Weight %
C K	67.3
O K	3.4
S K	0.2
Zn K	1.4
Au L	27.6
Total	100.0

Table S5: Physisorption data.

Sample	Surface area BET ($m^2 g^{-1}$)	Total pore volume ($cm^3 g^{-1}$)	Pore surface area ($m^2 g^{-1}$)
150	49.6697	0.553295	55.6890
300	54.7288	0.554955	61.3026
450	295.8339	1.028325	195.8634
600	82.9960	0.619985	76.1633
450_L	230.8507	0.761477	123.3706

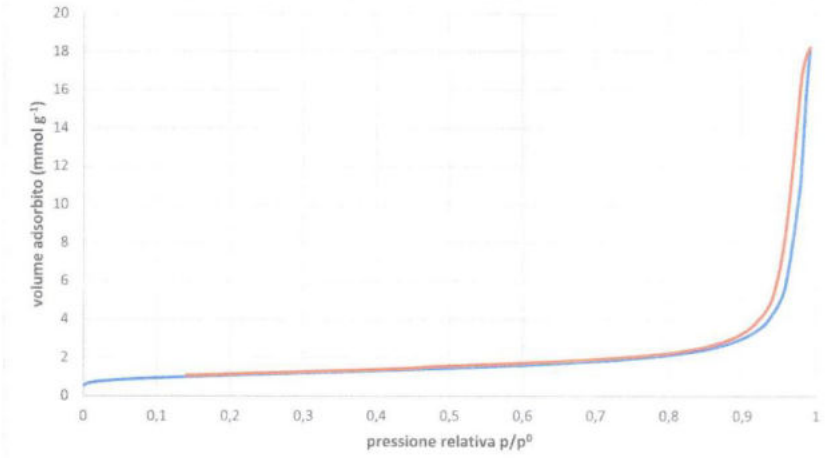

Figure S6: Absorption isotherm for sample 150.

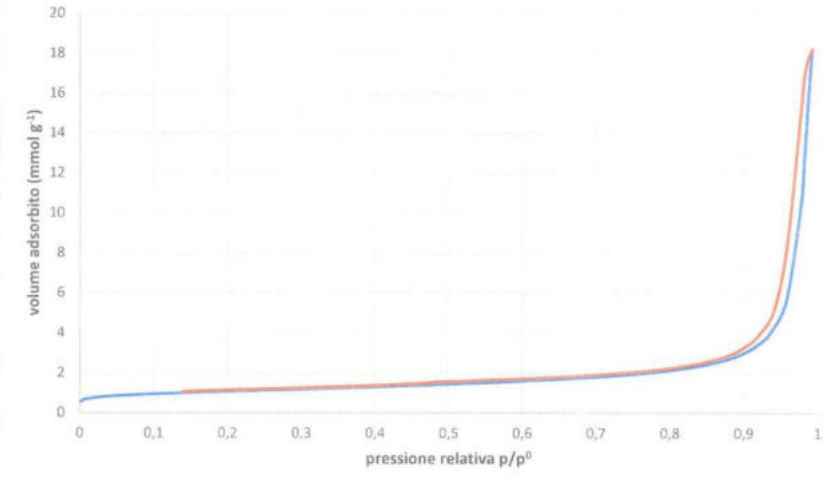

Figure S7: Absorption isotherm for sample 300.

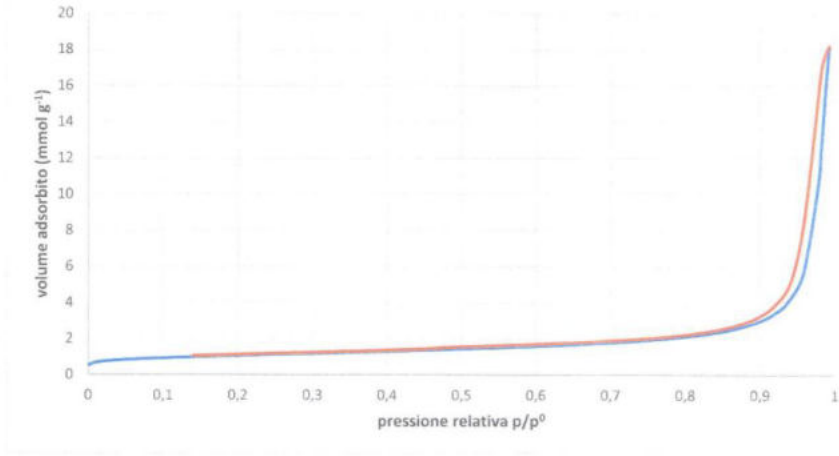

Figure S8: Absorption isotherm for sample 450.

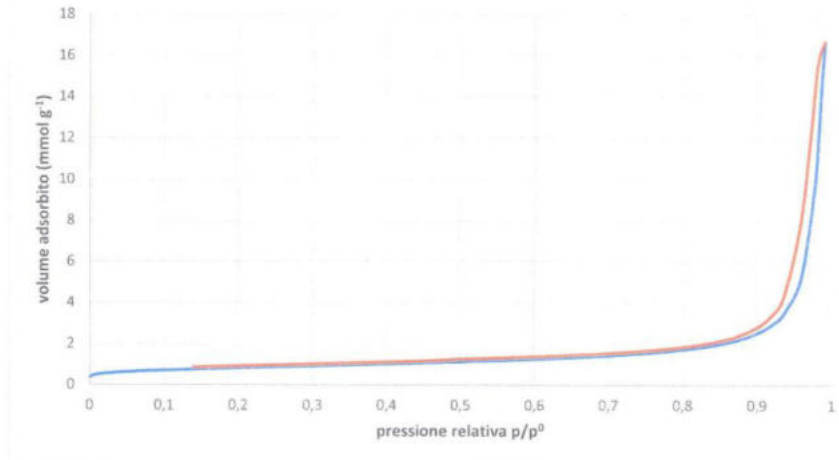

Figure S9: Absorption isotherm for sample 600.

7 Assembly stack Fuel cell

To complete the research of my work, the complete fuel cell was tested for each electrocatalyst studied. As previously described, a cell fuel is an electrochemical device in which it converts the free energy of the spontaneous chemical reaction into electrical energy. A specific electrolyte separates the two electrodes of a cell, anode and cathode, where oxidation and reduction reactions occur respectively. The fuel is fed to the anode and during the oxidation reaction the electrons are released at the anode catalyst layer. The electrons generated on the negative electrode through an external circuit flow towards the positive electrode where the reduction reaction occurs (reduction of an comb rent, oxygen or air). To closing the circuit, a flow of ionic species occurs in the electrolyte. Fuel cell may operate under continues flow of fuel (active fuel cell) or operate consuming the fuel contained in an tank directly connected to the anode (passive fuel cell).

7.1 Component of fuel cell

The core of a fuel cell is the so-called membrane electrode assembly (MEA). MEA the true "soul" of the fuel cell, is a sheet in which the solid electrolyte is located between the anode and cathode layers (also the gas diffusion layers) as in a “sandwich”.

Polymer Electrolyte Membrane (PEM) is membrane designed to conduct proton or hydroxyl ions while they don’t allow the passage of gaseous species such hydrogen and oxygen. This is fundamental condition to avoid the “crossover” of reactants with the loses of efficiency. PEMs are constituted by pure or composite polymer membranes Moreover it can be embedded with other materials into their polymer matrix. The essential

requisites for a membrane to be a good candidate for application in fuel cell are the following:

- High conductivity, to guarantees low ohmic losses
- Low permeability for reactants, to guarantees high efficiency to avoid the crossover of the fuel and second to evited the possibility of the cathode electro catalyst to operate both for oxidation of the fuel and oxygen reduction.
- Homogeneity of thickness, to avoid the formation of so called "hot spot" caused by a not homogeneous thickness that could be bring a differences local current density (high temperature) that may lead to local membrane breakdown.
- Good thermal stability, cell temperatures may reach up to over 80°C and its durability is required.
- Good mechanical resistance.

7.1.1 Catalyst Layers

The anode and cathode electrodes of a fuel cell are made by a two separated catalyst layers deposited on to opposite site of the PEM. The essential requisites for a catalyst layer to be a good candidate for application in fuel cell are the following:

- High surface area support material, to guarantees the dispersion of the electroactive material and also allows the fast transport of products and reactants. Moreover, to drive the electrons to the current collectors and to the external circuit, for this reason the support materials must have a good conductivity. At the end the stability represents a fundamental require as to avoid the corrosion phenomena especially on the cathode side.

- Electroactive phase, in fuel cell representative a crucial step in oxygen reduction reaction to enhance the velocity of the kinetics of the spontaneous reaction.
- The ionomer, to guarantees un additional ionic conductivity to the catalyst layers. Usually the ionomer is constituted by a number of monomeric units of polymer which constitute the PEM.
- A binder, its role is this hold together all components, above described.

Gas Diffusion Layer (GDL)

GDLs are usually made of carbon-fibre materials and their roles are:

- Distributes gases homogeneously, to prevent local hotspot and catalyst flooding (removing heat and excess water)
- To collect the electrons to or from a metal collector located beside of the GDL

To complete the fuel cell stack, it needs the presence of bipolar plates (usually high density graphite) to electrically connect each single cell, supply reagent gases and remove reaction products from MEA

7.2 FCs Performance parameters

7.2.1 Polarization characteristics

The quality and performance of FCs are joint to a variety of irreversible losses. The polarization curves are the way to valuated the losses in a fuel cell, here in were recorded a potential value output in response the applied electrical loading. Figure 7.1 showed three distinct polarization region in a real fuel cell:

- Activation region (Ƞact), the potential value is determinate electrochemical kinetics (overpotential for both anode and cathode reactions)
- Ohmic region polarization region, in this case the losses depend and obey Ohm's law (enhancement of the electrical resistance both the electronic, ionic conductors and quality of the contacts)
- Polarization of concentration, this type of loss occurs during the limits of mass transport and came from a depletion of reactant concentration in proximity of electrode. This phenomena be due to slow diffusion of the fuel through the electrode pores, solution/dissolution of reactants/products into/out of the electrolyte and the diffusion of reactants/products through the electrolyte to/from the electrochemical reaction site

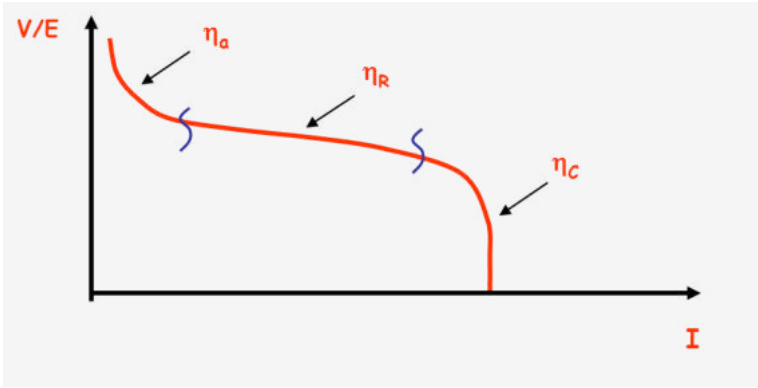

Fig. 7.1 Polarization and power density curves

Power density curve show a different graphical system to representation of the polarization curve. In this case, the correlation is between the current density and power density (define as the product of J and the potential)

7.2.2 Main operating parameters

The FC performances are closely linked, in addition to the nature of the catalyst, the MEA and the fuel, a specific operating condition:

- Temperature; Higher temperature, in addition to improve kinetics sluggish, increases the mass transport properties such as diffusion and even charge transport in ionic conductors. Working over 100°C temperature is dangerous for the stability of the PEM and al great production of water at cathode can bring a diminution of the partial pressure of oxygen. For practical purpose it is widely recognized the safety of the PEM and the better temperature for the PEMFCs is around 80°C.
- Stoichiometric Ratio; represent the ratio between the amount of actual reactant and reactant needed to exactly complete a reaction. A higher stoichiometric ratio increases the possibility that sufficient reactant reacts at each electrodes of Fuel Cell. In the case of PEMFCs fed with H2/O2, the good value is around 2.
- Gas pressure (liquid fuel concentration), partial pressure of gas reactant influenced strongly the performance of FCs. Although increase the value of the pressure the performance of FCs improve, high pressure requires more sophisticated device and may create problems like leakage The optimal operating working range for the fuel cell is among 1 and 3 atm.
- Humidity, the right humidification, the amount of water, allows the membrane to correctly transport of protons as water molecules. On the other hand excessive humidification leads a flooding phenomenal.

Operating working, FCs require gas supply with precise control of the relative humidity.

Introduction

State of the art low temperature proton exchange membrane fuel cells (PEM-FCs) are compact, yet high power-density systems ideal for automotive application [1]. Corrosion problems associated with the acidic nature of the proton exchange membrane (PEM) and the high cost of the platinum based anodic and cathodic electrocatalysts and of the Nafion® membrane, are the main limiting factor for these devices. Replacing the PEM with an alkaline anion exchange polymeric electrolyte (AEM) is one way to overcome these problems. H_2/O_2 fed anion exchange membrane fuel cells (AEM-FCs) are the most attractive alternative to traditional PEMFCs. In fact, the alkaline environment is less corrosive for FC components and allows in principle the use of non-noble metal based catalysts [2,3,4]. Platinum-based electrocatalysts are the main limiting factor hindering the large scale development of proton exchange membrane fuel cells, due to the high cost of this metal and to the high Pt loading necessary to speed up the sluggish ORR reaction in H_2/O_2 PEMFCs . Another limiting factor of platinum based catalysts is the CO poisoning effect. Unfortunately, Pt and its alloys are the best catalytic materials for the hydrogen reactions and for the oxygen reduction reaction performed in acidic environments. Platinum is also the only metal that can tolerate the strong acidic environment of proton exchange membranes [5-7].

Operating in an alkaline environment is the only way to overcome these issues as in principle non platinum electrocatalysts, even non noble based electrocatalysts, can be used and the reactions kinetics are generally faster

with respect to acidic conditions. Alkaline conditions are also much less corrosive for FCs components . The main drawback of traditional Alkaline Fuel Cells is the liquid electrolyte, a highly concentrated KOH aqueous solution, that suffers from drying and flooding effects and of poisoning due to absorption of atmospheric CO_2 [5,7].

Regarding the cathodic catalyst, in alkaline environment platinum can be replaced by choice of non-noble metals In this regard the potential cathode electrocatalyst object of this research project, above described and studied in half cell, was tested in complete fuel cell.

7.3 Experimental Section (Fuel cell testing)

7.3.1 Membrane electrode assembly (MEA) fabrication

The anodic and the cathodic electrodes (5 cm^2) were obtained by spreading an ink of the catalytic powder sprayed onto a Toray TGP-H-60 carbon paper gas diffusion substrate (Alfa Aesar, non-teflonated), and dried in air (Fig. 7.2)

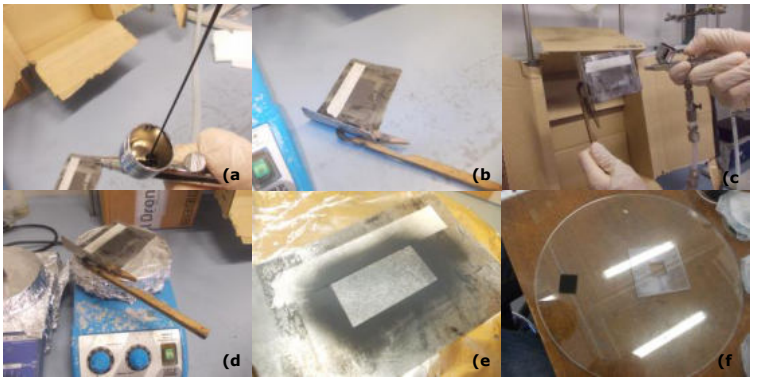

Fig. 7.2 Spreading ink of the catalytic powder sequences onto a Toray TGP-H-60; a)

The inks were prepared by mixing the catalytic powder with bidistilled water, 2-propanol and the radiationgrafted ETFE-based anion-exchange ionomer powder (IEC =1.24 0.06 mmol g/1) [10] in a 5 mL high density polyethylene vial [10]. The mixture was suspended with three pulses of ultrasound of 20 W power at the frequency of 20 kHz (Bandelin Sonor pulse UW 2200 SERIES) for 30 min. The choice of the cathodic catalyst for the complete cell test was made on the basis of the samples being studied in this thesis which obtained the best results in half a cell: Eon, number of electrons for the O_2 molecule. The table 7.1shows the catalyst used for cathode inks and the relative quantity of catalyst for the surface unit in addition to the value of the precious metal (sample of Pd-MWCNT). For all MEAs were used the same anodic electrodes contening 0,489 $mg_{PtRu/C.}*cm^{-2}$ using a catalytic powder composite of PtRu/C (20 wt% Pt and 10 wt% Ru) for the preparation of the ink. [11].

Entry	Cathode Catalyst	$mg_{cat.}*cm^{-2}$	$Mg_{Pd}*cm^{-2}$
MEA509	**CH_4_450°**	1,00	-
MEA510	**CH_4_450°**	1,35	-
MEA511/513	**MWCNT HL2** **Pd(II)** 86,1%	2,86	0,064

Table 7.1 Cathode catalyst loading

The anion exchange solid polymer membrane used in the AEM-FCs was a high-density polyethylene (HDPE)-based radiation-grafted anion-exchange membrane (RG-AEM) [10] that achieves a surprisingly high

peak power density and a low in situ degradation rate (with configurations tailored to each)

All electrodes and AEMs were immersed in aqueous KOH solution (1 M) for 1 h and then washed thoroughly in water (to remove excess KOH) before assembly into a 5 cm^2 fuel cell fixture using 5 m torque (Fig. 7.3).

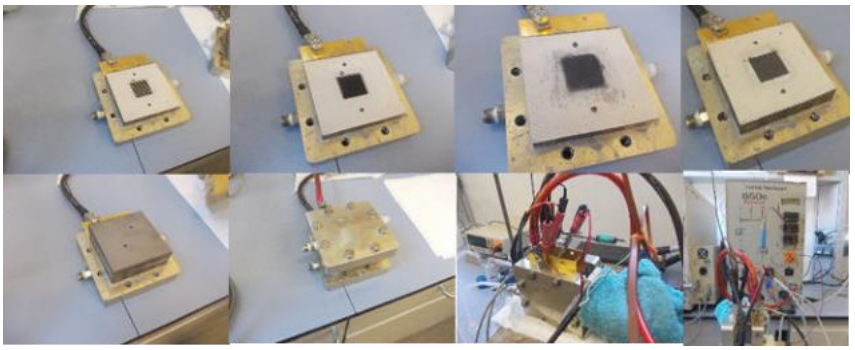

Fig. 7.3 Membrane Electrodes Assembly

7.3.2 Fuel cell performance data collection

An 850e fuel cell test station (Scribner Associates, USA) was used for testing. The fuel cell temperature and the dew point for both supplies of anode and cathode gas (calculated relative humidity, UR) were chosen in order to determine the best operating condition to obtain the maximum efficiency of the cell in terms of specific power supplied. These values will be reported in the following paragraphs for each sample/ experiments. All followers (heated lines between the fuel cell tester and the fuel cell device) were set to the same temperatures as the gas dew points. H_2 and O_2 gas feeds with flow rates of 1 and 2 L min^{-1} (SLPM) were supplied to the anode and cathode, respectively, with no back-pressurization. The MEAs were

activated by discharging the cell at a constant voltage of 0.5 V during cell heating, until a steady current density was observed. Beginning-of-life AEMFC performance data were collected under controlled galvanostatic discharge steps where data (at each current density) were recorded after potentials had stabilized. The internal ohm resistances were estimated using the 850e instrument's internal current interrupt method.

7.3.3 MEA Sample CH_4_450°

The table 7.2 shows the operating parameters for the study of the polarization and power density curves (Fig. 7.4) of the various scans relating to MEA_509.

Sample	OCV (V)	Temp (°C)	Temp Cathode (°C)	Temp Anode (°C)	Flow Cathode (l/min)	Flow Anode (l/min)	RH Cathode (%)	RH Anode (%)	Resistance milli omh
MEA509_1	72,66	65	62	62	1,95	0,97	87	87	27
MEA509_2	76,18	65	62	62	1,95	0,97	87	87	14-15
MEA509_3	75,87	65	62	62	1,95	0,97	87	87	14-15
MEA509_4	74,80	64	62	62	1,94	1,95	91	91	14-15
MEA509_5	75,72	65	62	62	1,94	1,94	87	87	13-14

Table 7.2 MEA509 Operating parameters

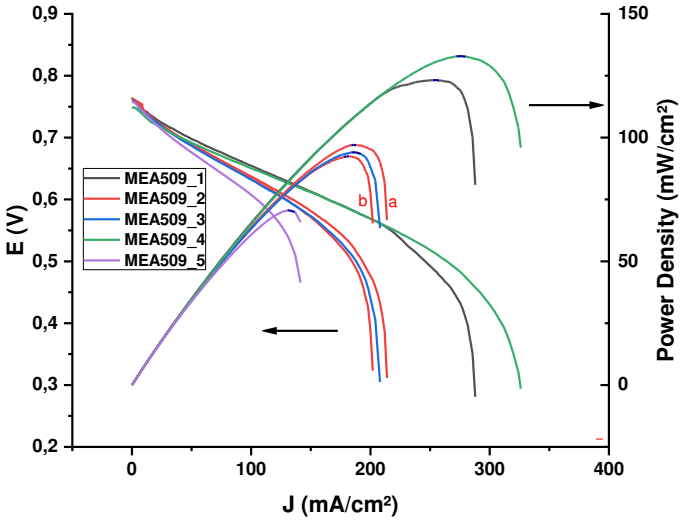

Fig. 7.4 Polarization and power density curves for the MEA 509

The results relating to the performance of the complete cell of the CH_4_450 ° sample are summarized in table 7.3. It is possible to observe the achievement of a peak of power density in the scan 4, of 132 mW / cm^2.

Sample		J	Power	Power Density (MAX)	E	J (MAX)	Power	Power Density (MAX)	E
		(mA/cm²)	(Watts)	(mW/cm²)	(V)	(mA/cm²)	(Watts)	(mW/cm²)	(V)
MEA509_1		255,66	0,61643	123,29	0,48223	287,94	0,40463	80,925	0,28105
MEA509_2	a	185,97	0,48535	97,069	0,52195	213,95	0,33298	66,596	0,31127
	b	179,88	0,462	92,399	0,51367	202,03	0,32661	65,321	0,32332
MEA509_3		188	0,47012	94,023	0,50013	208,02	0,31716	63,433	0,30494
MEA509_4		276,02	0,66468	132,94	0,48161	326,12	0,47975	95,95	0,29421
MEA509_5		131,87	0,35316	70,631	0,53562	141,44	0,3293	65,86	0,46562

Table 7.3 MEA509 Data Analysis

A second complete cell (MEA_510) containing the CH_4_450 ° sample was assembled using an ink containing a catalyst load greater than about

30 compared to MEA_509. The table 7.4 shows the operating parameters relating to the study of polarization and power density curves (Fig. 7.5) of the various scans relating to MEA_510.

Sample	OCV (V)	Temp (°C)	Temp Cathode (°C)	Temp Anode (°C)	Flow Cathode (l/min)	Flow Anode (l/min)	RH Cathode (%)	RH Anode (%)	Resistencemilliomh
MEA510_1	0,76	55	52	52	1,97	1,00	86	86	16-17
MEA510_2	0,74	59	54	54	1,96	1,00	79	79	22-17
MEA510_3	0,72	50	45	45	1,94	1,01	77	77	20

Table 7.4 MEA509 Operating parameters

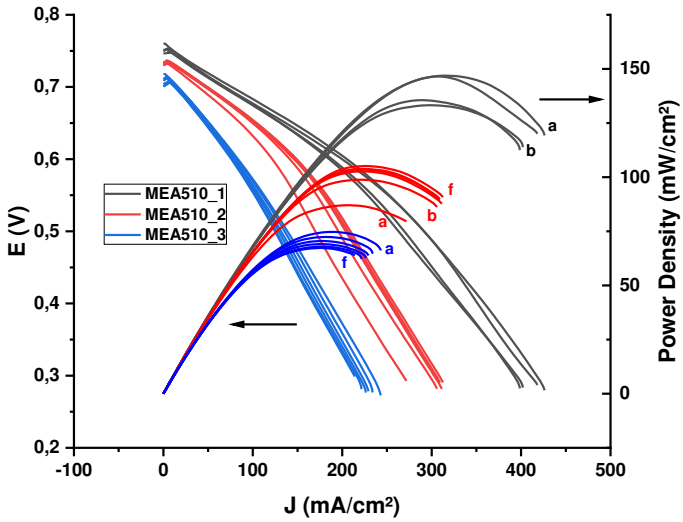

Fig. 7.5 Polarization and power density curves for the MEA510

The results related to the performance of the MEA510 are summarized in table 7.5 It is possible to observe the achievement of a peak of power density in scan 1 in the first cycle, of just under 150 mW / cm^2.

Sample		J	Power	Power Density (MAX)	E	J (MAX)	Power	Power Density (MAX)	E
		(mA/cm²)	(Watts)	(mW/cm²)	(V)	(mA/cm²)	(Watts)	(mW/cm²)	(V)
MEA510_1	a	314,51	0,73452	146,9	0,46709	426,37	0,59649	119,3	0,2798
	b	297,09	0,66619	133,24	0,44848	401,88	0,56924	113,85	0,28329
MEA510_2	a	206,43	0,43527	87,054	0,42172	271,73	0,39765	79,53	0,29269
	b	221,87	0,49398	98,795	0,44528	305,88	0,43086	86,173	0,28172
	c	224,79	0,51342	102,68	0,4568	311,42	0,43857	87,715	0,28166
	d	221,06	0,51817	103,63	0,46881	308,79	0,44766	89,532	0,28994
	e	219,94	0,52529	105,06	0,47767	312,63	0,45422	90,843	0,29057
	f	220,43	0,51897	103,79	0,47087	309,28	0,44943	89,886	0,29063
MEA510_3	a	188,53	0,37371	74,742	0,39645	242,81	0,33099	66,198	0,27263
	b	182,04	0,36192	72,384	0,39763	233,76	0,32331	64,662	0,27662
	c	181,57	0,35251	70,501	0,38829	229,42	0,31941	63,882	0,27845
	d	177,63	0,3455	69,101	0,38901	226,25	0,3128	62,56	0,2765
	e	177,25	0,33968	67,937	0,38329	221,48	0,31151	62,301	0,2813
	f	176,96	0,33643	67,287	0,38023	214,14	0,31989	63,978	0,29877

Table 7.5 MEA510 Data Analysis

7.3.4 Discussion MEA CH_4_450°

The results of the complete cells containing as catalysts the carbon coming from the map of waste tyres, in particular the sample CH_4_450 °, show a comparable maximum power density, if not slightly better than works containing carbonaceous materials without noble metals [11]. As expected, the MEA_510 manages to deliver a greater maximum power to the MEA_509. This improvement is certainly linked to an increase in the concentration of (non-noble) metals in the cathode due to a higher catalyst load in ink preparation. Unfortunately, due to problems related to overvoltage phenomena due to diffusion, both cells show stability problems.

7.3.5 MEA Sample MWCNT HL2 Pd(II)

Table 7.6 shows the operating parameters related to the study of polarization and power density curves (Fig. 7.6) of the various scans relating to MEA511.

Sample	OC V (V)	Temp (°C)	Temp Cathode (°C)	Temp Anode (°C)	Flow Cathode (l/min)	Flow Anode (l/min)	RH Cathode (%)	RH Anode (%)	Resistence milli omh
MEA511_1	72	50	45	45	1.97	1.00	77	77	20
MEA511_2	68	60	54	54	1,97	1,00	75	75	27
MEA511_3	69	60	54	54	1,97	1,00	75	75	20
MEA511_4	7,2	60	54	54	1,96	1,00	75	75	22
MEA511_5	69	65	58	58	1,96	1,00	72	72	22

Table 7.6 MEA511 Operating parameters

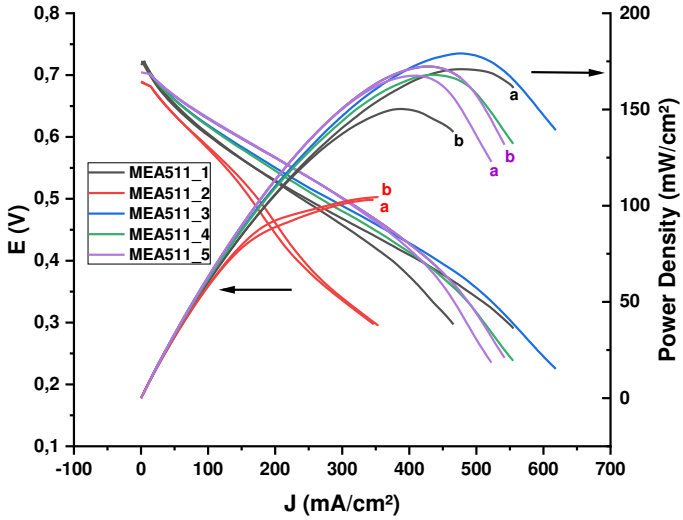

Fig. 7.6 Polarization and power density curves for the MEA511

The results relating to the performance of the complete cell of the MWCNT HL2 Pd (II) sample are summarized in table 7.7. The performance results related to MEA_511 are very variable, as in this case the best operating conditions were looked for with particular attention. It is possible to observe the achievement of a peak of power density in scan 3, of just under 179 mW / cm^2.

Sample		J	Power	Power Density (MAX)	E	J (MAX)	Power	Power Density (MAX)	E
		(mA/cm²)	(Watts)	(mW/cm²)	(V)	(mA/cm²)	(Watts)	(mW/cm²)	(V)
MEA511_1	a	474,03	0,85476	170,95	0,36064	555,02	0,80556	161,11	0,29028
	b	389,69	0,75123	150,25	0,38555	465,82	0,69156	138,31	0,29692
MEA511_2	a	345,17	0,51518	103,04	0,29851	345,17	0,51518	103,04	0,29851
	b	353,69	0,52124	104,25	0,29474	353,69	0,52124	104,25	0,29474
MEA511_3		476,1	0,89552	179,1	0,37619	618,4	0,69623	139,25	0,22517
MEA511_4		434,92	0,83974	167,95	0,38616	554,96	0,66084	132,17	0,23816
MEA511_5	a	407,27	0,83781	167,56	0,41143	522,44	0,6142	122,84	0,23513
	b	430,52	0,86159	172,32	0,40026	541,94	0,65822	131,64	0,24292

Table 7.7 MEA511 Data Analysis

Once the best operating parameters were identified, a second complete cell was assembled (MEA513). Table 7.8 shows the operating parameters relating to the study of polarization and power density curves (Fig. 7.7) of the various scans relating to MEA513.

Sample	OCV (V)	Temp (°C)	Temp Cathode (°C)	Temp Anode (°C)	Flow Cathode (l/min)	Flow Anode (l/min)	RH Cathode (%)	RH Anode (%)	Resistence milli omh
MEA513_1	0,62	61	54	54	1,97	1,00	72	72	25
MEA513_2	0,62	60	54	54	1,97	1,00	75	75	25
MEA513_3	0,62	60	54	54	1,97	1,00	75	75	23
MEA513_4	0,65	60	54	54	1,96	1,00	75	75	20

Table 7.8 MEA513 Operating parameters

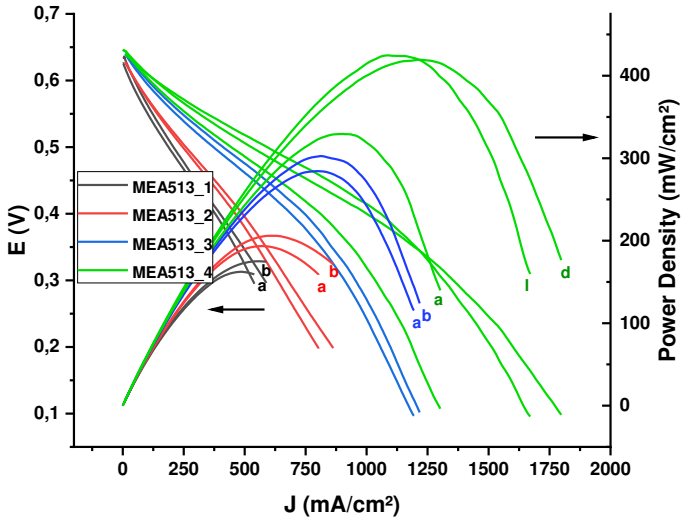

Fig. 7.7 Polarization and power density curves for the MEA513

The results relating to the performance of the MEA_513 are summarized in table 7.9. It is possible to observe the achievement of a peak of maximum power density in the scan 4 of over 400 mW / cm^2.

Sample		J	Power	Power Density (MAX)	E	J (MAX)	Power	Power Density (MAX)	E
		(mA/cm²)	(Watts)	(mW/cm²)	(V)	(mA/cm²)	(Watts)	(mW/cm²)	(V)
MEA513_1	a	485,96	0,81154	162,31	0,334	539,81	0,79601	159,2	0,29492
	b	552,55	0,87554	175,11	0,31691	589,09	0,87208	174,42	0,29608
MEA513_2	a	549,62	0,96557	193,11	0,35136	802,63	0,7933	158,66	0,19767
	b	613,96	1,0302	206,04	0,33559	862,67	0,85526	171,05	0,19828
MEA513_3	a	803,82	1,4216	284,32	0,35371	1193,9	0,57733	115,47	0,09671
	b	811,67	1,513	302,6	0,37281	1217,9	0,61984	123,97	0,10179
	a	901,95	1,6472	329,44	0,36525	1302	0,69879	139,76	0,10734
	b	958,25	1,746	349,19	0,36441	1397,7	0,74964	149,93	0,10727

MEA513_4	c	1148,1	1,979	395,8	0,34474	1594,3	1,0081	201,61	0,12646
	d	1219,9	2,0973	419,46	0,34384	1798	0,88232	176,46	0,09815
	e	1127,6	2,0173	403,47	0,35782	1613,1	0,79962	159,92	0,09914
	f	1035,7	1,9711	394,23	0,38065	1537,5	0,76939	153,88	0,10008
	g	1007,4	1,9522	390,43	0,38757	1470	0,6982	139,64	0,09499
	h	1091,2	2,0804	416,08	0,38132	1574,5	0,76063	152,13	0,09662
	i	1108,8	2,098	419,61	0,37844	1645,7	0,80729	161,46	0,09811
	l	1085,8	2,1234	424,68	0,39112	1671	0,79819	159,64	0,09553

Table 7.9 MEA513 Data Analysis

7.3.6 Discussion MWCNT HL2 Pd(II)

The results of the complete cells containing as a catalyst the MWCNT HL2 Pd (II) sample, show a maximum power density, in particular in MEA_513, of considerable interest. Specifically, it has been observed that it is able to deliver a specific power density of 6.25 W / mg_{Pd} cm^2. This result is comparable, if not slightly higher, to a work by Wang et al. [10] (5 W / mg_{Pd} cm^2). This work of literature was taken as a reference, as it presents the same setup in the assembly of the MEA (anode and AEM) except the cathode. The behaviour of the MEAs containing the MWCNT HL2 Pd (II) sample, once the best operating parameters have been found, appears to be completely different with respect to the cells composed of carbons cathode catalyst. Surely the explanation of this phenomenon lies in the stabilization of the catalyst with the increase in the work of the MEA itself, effectively reducing the overvoltages linked to the diffusion.

8 Conclusion

The oxygen reduction reaction (ORR) plays an important role in the industrial sector, especially in systems for the conversion of chemical energy into electrical energy, such as fuel cells. However, the technical applications are limited by the kinetics of the process and the difficulty in regulating the catalytic activity. To date, platinum is the metal that shows the greatest catalytic activity but its high cost actually limits its use in a massive form. In this context, the study of electrocatalysts is aimed at obtaining catalysts with a low platinum content, up to completely replacing them with less precious metals or materials. During these three years of doctorate two types of possible cathodic catalysts have been studied to be used in fuel cells.

One deriving from the reuse of waste material and one coming synthetically. In the first case, a pyrolysis coal was tested, using a microwave oven, out of motor vehicle tires. The second type, multiwalled carbon nanotubes, functionalized with binders, with and without a metal in particular palladium were evaluated. While for char obtained from MAP the winning card lies in the fact that the material used is at "cost O", for the functionalized carbon nanotubes studied they are an important alternative to classical catalysts, since the adsorption on the surface of a binder organic that complex cations of an active metal against ORR, like Pd (II), allows to obtain catalytic sites constituted by single ions uniformly distributed on the surface of the nanotube with the consequence of a decrease in terms of mass of the metal content noble clerk.

Electrochemical parameters such as the average number of electrons exchanged and the onset potential are considered as keys for understanding the complex chemistry of the O_2 reduction process in an alkaline aqueous

environment. The experimental methods used to determine the number of electrons exchanged are the Koutecky-Levich method (RDE) and the RRDE method.

The data collected in this doctoral thesis study show an excellent electrocatalytic performance in the reduction of half-cell oxygen both for the char obtained from MAP of waste tyres, in particular for the CH_4_450 ° sample and for the MWCNT HL2 Pd (II) synthesis sample which surprisingly presents a positive potential shift with respect to a platinum electrode of almost 50 millivolts, besides exchanging almost 4 electrons per water molecule. From the data obtained it can be deduced that the complexation of Pd (II) of an azamacrocycle (HL2) adsorbed on the graphitic surface of carbon nanotubes, allows to significantly reduce the mass of Pd with respect to the catalysts in which the metal is present in the massive state, without cause loss of catalytic activity.

Subsequently the samples were tested in a complete cell. As regards the CH_4_450 ° sample, the results obtained confirm only partially those observed in the half-cell. If on the one hand the results relating to the maximum power reached are in line with those present in the literature of similar works which use materials of a carbonaceous nature free of precious metals as cathode catalysts, the MEA does not seem to have good stability over time. Although the study on the complete cell presented some difficulties, it should not be forgotten that the material used comes after a treatment of a waste. Given that increasing the catalyst load on the MIO assembly, consequently the quantity of metals, P max tends to increase, further studies must be carried out in this sector in order to maximize the improvement of results.

As regards the performance of the MEA containing the cathodic catalyst the sample MWCNT HL2 Pd (II), the results obtained are extremely convincing. In fact the value of the specific maximum power, or the power density per unit of mass of precious loaded on the catalyst, turns out to be better than other articles present in the literature. Furthermore, a good level of performance was observed over time. Certainly further studies must be carried out as, also in the anodic compartment, the MWCNT HL2 Pd (II) sample is used both in alkaline and direct alcohol cells.

References

1. M. K. Debe, Nature 2012, 486, 43–51.

2. J. Ohyama, T. Sato, A. Satsum, J. Power Sources 2013, 225, 311–315.

3. D. J. Ham, C. Pak, G. H. Bae, S. Han, K. Kwon, S. A. Jin, H. Chang, S. H. Choi, J. S. Lee, ChemComm. 2011, 47, 5792–5794.

4. M. Piana, M. Boccia, A. Filpi, E. Flammia, H. a. Miller, M. Orsini, F. Salusti, S. Santiccioli, F. Ciardelli, A. Pucci, J. Power Sources 2010, 195, 5875–5881.

5. Y.J. Wang, J. Qiao, R. Baker, J. Zhang, Chem Soc Rev 2013, 42, 5768.

6. T. Fujigaya, C. Kim, K. Matsumoto, N. Nakashima, ChemplusChem 2014, 79, 400–405.

7. [62] S. F. Lu, J. Pan, B. Huang, L. Zhuang, J. T. Lu, Proc. Natl. Acad. Sci. U. S. A. 2008, 105, 20611–20614.

8. [63] Y. S. Li, T. S. Zhao, Z. X. Liang, J. Power Sources 2009, 187, 387–392.

9. [64] J. Xu, P. Gao, T. S. Zhao, Energy Environ. Sci. 2012, 5, 5333.

10. L. Wang, X. Peng, W. E. Mustain and J. R. Varcoe , Energy & Environmental Science Issue 5, 2019

11. L. Wang, M. Bellini, H. A. Miller and J. R. Varcoe, J. Mater. Chem. A, 2018, 6, 15404–15412 | 15405 J. Mater. Chem. A, 2018, 6, 15404 DOI: 10.1039/c8ta04783a.

9 Publications During the PhD period

Still within and in line with the research project “Electrochemical study, design and realization of modified substrate of energy interested with low environmental impacts” carried out in these three years doctorate, in addition to the study of catalysts for fuel cells, I dealt with carry out further research in the electrochemical field. In particular I used electrochemical technique known as electrochemical atomic layer deposition (E-ALD) to manufacture high-quality monolayers and multilayers of metal on materials. With E-ALD, we can exploit the potential deposition (UPD) methodology (i.e., the property of some materials to be deposited as a monolayer before massive electrochemical deposition). In addition, E-ALD allows the composition, morphology, and structure of an aqueous solution at low temperature to be controlled. The major goal of our research has been to demonstrate that it demonstrates that E-ALD can be used to efficiently fabricate high-quality monolayers and multilayers of pseudo-2D materials. This research has resulted in the publication in scientific journals of the sector.

materials

MDPI

Article

Investigations on the Electrochemical Atomic Layer Growth of Bi_2Se_3 and the Surface Limited Deposition of Bismuth at the Silver Electrode

Walter Giurlani [1,2,*], Andrea Giaccherini [2,3], Nicola Calisi [2,4], Giovanni Zangari [5], Emanuele Salvietti [1,2], Maurizio Passaponti [1,2], Stefano Caporali [2,4,6,7] and Massimo Innocenti [1,2,*]

1 Dipartimento di Chimica, Università degli Studi di Firenze, via della Lastruccia 3, 50019 Sesto Fiorentino, Italy; emanuele.salvietti@unifi.it (E.S.); maurizio.passaponti@unifi.it (M.P.)
2 Consorzio Interuniversitario Nazionale per la Scienza e Tecnologia dei Materiali, via Giusti 9, 50121 Florence, Italy; andrea.giaccherini@unifi.it (A.G.); nicola.calisi@unifi.it (N.C.); stefano.caporali@unifi.it (S.C.)
3 Dipartimento di Scienze della Terra, Università degli Studi di Firenze, via La Pira 4, 50121 Firenze, Italy
4 Dipartimento di Ingegneria Industriale, Università degli Studi di Firenze, via S. Marta 3, 50139 Florence, Italy
5 Department of Materials Science and Engineering, University of Virginia, Charlottesville, VA 22904, USA; gz3e@virginia.edu
6 Istituto dei Sistemi Complessi, Consiglio Nazionale delle Ricerche, via Madonna del Piano 10, 50019 Sesto Fiorentino, Italy
7 Istituto di Geoscienze e Georisirse, Consiglio Nazionale delle Ricerche, via La Pira 4, 50121 Florence, Italy
* Correspondence: walter.giurlani@unifi.it (W.G.); m.innocenti@unifi.it (M.I.); Tel.: +39-055-457-3097 (W.G.); +39-055-457-3102 (M.I.)

Received: 28 June 2018; Accepted: 8 August 2018; Published: 14 August 2018

check for updates

Abstract: The Electrochemical Atomic Layer Deposition (E-ALD) technique is used for the deposition of ultrathin films of bismuth (Bi) compounds. Exploiting the E-ALD, it was possible to obtain highly controlled nanostructured depositions as needed, for the application of these materials for novel electronics (topological insulators), thermoelectrics and opto-electronics applications. Electrochemical studies have been conducted to determine the Underpotential Deposition (UPD) of Bi on selenium (Se) to obtain the Bi_2Se_3 compound on the Ag (111) electrode. Verifying the composition with X-ray Photoelectron Spectroscopy (XPS) showed that, after the first monolayer, the deposition of Se stopped. Thicker deposits were synthesized exploiting a time-controlled deposition of massive Se. We then investigated the optimal conditions to deposit a single monolayer of metallic Bi directly on the Ag.

Keywords: bismuth; bismuth selenide; topological insulator; E-ALD; UPD

1. Introduction

Bismuth (Bi) and antimony chalcogenides, where the chalcogenide is selenium (Se) or tellurium (Te), exhibit excellent thermoelectric properties, achieving thermoelectric figure of merit (ZT) values of about 1 [1]. These materials commonly crystallize in a rhombohedral structure and exhibit semiconducting behavior (band gap ~0.3 eV). Beyond thermoelectric behavior, these materials show an insulating response in the bulk material while exhibiting metallic conductivity at grain boundaries or surfaces; surface states in particular, are protected via time reversal symmetry, such that electron scattering does not occur [2]. Recently, it has also been shown that the electrochemical growth of Bi_2Se_3 at low temperatures results in the formation of an orthorhombic structure with a higher band gap of about 1.1 eV [3,4]. Of interest, in the context of light absorbers and solar cells, the same behavior

Chapter 5

E-ALD: Tailoring the Optoeletronic Properties of Metal Chalcogenides on Ag Single Crystals

Emanuele Salvietti, Andrea Giaccherini, Filippo Gambinossi, Maria Luisa Foresti, Maurizio Passaponti, Francesco Di Benedetto and Massimo Innocenti

Additional information is available at the end of the chapter

http://dx.doi.org/10.5772/intechopen.71014

Abstract

Technological development in nanoelectronics and solar energy devices demands nanostructured surfaces with controlled geometries and composition. Electrochemical atomic layer deposition (E-ALD) is recognized as a valid alternative to vacuum and chemical bath depositions in terms of growth control, quality and performance of semiconducting systems, such as single 2D semiconductors and multilayered materials. This chapter is specific to the E-ALD of metal chalcogenides on Ag single crystals and highlights the electrochemistry for the layer-by-layer deposition of thin films through surface limited reactions (SLRs). Also discussed herein is the theoretical framework of the under potential deposition (UPD), whose thermodynamic treatment open questions to the correct interpretation of the experimental data. Careful design of the E-ALD process allows fine control over both thickness and composition of the deposited layers, thus tailoring the optoelectronic properties of semiconductor compounds. Specifically, the possibility to tune the band gap by varying either the number of deposition cycles or the growth sequence of ternary compounds paves the way toward the formation of advanced photovoltaic materials.

Keywords: E-ALD, Ag(111), thin films, metal chalcogenides, UPD, photovoltaics

1. Introduction

Improving the efficiency of the deposition techniques of compound semiconductors could be crucial for the future sustainable micro and nano-electronic industry. A common challenge

ECS Transactions, 80 (10) 749-756 (2017)
10.1149/08010.0749ecst ©The Electrochemical Society

Morphology and Composition of Cu_2S Ultra-Thin Films Deposited by E-ALD

F. Russo[a], A. Giaccherini[a], E. Salvietti[a], E. Berretti[a], M. Passaponti[a], A. Lavacchi[b†], G. Montegrossi[c], E. Piciollo[d], F. di Benedetto[e] and M. Innocenti[a,b,†]

[a] Department of Chemistry, University of Florence, Via della Lastruccia 3, 50019, Sesto Fiorentino (FI), Italy
[b] CNR – Istituto dei Composti Organometallici (ICCOM), Via Madonna del Piano 10, 50019, Sesto Fiorentino (FI), Italy
[c] The Institute of Geosciences and Earth Resources, CNR, Firenze (FI), Italy
[d] LEM, Via Valiani 55, 52021 Levane, Arezzo, Italy
[e] Department of Earth Sciences, University of Florence, Via la Pira 4, 50121, Firenze (FI), Italy
[†]Active ECS Member

CIGS are very promising semiconducting materials for solar energy conversion, but at the same time are considered unfavorable for the large scale exploitation. Thus, the scientific community is focusing attention on new compounds based on economic and low-environmental impact elements such as Cu, Sn, Fe and Zn. Exploiting electrodeposition by means of Electrochemical Atomic Layer Deposition (E-ALD) it is possible to grow ultra-thin films of semiconductors with tunable properties, such as copper sulphides films grown on Ag(111) single crystals. Considering the E-ALD scheme one would expect a CuS hexagonal structure (covellite) with no any important electronic properties, but recently operando Surface X-Ray Diffraction (SXRD) studies were able to show the presence of a chalcocite phase (Cu_2S). In this communication we report a morphological and compositional study, confirming the composition and morphology expected from the results of the SXRD operando measurements pointing to the growth of Cu_2S by means of E-ALD.

Introduction

The task for renewable energy resources is focusing the scientific community attention on the development of new materials, based on economic and low-environmental impact elements such as Cu, Zn and Sn. These materials are expected to have a very favorable Full Life Cycle Assessment (FLCA) and are mainly involved in the development of new semiconductors ultra-thin films. In order to achieve an optimal control of the electronic and transport properties of the films, it is possible to exploit a deposition technique alternative to high-pressure and high-temperature methods, called Eletrochemical Atomic Layer Deposition (E-ALD).[1,2] This technique is able to build a film monolayer-by-monolayer, alternating the deposition of a monolayer of a metallic element with one of

Applied Surface Science 432 (2018) 53–59

Contents lists available at ScienceDirect

Applied Surface Science

journal homepage: www.elsevier.com/locate/apsusc

Full Length Article

Operando SXRD of E-ALD deposited sulphides ultra-thin films: Crystallite strain and size

Andrea Giaccherini[a,*], Francesca Russo[a], Francesco Carlà[b], Annalisa Guerri[a], Rosaria Anna Picca[c], Nicola Cioffi[c], Serena Cinotti[a], Giordano Montegrossi[d], Maurizio Passaponti[a], Francesco Di Benedetto[d,e], Roberto Felici[f], Massimo Innocenti[a]

[a] Department of Chemistry, Università Degli Studi di Firenze, Via della Lastruccia 3-13, 50019, Sesto Fiorentino (FI), Italy
[b] ESRF, 6, Rue Horowitz, F-BP 220, 38043, Grenoble, Cedex, France
[c] Department of Chemistry, Università degli Studi di Bari, Via E. Orabona, 4-70125 Bari, Italy
[d] IGG-CNR, via G. La Pira 4, 50121, Italy
[e] Department of Earth Sciences, Università Degli Studi di Firenze, Via La Pira 4, 50121 Firenze, Italy
[f] SPINCNR, Area della Ricerca di Roma 2 – Tor Vergata, Via del Fosso del Cavaliere 100, 00133 Roma, Italy

ARTICLE INFO

Article history:
Received 8 March 2017
Received in revised form 21 July 2017
Accepted 31 July 2017
Available online 5 August 2017

Keywords:
SXRD
ECALE
E-ALD
Photovoltaics
Water-splitting
Ultra-thin films

ABSTRACT

Electrochemical Atomic Layer Deposition (E-ALD), exploiting surface limited electrodeposition of atomic layers, can easily grow highly ordered ultra-thin films and 2D structures. Among other compounds Cu_xZn_yS grown by means of E-ALD on Ag(111) has been found particularly suitable for the solar energy conversion due to its band gap (1.61 eV). However its growth seems to be characterized by a micrometric thread-like structure, probably overgrowing a smooth ultra-thin films. On this ground, a SXRD investigation has been performed, to address the open questions about the structure and the growth of Cu_xZn_yS by means of E-ALD. The experiment shows a pseudo single crystal pattern as well as a powder pattern, confirming that part of the sample grows epitaxially on the Ag(111) substrate. The growth of the film was monitored by following the evolution of the Bragg peaks and Debye rings during the E-ALD steps. Breadth and profile analysis of the Bragg peaks lead to a qualitative interpretation of the growth mechanism. This study confirms that Zn lead to the growth of a strained Cu_2S-like structure, while the growth of the thread-like structure is probably driven by the release of the stress from the epitaxial phase.

1. Introduction

The energy issue of modern society is linked to the limited availability of non-renewable fuels coupled to the increasing levels of global pollution, approaching an environmental overshoot. This implies the need for a rapid development in materials and techniques for renewable energy applications. An increase in efficiency and sustainability of the solar cells necessarily requires the use of materials consisting of elements whose availability will support the diffusion of the photovoltaic technology at a global level over the actual extent represented by the silicon-based solar cells. At the same time, the use of such materials should ensure a lower environmental impact, in a Full Life Cycle Assessment (FLCA), and the device production must be done through less energy-intensive methods, thus increasing the Energy Return Over Energy Investment (EROEI). For these reasons, the scientific community is focusing its attention on new compounds based on economic and low-environmental impact elements such as Cu, Sn, Fe and Zn. A possibility to obtain high quality thin film semiconductors relies on exploiting electrochemical deposition. This technique is a very attractive method to produce compound semiconductors with different stoichiometry and high crystallinity because of its easiness of implementation, its relatively low cost, its capability of growing the selected materials onto substrates of any shape and dimensions.

Chalcogenide nanomaterials are interesting candidates for photovoltaic applications due to the reasons well-explained by Innocenti et al. [1]. Chalcogenides can be grown by means of Electrochemical Atomic Layer Epitaxy (ECALE) [2]. This technique consists in the electrodeposition of alternating metallic and non-metallic monolayers in a cycle which can be repeated several times and which exploits reactions limited by the surface (SLR – Surface Limited Reactions), including UnderPotential Depositions (UPD). This method is also referred as E-ALD (Electrochemical Atomic Layer Deposition), when the deposit cannot be considered strictly epitaxial [3].

* Corresponding author.
E-mail address: andrea.giaccherini@unifi.it (A. Giaccherini).

http://dx.doi.org/10.1016/j.apsusc.2017.07.294
0169-4332/

Substantia
An International Journal of the History of Chemistry

Firenze University Press
www.fupress.com/substantia

Citation: M. Innocenti, W. Giurlani, M. Passaponti, A. De Luca, E. Salvietti (2019) Electrodeposition and innovative characterization of precious metal alloys for the Galvanic and Jewel industry. *Substantia* 3(1) Suppl.: 29-37. doi: 10.13128/Substantia-602

Data Availability Statement: All relevant data are within the paper and its Supporting Information files.

Competing Interests: The Author(s) declare(s) no conflict of interest.

Electrodeposition and innovative characterization of precious metal alloys for the Galvanic and Jewel industry

Massimo Innocenti, Walter Giurlani, Maurizio Passaponti, Antonio De Luca, Emanuele Salvietti

Department of Chemistry "Ugo Schiff", University of Florence, via della Lastruccia 3, 50019 Sesto Fiorentino (FI), Italy

Abstract. In recent years the idea that metals, oil and, more generally, natural resources are not endless has been firmed. Furthermore, people become aware that humanity must not only increase the production of customer-goods, but they also must produce them with respect for the environment, trying to limit either dangerous processing techniques and hazardous materials. The elimination of many metals from alloys has also reduced the possibility to modify or to produce a wide range of precious jewels and new materials. For such reasons it is essential to develop new techniques for manipulation and preparation of precious jewellery products. Nowadays this economic policy drives many companies and even the single craftsmen to a cultural innovation and technological growth. Many small and medium-sized companies ask the University for a technological support, otherwise impossible to achieve alone for high costs. The basic research of University has become an important point for the development of the goldsmith sector and for the increase in production and variety of new jewels. This important collaboration between universities and industries is called "the Third Mission for the University". This collaboration is important from a cultural, as well as from a productive point of view. Nowadays, the symbiosis "Research centre - Goldsmith company", allows the company to expand internationally its market, thus making the whole industrial sector competitive and innovative. This union is extremely important not only for the goldsmith sector but for the entire National economy.

Keywords. Electrodeposition, Surface Analysis, Galvanic, Jewel.

INTRODUCTION

Since several years, industrialists, politicians and scientists have become aware that the energy resources of our planet may sooner or later end since they are limited. Awareness contributed to move towards the development of numerous renewable energy sources. Alternative energies and new renewable sources supported by developing technologies are already a big market creating many, high quality jobs. National research on major societal challenges, such as renewable energies, synthesis of new materials or creation of technological poles, will have more impact if efforts would be combined at the

ECS Transactions, 80 (10) 757-766 (2017)
10.1149/08010.0757ecst ©The Electrochemical Society

Color Measurements In Electroplating Industry: Implications For Product Quality Control

Walter Giurlani[a,z], Filippo Gambinossi[a], Emanuele Salvietti[a], Maurizio Passaponti[a], Massimo Innocenti[a,*]

[a] Dipartimento di Chimica, UNIFI, via della Lastruccia 3, 50019, Sesto Fiorentino (Firenze), Italy
*Electrochemical Society Member
[z]walter.giurlani@unifi.it

Electroplating industry constantly requires accurate color references as part of quality control decision on manufactured goods and accessories. Especially in the metal finishing sector color inconsistency due to variable instrumental settings and product geometry would cause communication problems between producer and customer. In this respect we focused on electroplated color evaluation operated by colorimeters generally used in fashion manufacturing, and compared the results with a laboratory spectrophotometer. Implications of surface finish, texture, and instrumental settings on color tolerance of cataphoretic coatings were discussed. Based on the recommendations of the Commission Internationale de l'Eclairage (CIE) we show a correlation between perceptual color differences and sampled areas. Increased surface roughness levels off color tolerance among different colorimeter's apertures, though deviations remain high, $\Delta E > 2$. Color reproducibility from three local fashion companies is presented for electroplated metal finished samples. We show that there are significant differences between industrial and laboratory measurement, near the limits of naked eye perceptibility of two different colors $1 < \Delta E < 3$.

Introduction

Color measurement is one of the most important aspects for a variety of industrial applications. The precise color determination has a central role in the quality control of end products for food, textiles, automotives and metal finishing sectors (1-4). Especially for electroplating, color inspection is a primary indicator of surface quality. Alteration of lightness, hue, and saturation are usually associated with surface defects or changes in galvanic baths composition and deposition efficiency (5). With the improvement in technology and scientific development industrial quality control has been moving from operator-dependent processes towards more objective automated vision systems. The vast majority of the electroplating industries employs colorimetry to assess the quality of their products and to make the so-called 'pass/fail' decisions. Though color measurements are easily accessible, different instrumental settings and sample geometries might lead to uneven data. Variations in surface texture, angle of observation, deposition cycles and measurement protocols could drastically affect the reproducibility of analysis, thus resulting in communication problems between producer and customer. Specifically, in the

Article

Journal of
Nanoscience and Nanotechnology
Vol. 19, 1–6, 2019
www.aspbs.com/jnn

High Density Nanostructured Soft Ferrites Prepared by High Pressure Field Assisted Sintering Technique

M. Petrecca[1], M. Albino[1], I. G. Tredici[3], U. Anselmi-Tamburini[3], M. Passaponti[1], A. Caneschi[1], and C. Sangregorio[2,*]

[1]Dip. di Chimica, "Ugo Shiff", Università degli Studi di Firenze, via della Lastruccia 3-13, I-50019 Sesto Fiorentino, and Consorzio INSTM, Italy
[2]CNR-ICCOM, via Madonna del Piano 10, I-50019 Sesto Fiorentino, and Consorzio INSTM, Italy
[3]Dip. di Chimica, Università degli Studi di Pavia, v.le Taramelli 12, I-27100 Pavia, Italy

The synthesis of highly compacted, nanostructured soft magnets is highly desirable due to their promising properties for the development of electronic devices working at frequency higher than 2 MHz. In this work we investigated the potentiality of High Pressure Field Assisted Sintering Technique (HP-FAST). To this aim, we first synthesized soft Mn–Zn Ferrite magnetic nanoparticles (MNPs) through an easy-scalable, eco-friendly strategy based on aqueous co-precipitation in basic media, starting from transition metals chlorides. Powder X-ray diffraction (PXRD) and Transmission Electron Microscopy (TEM) analyses evidenced the formation of crystalline nanoparticles with the cubic spinel structure and average crystal size of 7.5 nm. Standard magnetometric measurements showed a saturation magnetization value of ca. 56 emu/g and no magnetic irreversibility at room temperature. The MNPs were then compacted applying an uniaxial pressure over a toroidal shaped die. In order to obtain a material with a density close to the bulk one, the as-prepared green toroids underwent either a classic sintering treatment, obtaining a microstructured system, or to High Pressure Field Assisted Sintering Technique (HP-FAST), which allowed for preserving the nanostructure. The relative permeability and core losses of the toroidal samples were evaluated in the frequency range 1–2 MHz using an in-house built setup. The comparison of the behavior of samples obtained by the two different sintering approaches showed the nanostructured samples had a much smaller relative magnetic permeability (ten times lower than the microstructured sample) and, consequently, higher core losses. However, when samples with similar μ_r were compared, a significant decrease of core losses at the larger frequencies was observed. This result suggests HP-FAST is a very promising approach to prepare high density nanostructured soft magnetic materials.

Keywords: Mn–Zn Ferrite, Soft Magnetic Materials, Nanostructure, Core Loss.

1. INTRODUCTION

Soft magnetic materials represent an economically relevant key element in modern technology, where they are widely used to realize electronic devices such as transformers, choke coils, inductors and high-frequency power electronics.[1,2] All these devices, indeed, comprise a soft magnetic core inserted in an electric circuit, working both in direct current (DC) or alternating current (AC).[3] The constant demand for increasing the efficiency and miniaturizing the size of electronic devices requires the use of ever increasing frequencies, which, at the same time makes energy dissipation more and more critical. The reduction of the energy dissipation as heat (power losses) is indeed, at present, the keystone for the effective use of soft magnetic cores in electronic devices. In the range of frequency of few MHz the main contributions to power losses are hysteresis, conductivity (eddy current loss) and residual losses.[4] Typical approaches to reduces hysteresis losses are based on increasing the magnetic permeability and/or decreasing the anisotropy by fine tuning the composition of ferrites and alloys, increasing the grain size of bulk metal alloys or using amorphous alloys.[5–7] On the other hand the reduction of eddy currents requires the

*Author to whom correspondence should be addressed.

Journal of Analytical and Applied Pyrolysis 130 (2018) 305–313

Contents lists available at ScienceDirect

Journal of Analytical and Applied Pyrolysis

journal homepage: www.elsevier.com/locate/jaap

Microwave assisted pyrolysis of crop residues from *Vitis vinifera*

Mattia Bartoli[a], Luca Rosi[a], Alessio Giovannelli[b], Piero Frediani[a], Maurizio Passaponti[a], Marco Frediani[a,*]

[a] Department of Chemistry, University of Florence, Via della Lastruccia, 3-13, 50019, Sesto Fiorentino, Italy
[b] CNR IVALSA Via Madonna del Piano 10, 50019, Sesto, Fiorentino, Italy

ARTICLE INFO

Keywords:
Vitis vinifera
Microwave
Pyrolysis
Biomass
Quantitative bio-oil composition

ABSTRACT

A fast pyrolysis of crop residues of *Vitis vinifera* has been realized using a multimode microwave (MW) oven using various MW absorbers. The combination of absorber/reactor arrangement address the process towards a high formation of bio-oil (34.9%) and gas (45.7%) or the production of large amount of bio-char (up to 71.4%).

Bio-oils were collected as dark brown liquids with low viscosity and density. They were characterized through analytical and spectroscopic methods and the compounds present were identified and quantified. Large amount of acetic acid (up to 172.5 g/L) and appreciable amount of aromatics (up to 39.5 g/L) were formed in all experiments. Bio-oil obtained using carbon as MW absorber and set-up B showed the lower water concentration (39.5 wt%).

Bio-chars formed in all tests showed almost the same calorific values, close to that of commercial pellets.

The MAP of vine residues is a sound way to reduce environmental risks for their disposal and gave usefully chemicals, mainly acetic acid, aromatics and fuels through a fast pyrolysis process.

1. Introduction

The primary energy demand was growing every year and in 2010 it was increased of 5% [1]. As a consequence the greenhouse gas emissions recorded a new peak, growing of 5.8% if compared to 2009 [2]. The increase of primary energy consumption between 2000 and 2009 was concentrated in few countries, mainly India and China, and it was driven by coal consumption even if this trend was decreased in the last years [3]. In Europe primary energy demand grew slowly in 2010 (3% if compared to 2009) [4] and the most interesting trend consists in an increased production from renewable sources [5].

In the same time the request of chemicals rises year by year and the use of renewable resource have been approached as a promising way to supply, at least partially, this demand [6]. Thermal treatments of biomass may give a contribution to the increasing request of energy and chemicals from renewable sources avoiding, in the same time, an increase in the production of CO_2 [7].

In the last 10 years microwave assisted pyrolysis (MAP) gained a remarkable interest for processing waste/contaminate plastic materials in order to obtain fuels or raw materials [8–18]. Also MAP of biomasses was studied by several authors [19–22] to obtain high quality bio-oils thanks to a fast heating at moderate temperature (500–700 K) followed by a rapid quenching of the volatile products formed [23–25]. Furthermore MAP does not require the use of a finely milled feedstock because MW allows a volumetric heating of sample [26]. The presence of water inside the material may enhance the heating rate and mitigate the temperature reached during pyrolysis avoiding an advanced cracking degradation. Even if biomass may absorb MW, the addition of a MW absorber improve significantly the quality/quantity of the products formed [19]. Vine (*Vitis vinifera*) cultivation is one of the major business in the agrochemical industry [27] and they produce large amount of pruning and grape residues. In Italy, the annual pruning vineyard residues accounted to 1 oven dry ton (odt) per hectare with an estimated managing cost for the farms of 50 Euro per year [28]. There are a lot of available technologies to dispose these residues such as mechanical recycling or composting [29], but combustion is the most used. Several authors studied thermal pyrolysis of grapes bagasse to produce fuels with [30] or without a catalyst [31,32]. In this work MAP of woody residues from vineyards was performed in a multimode batch oven using MW absorbers (carbon, iron powder, silicon carbide). A modified plant, containing a fractionating system inserted between the oven and the condensing system, was also tested. The aim of this work was to check an efficient disposal of waste residue of vineyards through a MAP process evaluating the yield of the pyrolyzed products using different reaction conditions. A great attention was devoted to the characterization of the three collected fractions (bio-char, bio-oil and gas) with particular attention to the liquid fraction.

* Corresponding author.
E-mail address: marco.frediani@unifi.it (M. Frediani).

https://doi.org/10.1016/j.jaap.2017.12.018
Received 8 August 2017; Received in revised form 13 December 2017; Accepted 26 December 2017
Available online 10 January 2018
0165-2370/

Physics and Chemistry of Minerals (2018) 45:935–944
https://doi.org/10.1007/s00269-018-0974-x

ORIGINAL PAPER

An XRPD and EPR spectroscopy study of microcrystalline calcite bioprecipitated by *Bacillus subtilis*

B. Perito[1] · M. Romanelli[2] · A. Buccianti[2,4] · M. Passaponti[3] · G. Montegrossi[4] · F. Di Benedetto[2,4]

Received: 22 November 2017 / Accepted: 3 May 2018 / Published online: 22 May 2018

Abstract
We report in this study the first XRPD and EPR spectroscopy characterisation of a biogenic calcite, obtained from the activity of the bacterium *Bacillus subtilis*. Microcrystalline calcite powders obtained from bacterial culture in a suitable precipitation liquid medium were analysed without further manipulation. Both techniques reveal unusual parameters, closely related to the biological source of the mineral, i.e., to the bioprecipitation process and in particular to the organic matrix observed inside calcite. In detail, XRPD analysis revealed that bacterial calcite has slightly higher c/a lattice parameters ratio than abiotic calcite. This correlation was already noticed in microcrystalline calcite samples grown by bio-mineralisation processes, but it had never been previously verified for bacterial biocalcites. EPR spectroscopy evidenced an anomalously large value of W_{δ}, a parameter that can be linked to occupation by different chemical species in the next nearest neighbouring sites. This parameter allows to clearly distinguish bacterial and abiotic calcite. This latter achievement was obtained after having reduced the parameters space into an unbiased Euclidean one, through an isometric log-ratio transformation. We conclude that this approach enables the coupled use of XRPD and EPR for identifying the traces of bacterial activity in fossil carbonate deposits.

Keywords Biogenic calcite · Spectroscopic signature · *Bacillus subtilis* · EPR · XRPD · Statistical analysis

Introduction

The study of formation of $CaCO_3$ by precipitation processes mediated by the activity of bacteria dates to Murray and Irvine, at the end of the nineteenth century (Ehrlich 2002). These processes are highly relevant in the global cycle of carbon, being able to affect the ecosystems in the lithogenesis and in the supply of carbon dioxide in the atmosphere (Hazen 2010). Indeed, a significant portion of the insoluble carbonate at the Earth's surface is of biogenic origin (Ehrlich 2002). On the other hand, bioprecipitation of calcite opens interesting perspectives on several potential applications. These include the bioremediation of aquifers, polluted either by natural processes or by industrial wastes (Lalonde et al. 2007; Kumari et al. 2016), the conservation of cultural heritage artefacts made up by calcareous stones (Navdeep-Kaur et al. 2013; Lopez-Moreno et al. 2014; Perito et al. 2014), the fixing of atmospheric CO_2 (Clark and Fritz 1997), the mineral separation by flotation in the industrial processes (Botero et al. 2007; Pollmann et al. 2016), and the improvement of technological concrete's properties (Sarkar et al. 2015; Vahabi et al. 2015).

The study of calcite bioprecipitation, either spontaneous or under laboratory conditions, has been the focus of numerous studies, resulting in the proposals of different mechanisms for this process being still debated nowadays. The phenomenon can be influenced by the environmental physico-chemical conditions and is correlated to both the metabolic activity and the cell surface structures of microorganisms (Castanier et al. 1999; Fortin et al. 1997; Perito and Mastromei 2011). Some studies point to the necessity of identifying an analytical marker able to safely distinguish the

Electronic supplementary material The online version of this article (https://doi.org/10.1007/s00269-018-0974-x) contains supplementary material, which is available to authorized users.

✉ F. Di Benedetto
francesco.dibenedetto@unifi.it

[1] Department of Biology, University of Florence, Florence, Italy

[2] Department of Earth Sciences, University of Florence, Florence, Italy

[3] Department of Chemistry, University of Florence, Sesto Fiorentino, Italy

[4] CNR-IGG, Florence, Italy